

AD-A185 232

THE EFFECTS OF BAND-LIMITED WHITE NOISE EXCITATION ON
LIQUEFACTION POTENTIAL IN LARGE-SCALE TESTS(U) AIR
FORCE INST OF TECH WRIGHT-PATTERSON AFB OH

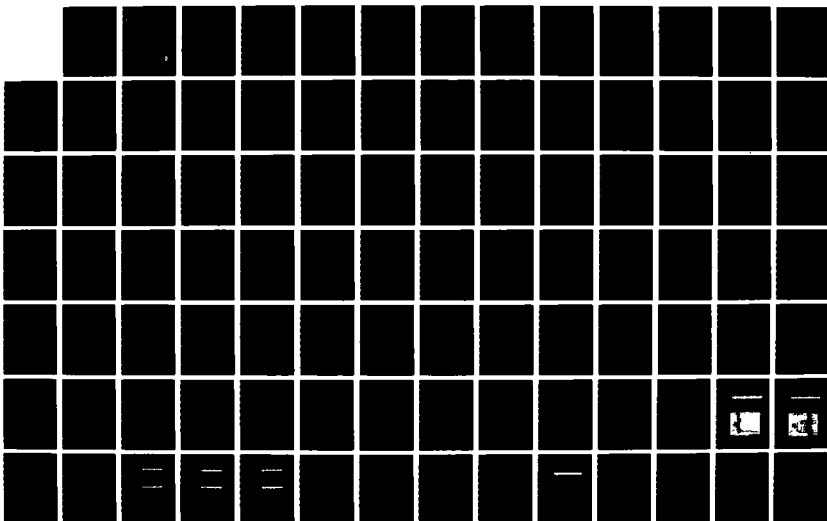
1/2

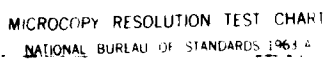
UNCLASSIFIED

D L JASINSKI 1987 AFIT/CI/NR-87-58T

F/G 8/18

NL





REPORT DOCUMENTATION PAGE

READ INSTRUCTIONS
BEFORE COMPLETING FORM

1. REPORT NUMBER AFIT/CI/NR 87-58T	2. GOVT ACCESSION NO.	3. RECIPIENT'S CATALOG NUMBER
4. TITLE (and Subtitle) The Effects of Band-Limited White Noise Excitation on Liquefaction Potential In Large-Scale Tests		5. TYPE OF REPORT & PERIOD COVERED THESIS/INSTRUMENTAL
7. AUTHOR(s) Dennis Lee Jasinski		6. PERFORMING ORG. REPORT NUMBER
9. PERFORMING ORGANIZATION NAME AND ADDRESS AFIT STUDENT AT: Ohio State University		8. CONTRACT OR GRANT NUMBER(s)
CONTROLLING OFFICE NAME AND ADDRESS AFIT/NR WPAFB OH 45433-6583		10. PROGRAM ELEMENT, PROJECT, TASK AREA & WORK UNIT NUMBERS
11. MONITORING AGENCY NAME & ADDRESS (if different from Controlling Office)		12. REPORT DATE 1987
		13. NUMBER OF PAGES 145
		15. SECURITY CLASS. (of this report) UNCLASSIFIED
		15a. DECLASSIFICATION DOWNGRADING SCHEDULE

6. DISTRIBUTION STATEMENT (of this Report)

APPROVED FOR PUBLIC RELEASE; DISTRIBUTION UNLIMITED

17. DISTRIBUTION STATEMENT (of the abstract entered in Block 20, if different from Report)

18. SUPPLEMENTARY NOTES

APPROVED FOR PUBLIC RELEASE: IAW AFR 190-1

Lynn E. Wolaver
LYNN E. WOLAVER 17 Aug 87
Dean for Research and
Professional Development
AFIT/NR

19. KEY WORDS (Continue on reverse side if necessary and identify by block number)

20. ABSTRACT (Continue on reverse side if necessary and identify by block number)

ATTACHED

DTIC
ELECTE
OCT 26 1987
S D
CD

DD FORM 1 JAN 73 1473

EDITION OF 1 NOV 65 IS OBSOLETE

87 10 1 280

AD-A185 232 DTIC FILE COPY

CHAPTER I
INTRODUCTION

During earthquakes, ground movement can cause soils to lose strength or stiffness resulting in structures settling and embankments sliding. A phenomenon contributing to this loss in strength and subsequent failures is called soil liquefaction. This title, however, does not refer to a single well-defined event, but rather to a complex set of interrelated phenomena which contribute to the occurrence of damage and failures during an earthquake. Numerous investigators have tried to model and predict the potential and probability of liquefaction occurring in soils. Since the early 1960's, considerable attention has been given to the development of laboratory testing procedures to provide improved methods of characterizing the liquefaction properties of soils. Various test apparatus have been designed or modified in an attempt to provide an accurate representation of the stress state generated in-situ by earthquakes. To this end a number of experimental devices including the cyclic triaxial, cyclic simple shear,

repeatable representation of conditions in-situ during an actual earthquake.

The testing program described in this thesis actually consisted of three distinct stages. The first stage involved the conduct of the same shaking table tests on isotropically consolidated samples as were performed by Mason [22] and Amato [1]. These tests were harmonic tests designed to illustrate that indeed consistent results were attainable from one investigator to another using the same testing apparatus. The second stage was designed to perform tests in which a heavy reaction mass was placed on top of the sand sample. These tests were conducted in order to compare the results of the present study with those reported by De Alba et al [9] since the De Alba results have for the past 12 years served as the benchmark in this area of study. Finally, the third stage of testing utilized band-limited white noise to reproduce a simulated earthquake loading pattern on in-situ soil deposits.

The following chapters of this thesis systematically present and describe the laboratory testing procedures used and the results obtained. Chapter II describes previous nonuniform loading studies on liquefaction potential and why pink noise is the most representative loading pattern in simulating in-situ conditions. Chapter III provides a description of the experimental testing apparatus and modifications made since the tests reported by Amato [1]

were conducted. Chapter IV contains the procedures followed for each liquefaction test and Chapter V summarizes the experimental results obtained during each of the three testing stages. Chapter VI presents conclusions and recommendations.

The three appendices which follow contain the time histories of the generated test data, as well as, the resulting Fourier amplitude spectra.



Location For	
US CR421	✓
NO. 186	
100-1000	
100-1000	
Date	
By (Name)	
Submitting Codes	
Dist	Field and/or Special
A-1	

THE EFFECTS OF BAND-LIMITED WHITE NOISE EXCITATION
ON LIQUEFACTION POTENTIAL IN LARGE-SCALE TESTS

A Thesis

Presented in Partial Fulfillment of the Requirements for
the degree Master of Science in the Graduate
School of The Ohio State University

by

Dennis Lee Jasinski, B.S.C.E., M.B.A.

* * * * *

The Ohio State University

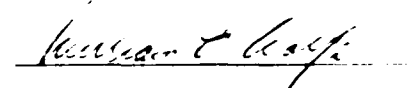
1987

Master's Examination Committee:

Ranbir S. Sandhu

Tien H. Wu

Approved by:



Advisor

Department of Civil Engineering

ACKNOWLEDGEMENTS

I would like to extend my sincere gratitude to Dr. William E. Wolfe, my thesis advisor, for his continual guidance and support throughout the course of my academic study. His instruction and encouragement were essential to the completion of this thesis. I am also grateful to Professors Ranbir S. Sandhu and Tien H. Wu for serving on my oral defense committee.

The investigation reported herein is part of the research performed at The Ohio State University and made possible through the Air Force Office of Scientific Research Grant 83-00-55 under the management of Dr. Spencer Wu.

The help of Messrs. Leonart Claussan and Richard Noll in modifying and maintaining the test equipment is greatly appreciated.

VITA

May 29, 1959 Born: Heidelberg, West Germany

1981 B.S.C.E., The University of
Wisconsin-Platteville, Platte-
ville, Wisconsin

1982-1985 Structural Projects Engineer,
3902d Air Base Wing, Offutt
Air Force Base, Nebraska

1986 M.B.A., The University of
Nebraska, Lincoln, Nebraska

FIELDS OF STUDY

Major Field: Geotechnical Engineering

Studies in liquefaction potential of saturated sands

TABLE OF CONTENTS

ACKNOWLEDGEMENTS	ii
VITA	iii
LIST OF TABLES	vi
LIST OF FIGURES	vii
CHAPTER	
I INTRODUCTION	1
II PREVIOUS STUDIES ON LIQUEFACTION	5
2.1 Introduction	5
2.2 Susceptibility Of Cohesionless Soils to Liquefaction	7
2.3 Random Vibrations	8
2.3.1 Band-limited white noise	11
2.3.2 White noise studies	12
2.3.3 Representation of earthquake motion	14
2.4 Equivalent Uniform Cycles	18
2.5 Liquefaction Testing Under Irregular Loadings	23
III INSTRUMENTATION.....	38
3.1 Introduction	38
3.2 Shaking Table.....	38
3.3 Sample Test Chamber.....	39
3.4 Instrumentation.....	42
IV TESTING PROCEDURE.....	45
4.1 Introduction.....	45
4.2 Sand Sample Preparation.....	45
4.3 Membrane Penetration.....	48
4.4 DataCollection.....	48

V	LIQUEFACTION TEST RESULTS.....	51
5.1	Introduction.....	51
5.2	Sample Saturation.....	52
5.3	Testing Material	53
5.4	Shear Stress Ratio	53
5.5	First Testing Stage	55
5.5.1	Results	55
5.5.2	Pore water pressure generation	56
5.5.3	Table excitation	59
5.6	Second Testing Stage	61
5.6.1	Results	61
5.6.2	Pore water pressure generation	65
5.6.3	Table and sample excitation	67
5.7	Third Testing Stage	69
5.7.1	Input motions	69
5.7.2	Results	71
5.7.3	Table and sample excitation	83
5.7.4	Spectrum analysis	85
5.7.5	Pore water pressure generation	85
VI	SUMMARY, CONCLUSIONS AND RECOMMENDATIONS	87
	REFERENCES	92
	APPENDICES	
A	TIME HISTORIES OF SAMPLE PORE WATER PRESSURE CHANGE	100
B	TIME HISTORIES OF TABLE AND SAMPLE EXCITATION	122
C	SPECTRUM ANALYSIS RECORDS.....	140

LIST OF TABLES

TABLE

2.1	Summary of factors affecting liquefaction potential of cohesionless soils	9
5.1	Applied isotropic test conditions and results...	57
5.2	Test conditions and results from reaction mass testing	63
5.3	Test conditions and results from pink noise excitation testing	75

LIST OF FIGURES

FIGURE

2.1	Effect of loading wave form on cycles to initial liquefaction	10
2.2	Typical band-limited white noise Fourier amplitude spectrum	13
2.3	Earthquake response spectrum	15
2.4	Fourier amplitude spectrum for the 1940 El Centro earthquake	16
2.5	Equivalent cycle concepts	20
2.6	Cyclic shear stresses on a soil element during earthquake excitation	24
2.7	Effect of nonuniform loading on pore water pressure increase	27
2.8	Irregular cyclic load test records	29
2.9	Effect of peak shear stress timing on pore water pressure increase	31
2.10	Laboratory simulation of liquefaction during the Niigata earthquake	33

2.11	Relation between the stress ratios and pore water pressures using the Niigata earthquake acceleration record	34
2.12	Relation between stress ratios and time to initial liquefaction	36
3.1	Large scale laboratory testing system	40
3.2	Sample test chamber	41
3.3	Pore water pressure measurement system	44
4.1	Second stage sample preparation	47
4.2	Membrane penetration testing	49
5.1	Grain size distribution curve	54
5.2	Comparison of first stage results with other isotropic tests	58
5.3	Comparison of renormalized results	60
5.4	Comparison of liquefaction potential test results	62
5.5	Comparison of second stage results with other investigators	64
5.6	Typical stage two test record	66
5.7	Comparison of stage two table and sample acceleration time history	68
5.8	Fourier spectra of stage three study and 1940 El Centro Earthquake	70
5.9	Typical spiked acceleration temporal and frequency record	73

5.10	Typical non-spiked acceleration temporal and frequency record	74
5.11	Typical Test C1 record	76
5.12	Typical Test C2 record	77
5.13	Typical Test C3 record	78
5.14	Typical Test C4 record	79
5.15	Comparison of time to liquefaction for stage three results	80
5.16	Comparison of results from this study with other investigators	82
5.17	Comparison of typical stage three table and sample acceleration time history	84
A.1	Pore water pressure transducer orientation	100

CHAPTER II

PREVIOUS STUDIES ON LIQUEFACTION

2.1 Introduction

Signs of liquefaction have been visible during and after many earthquakes around the world. In many cases, liquefaction has caused considerable damage. This was especially true when an earthquake occurred near the town of Niigata, Japan on June 16, 1964. The epicenter of the earthquake (magnitude of 7.3 on the Richter Scale) was located approximately 35 miles from Niigata, but the earthquake still induced extensive liquefaction of the sand deposits in the low-lying areas of the town [16]. Cracking of the ground surface associated with the initial emergence of water from the ground occurred. In some areas numerous sand vents could be observed after the earthquake subsided, sometimes surrounded by rings of sand carried to the surface by the upward-flowing water. As liquefaction developed over various areas of the city, automobiles, structures, and other objects settled or tilted into the resulting quicksand.

In the two decades since the Niigata earthquake, considerable progress has been made in identifying the geologic deposits and sandy soils which are most susceptible to liquefaction. Data bases have been compiled which correlate certain factors to liquefaction potential and are of great value to engineering practice and design. They have shown, for example, deposits that liquefy during one earthquake can again liquefy in subsequent earthquakes [23]. Tests on laboratory soil samples have shown cyclic straining causes pore water pressure to build up in a saturated soil as a result of soil particles being rearranged with a tendency toward compaction. However, if the water in a sample cannot drain from the soil during the applied load, gravity loading is transferred from the sand skeleton to the pore water pressure, with a consequent reduction in the capacity of the soil to resist loading. Eventually, the pore water pressure may become equal to the effective confining pressure. If it does, liquefaction (this has also been defined as initial liquefaction or cyclic mobility by some authors) is said to have occurred. This definition for liquefaction will be used throughout this thesis.

Several explanations have been proposed to account for the failure of structures as a result of liquefaction. Extensive reviews can be found in references 5, 23 and 37.

Regardless of which explanation of the physical phenomenon is adhered to, for failure to occur there must be both a prior susceptibility to loss of strength in the soil deposit and a triggering mechanism (such as an increase in pore water pressure). The two combine to initiate the progressive loss of strength within the saturated soil deposit.

Almost any saturated granular soil can develop increased pore water pressure when cyclicly loaded. These pore water pressures can become significant if the intensity and duration of earthquake loading are great enough. The engineer must then decide what intensity and duration of cyclic loading will cause liquefaction at a particular site, or, conversely, whether a soil deposit can survive a particular intensity of shaking without liquefying. A wide variety of testing methods have been utilized for determining the potential of liquefaction at a specific site, and most have highlighted the numerous factors affecting this potential.

2.2 Susceptibility of cohesionless soils to liquefaction

The results of tests from reconstructed soil samples in the laboratory have identified various factors influencing the susceptibility of soils to liquefaction. Saturated granular soils without cohesive fines (i.e. some silts, sands and even some gravels) are all susceptible to the

generation of residual pore water pressures. The density of the soil has also been shown to be a very important factor. This is because pore water pressures have been shown to build up more quickly in a loose versus a dense sand, causing the soil deposit to lose its initial resistance to shear after a shorter period of loading. Other factors affecting the amount of relative pore water pressure generated include: the amplitude of the cyclic loading; the past history of stressing; the size, shape, and gradation of particles; the confining pressure acting on the sample; the age of the deposit; the fabric of the soil; and the overconsolidation ratio of the soil. Table 2.1 [37] presents a brief summary of these factors.

A noteworthy factor influencing the potential of liquefaction is the loading waveform. Figure 2.1 [37] compares the effect of the loading waveform used in laboratory testing on the number of cycles to liquefaction. These test results show that the strength of sand samples subjected to rectangular, triangular, and sinusoidal loads behaved differently, with triangular and sinusoidal wave loading strengths being 13 to 30 percent higher than rectangular loadings, respectively.

2.3 Random Vibrations

An earthquake accelerogram is a random function that can be thought of as being composed of a nonperiodic

Variable Effect of	Testing Conditions and Materials	Effect (Result)
Testing laboratory and equipment	"standard sand" tested by eight different laboratories following specified testing procedures and conditions Monterey No. 0 sand	excellent agreement between laboratories provided strict adherence to testing procedures followed
Specimen preparation	specimens formed by pluviation through air or water, vibration or tamping in dry or moist condition Monterey No. 0 sand 50% D_{50} and other soils	weakest specimens formed by pluviation through air, while strongest formed by vibrating in moist condition. Difference in stress ratio for failure can be 100%
Reconstituted versus intact	"intact" (relatively undisturbed) specimens tested, then remolded and reconstituted to same density and retested under same conditions as intact. A variety of sands and specimen preparation techniques for reconstitution used	intact specimens stronger than reconstituted. Strength decreases range from 0 to 100% depending upon material and reconstitution method
Freezing intact specimens	intact specimens transported to laboratory in frozen and unfrozen condition reconstituted specimens frozen in laboratory and compared with unfrozen specimens	no effect, with testing variation, due to freezing
Confining stress, σ_3	tests conducted at a variety of confining stresses on variety of sands	within small range of pressures, cyclic strength is directly proportional to confining stress. cyclic stress ratio decreases with increasing confining pressure 0.0007 to 0.004 per psi increase in σ_3
Loading wave form	tests conducted using rectangular, rounded rectangular, triangular, and sine wave loading shapes irregular wave forms simulating earthquake stress histories evaluating equivalent cycle concept	order of increasing strengths: rectangular, degraded rectangular or triangular, sine. Sine wave approximately 30% stronger than rectangular equivalent cycle approach valid. Cyclic triaxial affected by extension more than compression
Frequency	frequencies with combined range of 1 to 1680 cpm for various sands. Typical ranges 1 to 20 or 5 to 60 cpm evaluated for one sand water and air used as confining media while evaluating frequency effects	slower loading frequencies have slightly higher strengths. For range of 1 to 60 cpm, effect is 10% water may affect results at 5 Hz
Specimen size	strengths of 15 ϕ and 70 mm dia specimens compared with strengths of 70 and 300 mm dia specimens	no effect for this range 300 mm dia specimens 10% weaker
Frictionless caps and bases	specimens tested with friction and frictionless caps and bases at frequencies slow enough to allow grease to function	no effect between full friction and frictionless caps and bases
Relative density	tests conducted on variety of cohesionless soils over wide range of stress and testing conditions	cyclic strength increases dramatically with increasing density. Linear relationship between cyclic stress ratio and relative density to approximately 60% D_r , but slope is dependent on soil type, fabric, confining pressure, and failure strain
Particle size and gradation	cyclic strengths of different soils at comparable testing conditions compared on basis of mean grain diameter D_{50} well graded material compared with uniformly graded material both having same D_{50} size	sands have $D_{50} = 0.1$ mm have least resistance to cyclic loading. As D_{50} increases from 0.1 to 30 mm, a 60% strength increase observed as D_{50} decreases from 0.1 mm to silt and clay sizes, rapid increase in strength observed well graded somewhat weaker than uniformly graded material
Prestraining	specimens liquefied by cyclic loading, reconsolidated and reliquified by applying same original cyclic load specimens prestrained to 50 to 80% pore pressure response, reconsolidated, and reloaded cyclicly	despite increase in density due to consolidation, liquefaction causes considerably weaker specimen prestraining greatly strengthens cyclic strength
Overconsolidation ratio (OCR)	specimens overconsolidated by consolidating to higher stresses and rebounded to lower testing stresses	OCR's of 1 to 4 and 1 to 8 increased cyclic simple shear stress ratios 75 and 150%, respectively OCR of 1 to 2 increased cyclic strengths 30 to 60% depending upon amount of fines. Amount of fines affect OCR
Consolidation ratio R_c	specimens consolidated anisotropically for variety of confining stresses and subjected to reversing and nonreversing cyclic stresses	maximum deviator stress required for failure increases with R_c ratio for given d_v . method of presenting data influences conclusions, r_v versus σ_v , recommended. Interrupted consolidation may not always provide conservative results

TABLE 2.1 SUMMARY OF FACTORS AFFECTING LIQUEFACTION
POTENTIAL OF COHESIONLESS SOILS (AFTER TOWNSEND)

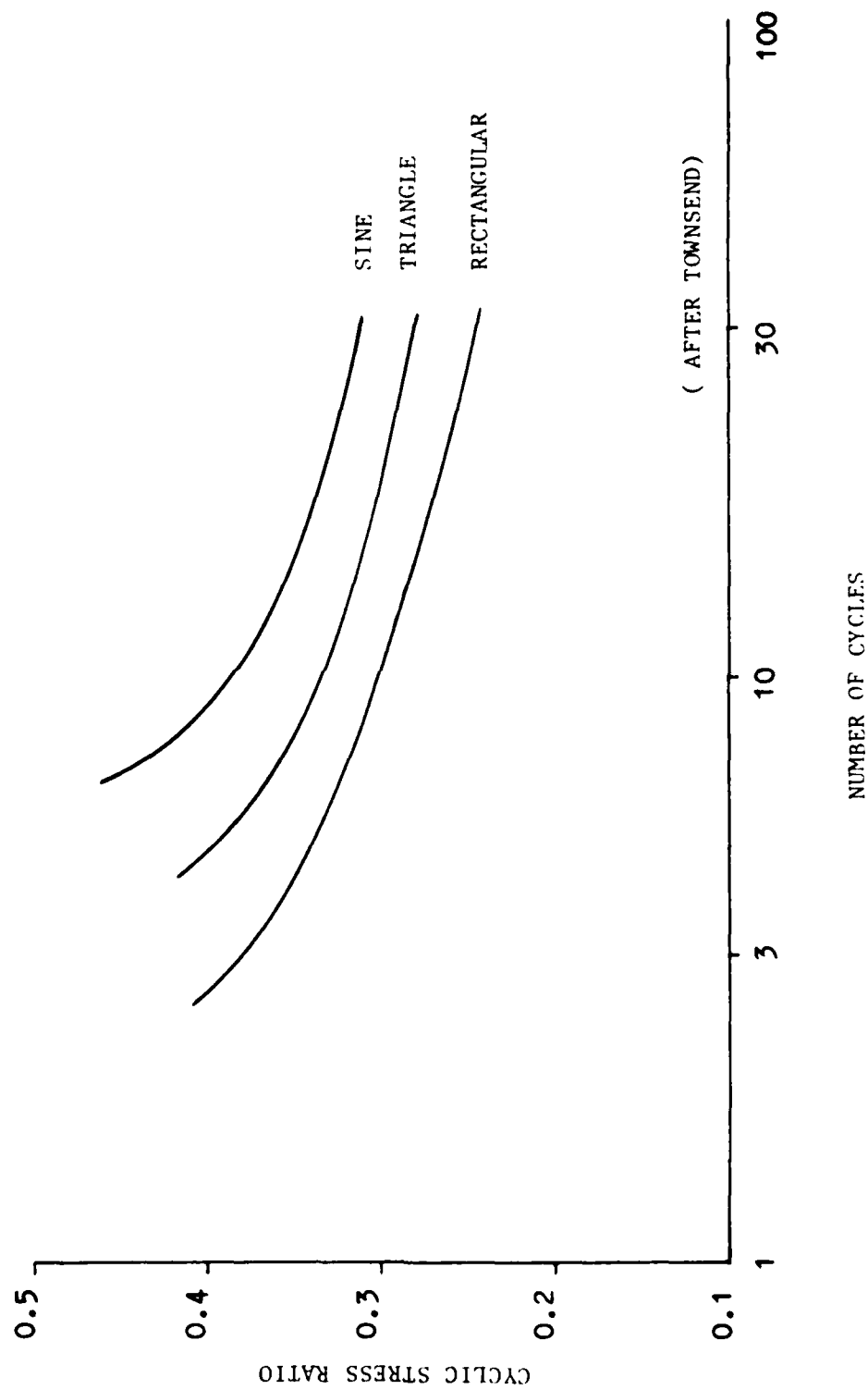


FIGURE 2.1 EFFECT OF LOADING WAVE FORM ON CYCLES TO INITIAL LIQUEFACTION

sequence of acceleration pulses. It is the area of a pulse that is a measure of its effectiveness in producing structural vibrations [29]. The amplitude of the pulse (e.g. the maximum acceleration) is often used to indicate the severity of the ground motion. This is satisfactory if the pulse durations are similiar in all earthquakes, but it is not a reliable measure if the pulses are of different durations [10]. The effect of the ground shaking therefore must also depend on the dominant frequency content of the earthquake motion and how it relates to the natural frequency of the soil strata and superimposed structures. Any method used in the laboratory to simulate an earthquake must incorporate these inherent earthquake properties.

2.3.1 Band-limited white noise

Earthquake accelerations were first modelled as random processes by Housner [13] who idealized accelerations as a series of pulses of a certain magnitude located randomly in time. In a subsequent paper [14], Housner represented accelerations as the sum of full period sine wave pulses distributed randomly in time, with frequency and amplitude taken from a calculated probability distribution. In the mid 1960's, a sufficient number of strong-motion earthquake accelerograms were recorded for investigators to determine that many earthquakes have a dominant frequency range of

zero to ten hertz [8] in common. Further research determined the naturally occurring frequency range of a strong-motion earthquake was adequately represented by a band-limited white noise excitation [24]. White noise implies a random process having a constant amplitude throughout the Fourier spectrum and is mathematically possible as the representation of an impulse excitation. Band-limited white noise has been defined as white noise over a specific frequency bandwidth in the Fourier amplitude spectrum and having zero amplitude throughout the remaining frequencies. Because band-limiting distorts the purity of white noise, the term pink noise is used to describe this random process [28]. The idealization of pink noise is shown in Figure 2.2 with true white noise represented by dashed lines.

2.3.2 White noise studies

Recent investigators [3,13,14,16,26,35] have verified Housner's theory that earthquake induced ground motion can be modeled by a series of either velocity or acceleration impulses of random amplitude and temporal spacing. Bycroft [3] studied the use of white noise in representing earthquake motion of a given intensity level. In his studies, Bycroft examined the maximum velocity response values resulting from 20 separate "bursts" of white noise having a duration of 25 seconds each. He limited the random

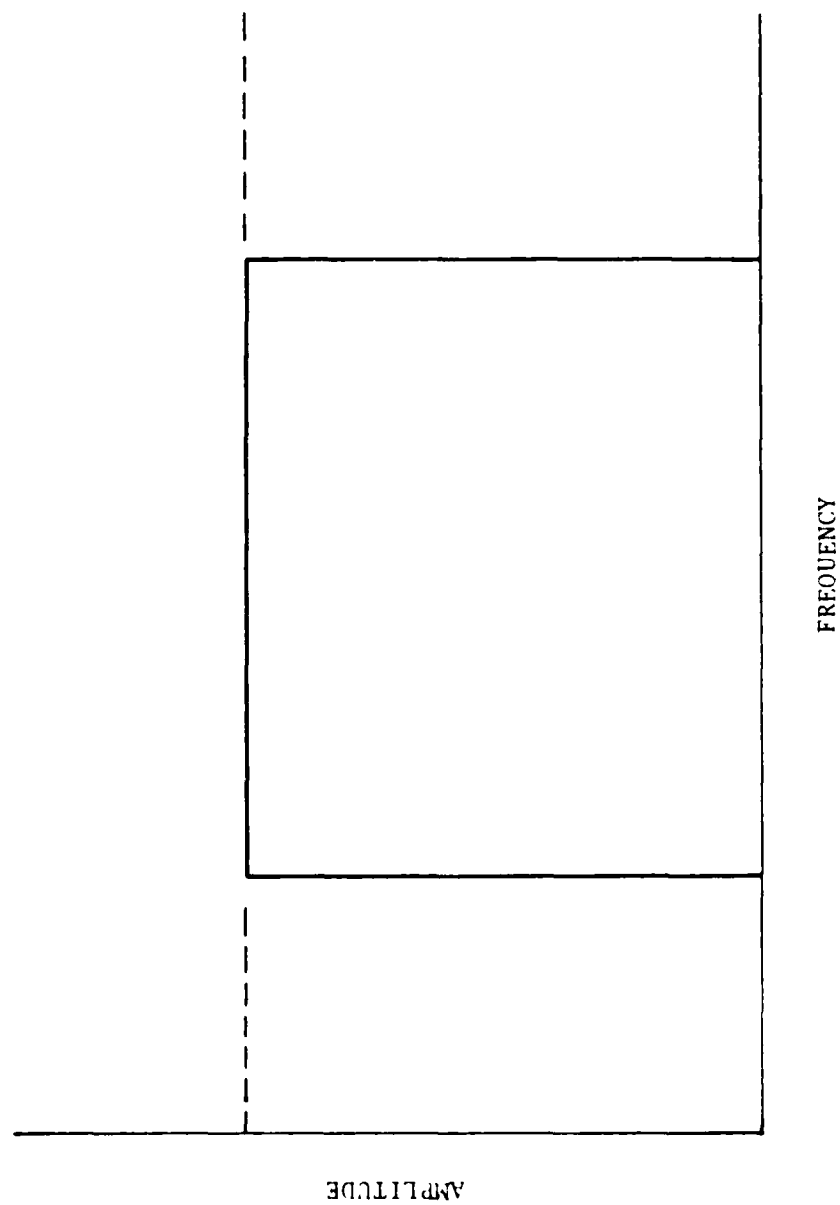


FIGURE 2.2 TYPICAL BAND-LIMITED WHITE NOISE FOURIER AMPLITUDE SPECTRUM

process to a band width of constant amplitude and 0-35 hertz. In order to compare his results with those of Housner's standard velocity spectra [13] (which he considered an accurate representation of naturally occurring earthquakes) Bycroft normalized his results to a Fourier amplitude spectrum showing agreement with that of Housner's. Figure 2.3 shows Bycroft's results and aids in the confirmation of the theory that pink noise is an accurate simulation of earthquake excitation.

2.3.3 Representation of earthquake motion

Ground measurements show that the assumption of a flat amplitude spectrum is extremely accurate in the proximity of bedrock but loses its accuracy near the surface, especially in weaker and less stiff layers [17].

An analysis of a large data base made up of naturally occurring accelerogram readings indicates that the Fourier amplitude spectrum represents, by integrating over the complete duration of each individual accelerogram separately, common characteristics:

- (1) they are all highly oscillatory in a random fashion;
- (2) representations of these oscillatory functions in the frequency domain contain peak values at ground motion frequencies usually in the range of zero to ten hertz; and

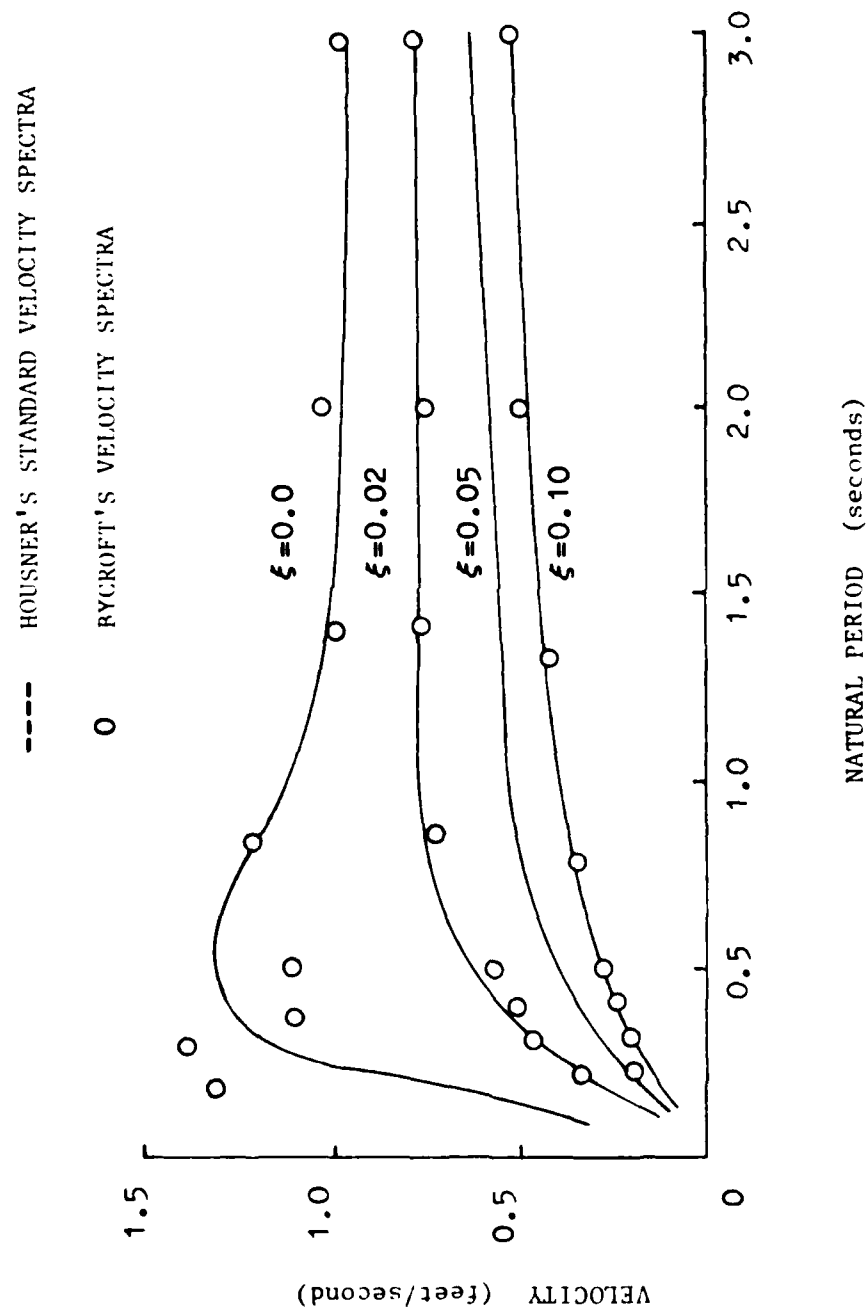


FIGURE 2.3 EARTHQUAKE RESPONSE SPECTRUM (AFTER HOUSNER, 1964)

(3) these Fourier amplitude spectra decay rapidly with increasing frequencies [27]. A typical Fourier amplitude spectrum is shown in Figure 2.4 for the El Centro earthquake of 1940.

In consideration of the aforementioned discussion, pink noise can be justified as an accurate laboratory simulation of strong earthquake induced ground accelerations in liquefaction studies because:

(1) A bandpass filter can be constructed in such a way as to include only those frequencies which are dominant in naturally occurring earthquakes. A standard earthquake can then be defined which can be used in all future seismic studies.

(2) Because of their high degree of randomness, past earthquakes will never be repeated exactly in nature. Two earthquakes having the same magnitude will have different effects on a particular soil sample as a result of their dissimilar time histories. Although a time history can be constructed to represent a typical or design earthquake, the simulated time history is only representative of an earthquake having a specific energy content at a particular point in time. Whereas pink noise is repeatable in the temporal and frequency domains, as well as, energy content. Also, the energy content of pink noise excitation is not a function of the temporal domain. Therefore, the effects of pink noise loading on different soil samples can be

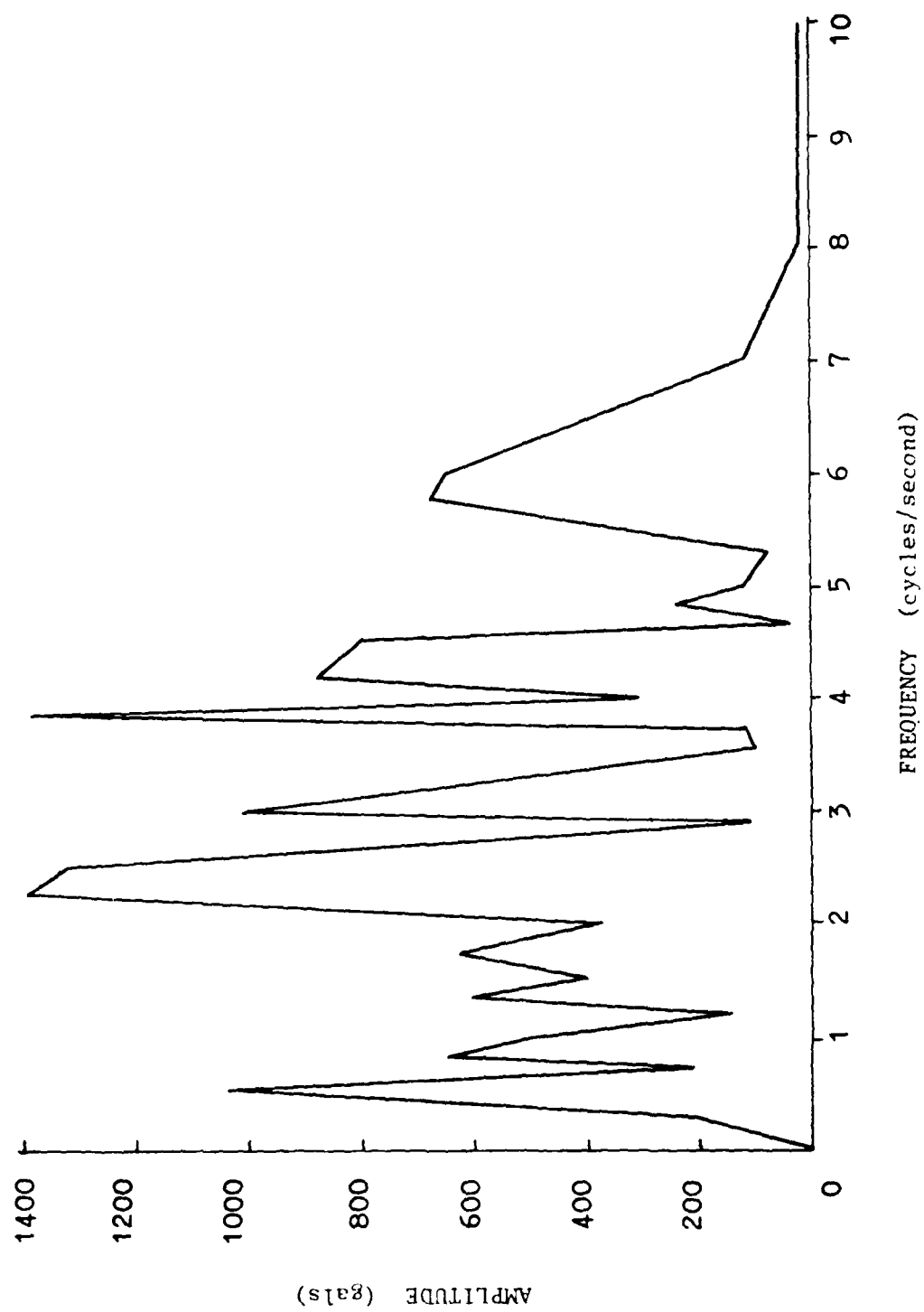


FIGURE 2.4 FOURIER AMPLITUDE SPECTRUM FOR THE 1940 EL CENTRO EARTHQUAKE (AFTER PENZIEN)

accurately analyzed as representative of all earthquake loadings.

(3) Laboratory qualification testing has been accomplished by Bycroft [3] and illustrates, through the comparison of velocity spectra, a good statistical fit with average earthquake spectra.

(4) If the laboratory soil sample can be constructed to represent an in-situ sample in the proximity of bedrock, the assumption of a flat frequency spectrum is reasonable.

(5) Both pink noise and naturally occurring earthquakes are gaussian random processes in the temporal domain.

2.4 Equivalent uniform cycles

While the time history of stresses applied to a sample in-situ during an earthquake is very irregular, the vast majority of laboratory liquefaction tests has utilized uniform or harmonic cyclic loading. Methods for converting irregular loading to an equivalent number of uniform cycles by appropriate weighting of the different stress amplitudes have been proposed [2,11,12,19,30,33]. The cumulative damage method and the equivalent uniform cycle method are the two currently most used for this conversion.

For most earthquake ground motions, the maximum pore water pressure increase occurs at the time when the largest peak ground acceleration occurs. Annaki [2] states this is especially critical in sands during the extension portion

of loading in cyclic triaxial testing. Hence only the time history of loading to that moment was considered in his studies when evaluating the equivalent number of uniform cycles. However, this ceases to be acceptable when there are subsequent peaks of acceleration almost as great as the largest peak ground acceleration.

Annaki and Lee [2] present a simple method to convert random or irregular excitations into a uniform cyclic pattern. They state the premise of their model is the assumption that the energy applied during any stress cycle has an accumulative damaging effect on the saturated sand sample. Also, assuming material linearity, this effect is independent of where in the time history a particular stress pulse is applied. The basis of their comparison model is expressed in terms of the damage or strength deterioration produced by the continued cyclic loading. Their procedure begins with the selection of an arbitrary "average" uniform cyclic stress level, S_e , to which all irregular stresses are then to be compared (see Figure 2.5). S_e is then defined as a percentage of the maximum cyclic stress (S_{max}) in the random time history: $S_e = R * S_{max}$; where R is dimensionless and was empirically derived to be between 0.65 and 0.85. However no means for identifying a specific value for R was presented. S_e can then be found on a plot of stress versus cycles to failure ($S-N$) for a uniform stress history. Next, the

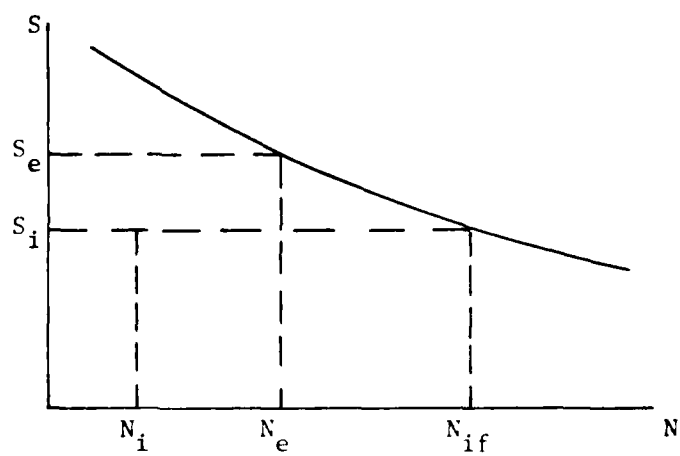
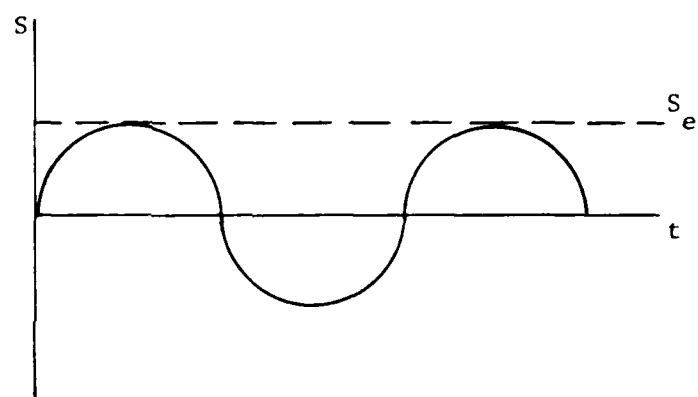
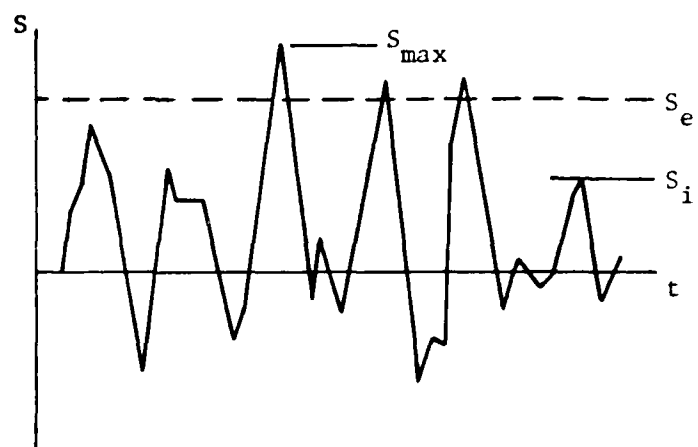


FIGURE 2.5 EQUIVALENT CYCLE CONCEPTS (AFTER ANNAKI AND LEE)

number of uniform cycles, N_e , of stress level S_e required to cause failure is found from the S-N graph. Lastly, picking an arbitrary stress level, S_i , from the random stress history and finding this value on the uniform S-N graph and its corresponding value of cycles to failure, N_{if} , can be found. N_i is the number of cycles occurring in the random time history of stress level S_i . Assuming linearity, this leads to a formulation for N_{eq} , the number of uniform stress cycles of level S_e which have a damaging effect on the soil sample equivalent to the entire random time history considered [2]:

$$N_{eq} = N_e \sum \frac{N_i}{N_{if}} \quad (2.1)$$

The limitations of this model lie in the fact constants and values must be selected (e.g. S_e , R , S_i) with no consideration of how often and when peak (or near peak) accelerations occur in the time history (which has been shown to be important by Martin et al [21]).

Halder and Tang [11,12] present a more speculative method to represent random loadings by an equivalent number of uniform cycles. They state that a reasonable intensity of 75 percent of the maximum shear stress in a random time history is equivalent to a certain constant level of a cyclicly loaded soil sample. This constant uniform time history is defined as the shear stress needed to cause failure of a laboratory specimen in one cycle of stress.

This value was empirically derived based on a statistical study which showed 75 percent to have a minimum effect on the value of equivalent cycles versus the magnitude of earthquake as compared to other values tested.

Seed and Idriss [30] have also presented a method with which to calculate an equivalent number of uniform shear stress cycles from a random stress time history. Their method entails counting the number of major stress peaks occurring within the first 15 seconds of ground motion. Additionally, the cumulative effects of smaller stress cycles occurring during this time period are equated to a number of major stress peaks regardless of when they occur. These two quantities of major stress peaks are summed and their average magnitude is determined. Therefore, by looking at any actual stress-time record during the first 15 seconds of shaking, an equivalent number of uniform stress cycles can be found for a constant magnitude.

Using the time histories from the 1964 Niigata earthquake, Seed and Idriss estimated that at all depths of the sand strata they examined, the equivalent number of stress cycles, N , equalled 10, and the magnitude of the equivalent uniform cyclic shear stress developed, τ_{dn} , increased in magnitude with increasing depth. Seed and Idriss found that the cyclic stress, τ_{10} , required to cause

liquefaction in 10 cycles could be given by:

$$\tau_{t_{10}} = \frac{C_o * Dr}{200} \text{ psf} \quad (2 . 2)$$

where Dr is relative density.

Results presented by Seed and Idriss show this equation to be in good agreement with experimental liquefaction results using uniform stress cycles in the stratum where liquefaction occurred after 10 seconds of ground motion. However, their procedure has limited application for samples whose time to liquefaction is greater than 10 seconds as may be the case for denser samples both in-situ and in the laboratory. Also, subsequent tests by Ishihara and Yasuda [15] show that the inclusion of smaller stress cycles after the onset of liquefaction appear to have no effect on the increase of pore water pressure, therefore should not be used in the calculation of the number of major stress peaks. On the other hand, results from tests conducted by Shen et al [32] point to the fact that smaller relative stress cycles occurring before and after the onset of liquefaction should not be discounted for the reasons addressed in the next section.

2.5 Liquefaction testing under irregular loadings

The predominant apparatus used in previous laboratory studies of liquefaction has been the cyclic triaxial device. Initial stresses on an element of soil tested in

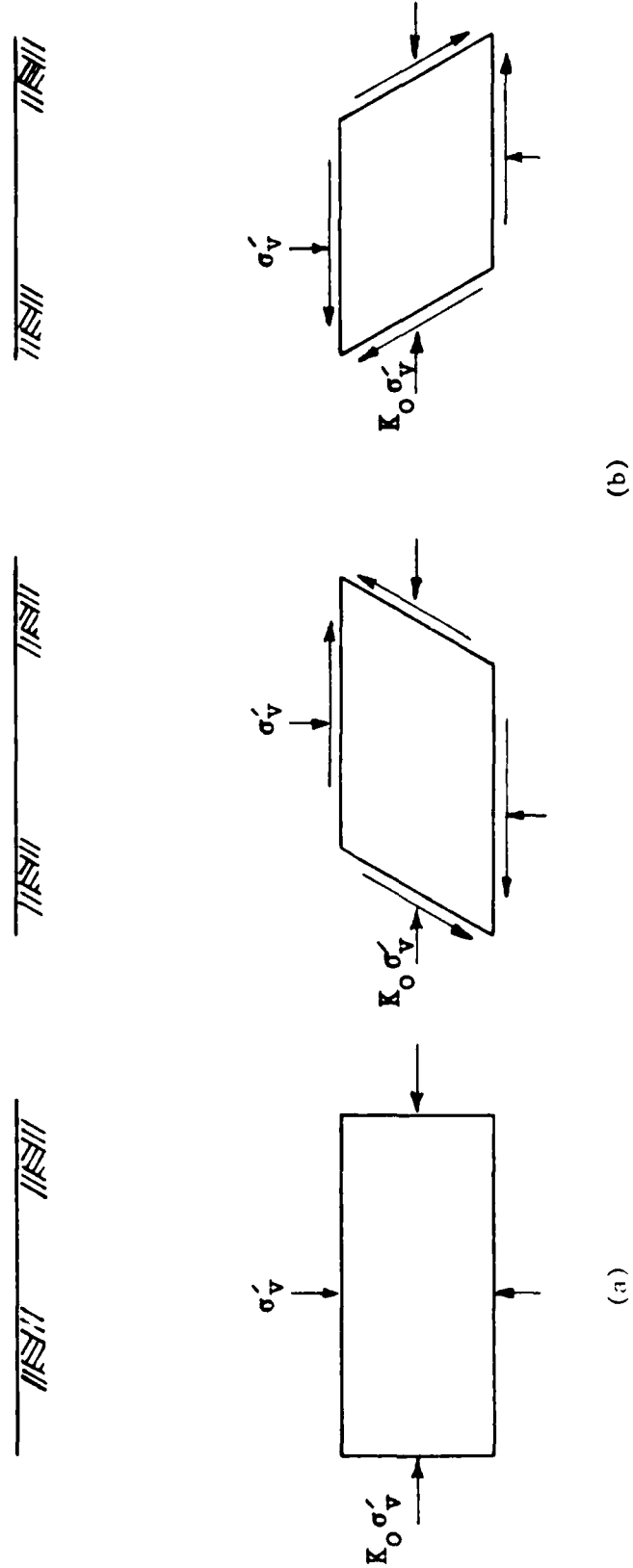


FIGURE 2.6 CYCLIC SHEAR STRESSES ON A SOIL ELEMENT DURING EARTHQUAKE EXCITATION

the cyclic triaxial device are shown in Figure 2.6(a). When loaded with a uniform cyclic deviator stress under undrained conditions, induced stresses on a 45 degree plane through the soil sample are shown in Figure 2.6(b). Numerous test results have been presented in the literature. Typically these results exhibited an increase in residual pore water pressure at the end of each applied stress cycle. The rate of generation of pore water pressure was seen to accelerate as liquefaction approached, at which point in time the strain amplitude also rapidly increased. On the other hand, documentation on the nature of pore water pressure increases due to irregular cyclic deviator stresses simulating actual earthquake loadings on an in-situ or a laboratory sample has been relatively scarce.

The irregular loading patterns investigators [6,15,16,18,20,21,25,32,34] have utilized in past cyclic triaxial liquefaction studies can be classified into one of the following two categories:

- (1) A nonuniform amplitude transient sinusoidal wave having a maximum shear stress loading at the beginning, middle, or end of the time history, or a combination thereof. Maximum positive and negative shear stresses are not necessarily equal.

- (2) Earthquake time histories corresponding to random loading where no restrictions on amplitude or frequency exist. The most common method has been to use an actual

record of an earthquake with the 1964 Niigata earthquake being the most widely used.

Martin et al [20] and Shibata et al [34] used the first category of irregular loading to illustrate the effect the relative position of the maximum stress(es) has on pore water pressure increase. Using various patterns of sinusoidal shear stress loading they were able to get distinct patterns of pore water pressure increase as shown in Figure 2.7. The significance of the relative position in the time history where the maximum stress amplitude occurs is very apparent. Time history A [20] has a large stress at the beginning of the record resulting in a rapid increase in pore water pressure. The rate of pore water pressure generation decreases as the applied shear stress level decreases. The opposite effect is illustrated in time history B [20] where a gradual increase in cyclic shear stress throughout the 20 cycles of applied load generates a gradual increase in pore water pressure. Time history C [20] has the same peak cyclic shear stresses as the first two time histories but they are randomly distributed. Only the peak cyclic shear stresses appear responsible for a sudden increase in pore water pressure while the smaller cyclic shear stresses induced only very gradual increases.

Shen et al [32] also conducted irregular loaded cyclic triaxial tests on sand samples to determine the affect of the location in the time history of the maximum shear

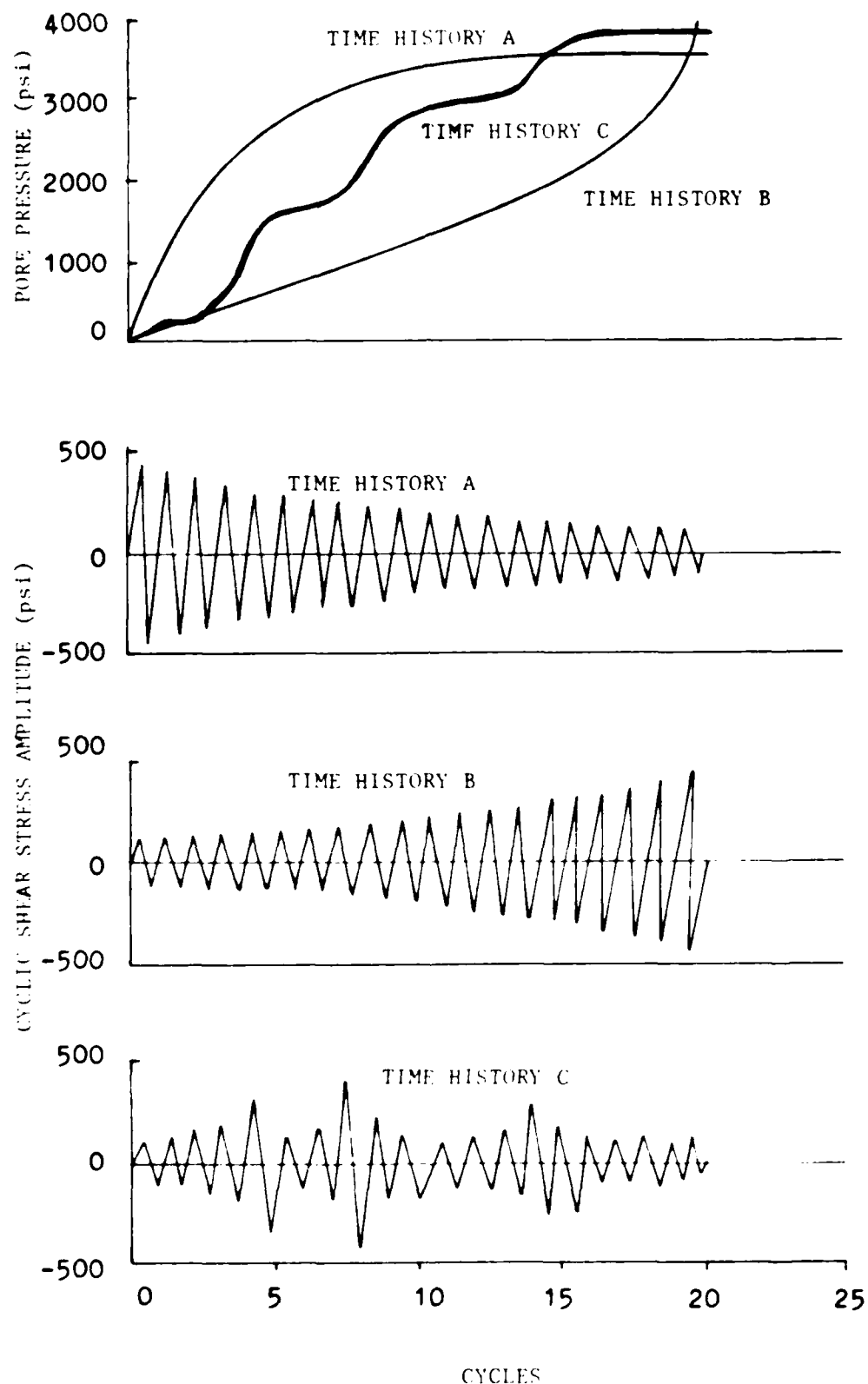


FIGURE 2.7 EFFECT OF NONUNIFORM LOADING ON PORE
WATER PRESSURE INCREASE (AFTER MARTIN ET AL, 1975)

stress. They used four combinations of a single magnitude 6.5 earthquake pattern (i.e. with the sign of the maximum shear stress reversed and a shift of the maximum shear stress to the middle of the time history). An example of the time history and test results for patterns 1 and 3 appear in Figure 2.8 where pattern 1 is the original and pattern 3 is a shift of the maximum shear stress to the center of the time history.

To correct for the problem of load attenuation as the sample deformations became large, Shen et al reduced the original frequency content of the pattern by a factor of 5. This meant the loads were applied in a frequency range of 0.1 to 0.3 hertz. They justified this reduction citing studies by Lee and Fitton [18], Silver et al [36], and Wong et al [39] which determined that for sinusoidal loadings triaxial test results were not adversely effected when the loading remained in the frequency range of 0.17 to 4.0 hertz.

The following observations can be made on their test results:

- (1) After the largest shear stress peak and corresponding increase in pore water pressure have occurred, additional smaller shear stress applications produced disproportionately large effects.

- (2) Regardless of when they occurred in the time history, the largest shear stress peaks induced the largest

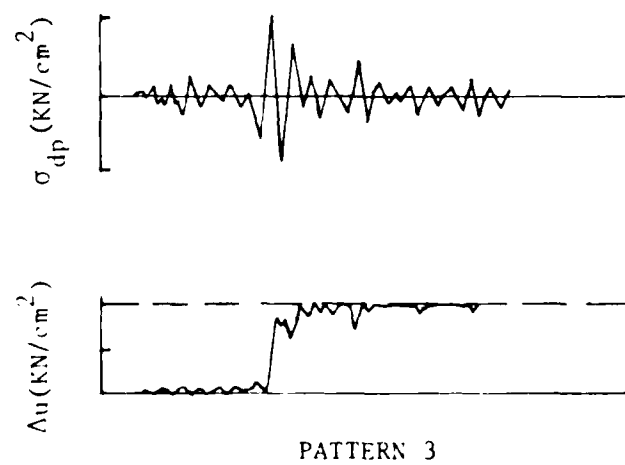
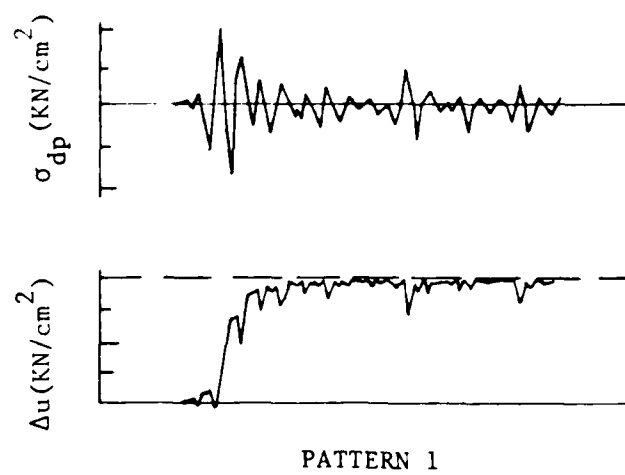


FIGURE 2.8 IRREGULAR CYCLIC LOAD TEST RECORDS (AFTER SHEN ET AL.)

increases in pore water pressure.

(3) Significant axial strain was not present before the application of the largest shear stress peak.

Figure 2.9 [32] is an illustration of the effect of the relative timing of the peak deviator stress on the pore water pressure increase. Pattern 1 was characterized as having the peak deviator stress at the beginning of the time history whereas pattern 3 had its peak deviator stress in the middle. All other test conditions were kept constant (e.g. relative density (D_r), confining pressure (σ'_{3c}), and the value of the peak deviator stress (σ'_{dp})_{max}). It is apparent that the first loading pattern had a more significant effect on the pore water pressure change than did the third in both magnitude and time to maximum change. The larger peaks at the beginning of the time history caused approximately twice the pore water pressure change in half the time. Since the pore water pressure increase is about the same for both samples prior to the application of the peak shear stress, the cumulative energy theory would predict the same eventual generation of pore water pressures at the conclusion of the time history for both patterns. However, since only half the pore water pressure change was induced by pattern 3, it appears that the smaller shear stress peaks preceding the maximum deviator stress provided a strengthening effect upon the sample. This is similiar to the effect of past strain upon

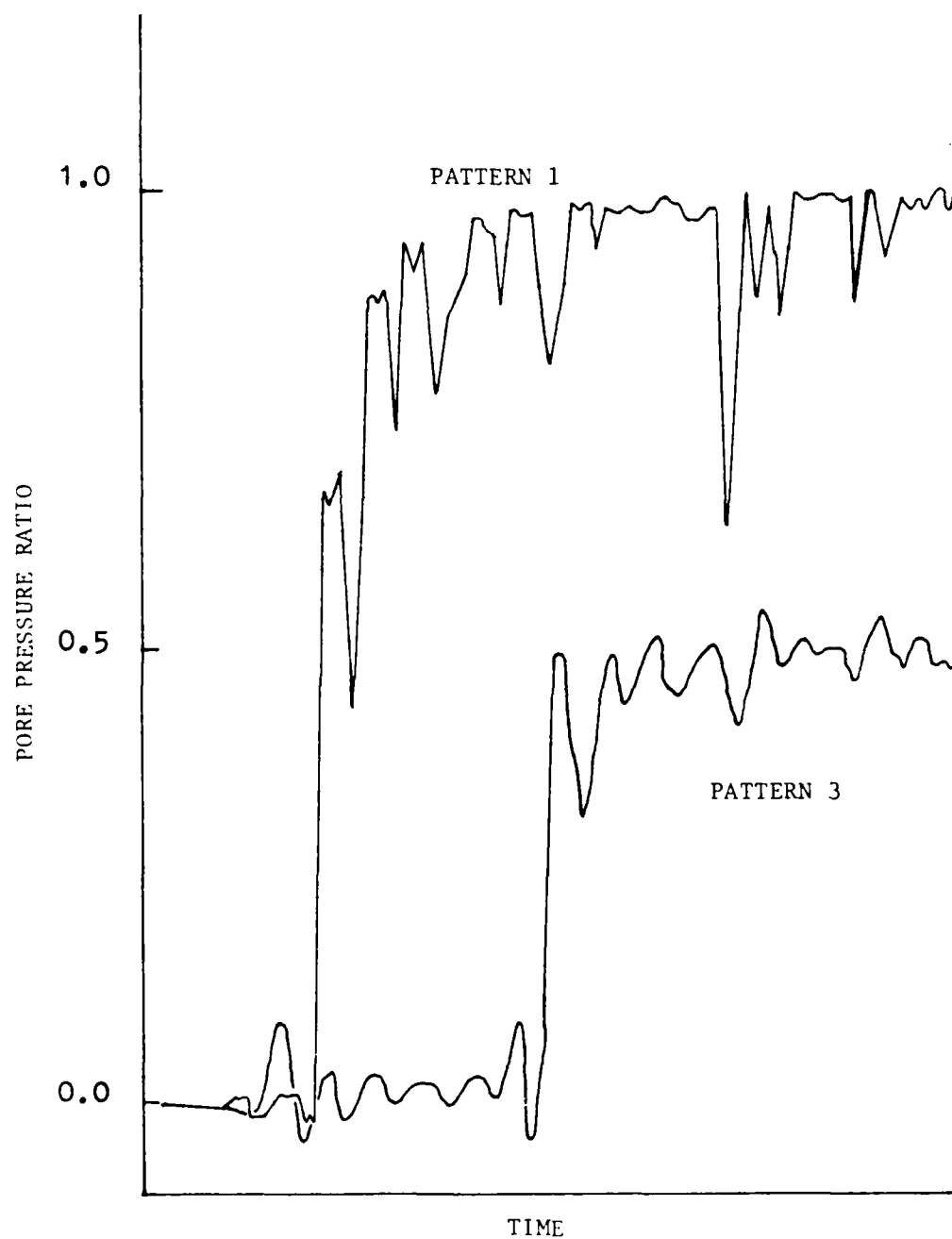


FIGURE 2.9 EFFECT OF PEAK SHEAR STRESS TIMING ON
PORE WATER PRESSURE INCREASE (AFTER SHEN ET AL.)

liquefaction potential as investigated by Seed et al [31] using a shaking table. Shen et al, however, found this effect to be insignificant with loose sand samples.

Using the two component acceleration record taken at the time of the 1964 Niigata earthquake, Ishihara and Yasuda [15,16] compared their experimental results with those obtained by applying a uniform time history load to the same soil samples in order to discover what correlations may exist in the generation of pore water pressure.

A typical test result from their study is shown in Figure 2.10. The investigators ran the same test twice using the same earthquake loading to illustrate the large difference in the generation of pore water pressure which occurs when a test is conducted employing the maximum stress on the compression side of the triaxial piston stroke (CM) versus the extension side (EM). It is notable that pore water pressure increase is abrupt at the instant the maximum deviator stress (σ_{max}) experiences a zero-crossing (returns to a zero stress applied state) from the extension stroke. Conversely, when the maximum stress occurs on the compression stroke, liquefaction occurs immediately after the second greatest stress is released from the extension side.

The values of pore water pressure, u , collected from each test performed by the investigators are shown in

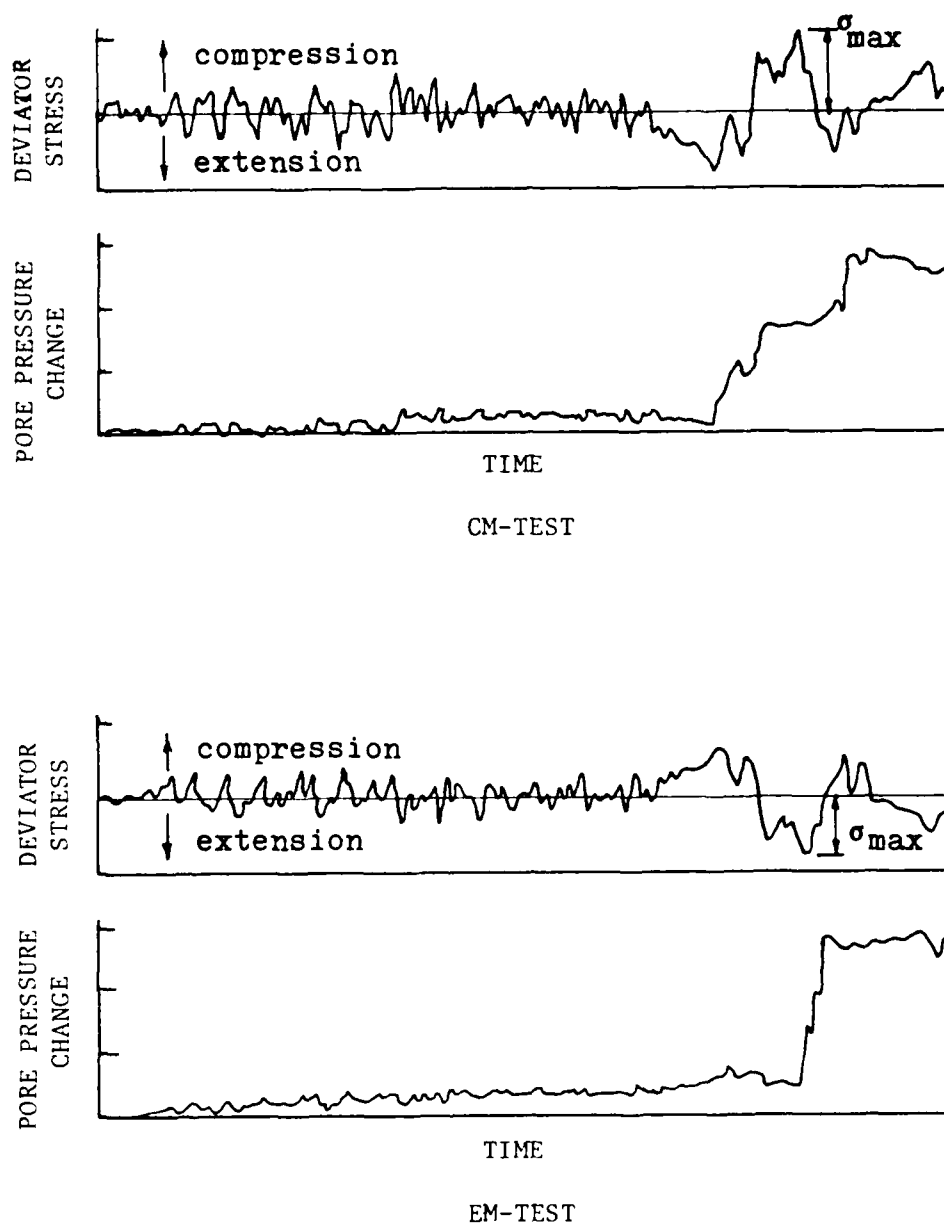


FIGURE 2.10 LABORATORY SIMULATION OF LIQUEFACTION DURING THE NIIGATA EARTHQUAKE (AFTER ISHIHARA AND YASUDA, 1972)

Figure 2.11 [15] versus the maximum axial stress, σ_{max} , with these values normalized to the confining pressure, σ_c . It appears evident that once the pore water pressure reached 50 percent, even a small amount of increase in the stress ratio was sufficient to induce liquefaction. The stress ratio corresponding to the pore water pressure ratio of 1.0 is then denoted as the minimum stress ratio at which liquefaction can occur under a given pattern of load variation. Figure 2.11 also shows again the greater susceptibility to liquefaction of the EM tests, a phenomenon the investigators were unable to explain but may highlight one limitation of the cyclic triaxial cell in dynamic testing, i.e. the asymmetry of the direction of stress alteration.

Ishihara and Yasuda [15,16] also conducted constant-amplitude cyclic tests for comparison purposes utilizing a one hertz uniform load. The magnitude of the applied deviator stress required for liquefaction in a given number of cycles was found and plotted as shown in Figure 2.12 [15]. This figure is useful in considering the relative effect of the wave shape and where their peak shear stresses occur on the liquefaction potential of saturated sands. It also sets forth a starting point from which to compare uniform and random time histories.

The present study is designed to further the investigation of the effect of random loading on the

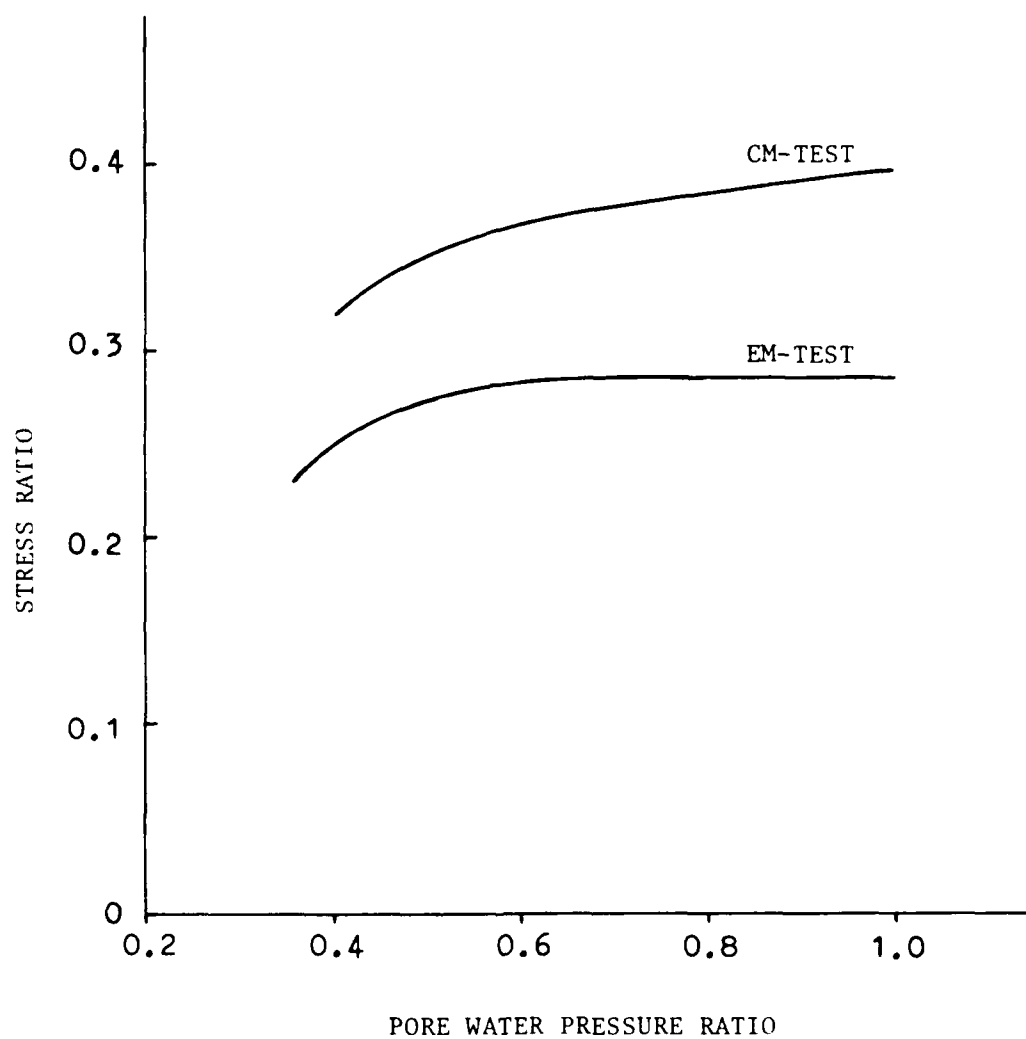


FIGURE 2.11 RELATION BETWEEN THE STRESS RATIOS AND PORE WATER PRESSURES USING THE NIIGATA EARTHQUAKE ACCELERATION RECORD (AFTER ISHIHARA AND YASUDA, 1972)

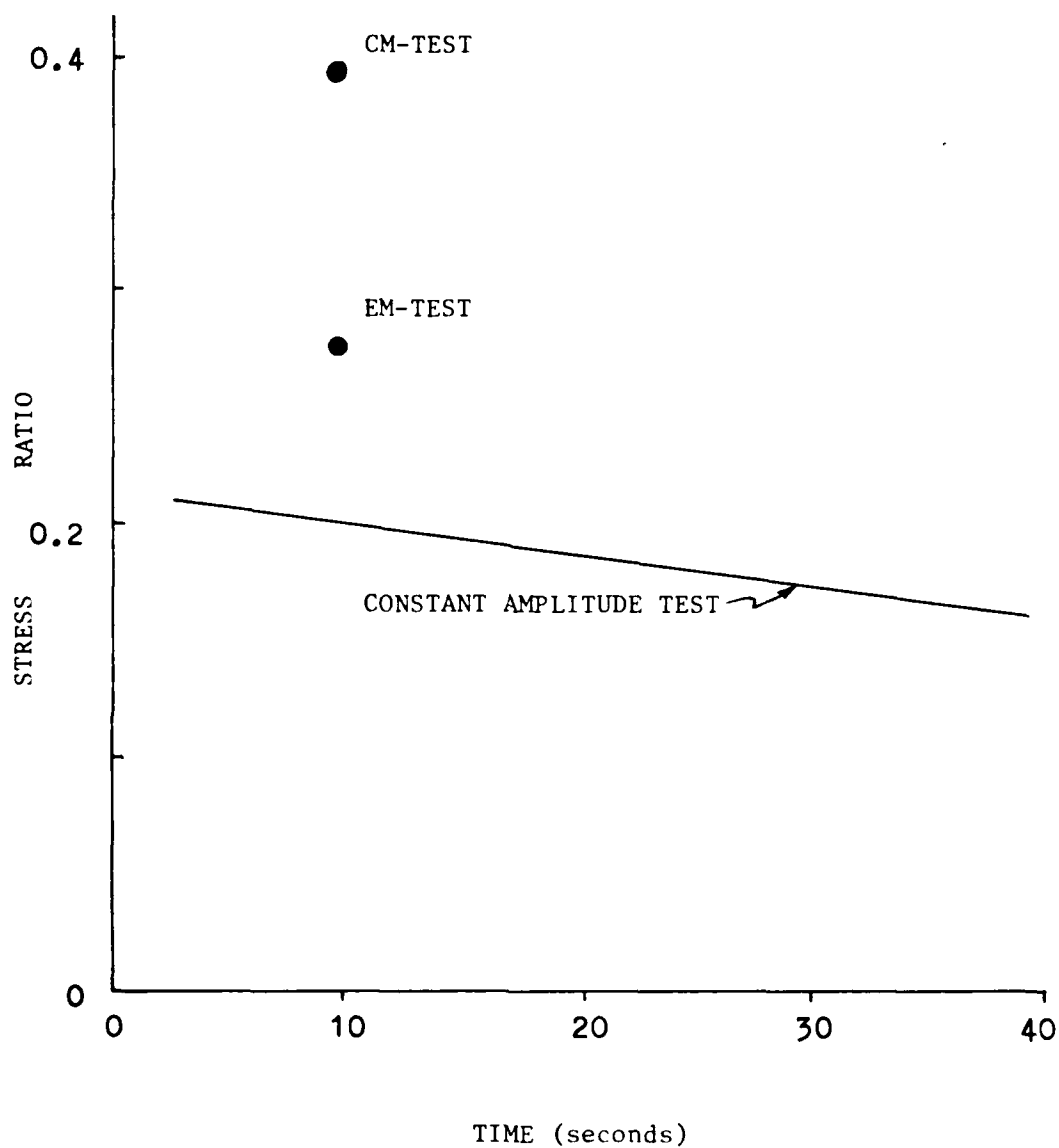


FIGURE 2.12 RELATION BETWEEN STRESS RATIOS AND TIME TO INITIAL LIQUEFACTION (AFTER ISHIHARA AND YASUDA, 1972)

liquefaction potential of cohesionless soils. Random loading functions have been proposed by previous researchers to be a better representation of strong earthquake motion than uniform loads. Past research on the effects of random loading has primarily utilized small scale tests. Because numerous uniformly loaded tests have also been conducted with small scale apparatus, comparison of the two loading types has been published. However, large scale testing apparatus have been proposed by recent investigators as more representative of in-situ conditions during earthquakes [1,9,22]. These investigators have subsequently proposed values of liquefaction potential for uniformly loaded sand samples. The purpose of the study described in this thesis is to combine the ability of random loading and large scale testing apparatus to represent in-situ conditions of a sand deposit subjected to an earthquake loading. The results of this study can then be compared to either loading pattern on either testing apparatus.

CHAPTER III

INSTRUMENTATION

3.1 Introduction

In an effort to realistically reproduce in-situ conditions under which earthquakes will induce liquefaction, large-scale tests were conducted in the Soil Dynamics laboratory at The Ohio State University. All the salient aspects of the shaking table and sample test chamber used during these tests have been described in great detail by Mason [22] and Amato [1]. Collection of the large-scale laboratory results was detailed by Amato [1] with modifications described in this chapter.

3.2 Shaking table

The first two stages of the experimental testing program utilized a ten hertz periodic acceleration input signal generated by a Materials Test System (MTS) series 810 testing system function generator and supplied to its dynamic response controller. The dynamic response controller then conditioned the acceleration program signal and transmitted the signal to an electro-hydraulic servovalve connected to an actuator which was in turn

attached to the shaking table. An accelerometer mounted on the shaking table provided a feedback signal to the dynamic response controller. Comparing the transmitted and feedback signals enabled the dynamic response controller to compensate for any differences between the two signals. The system is illustrated in Figure 3.1. The dynamic response controller provided the major electronic control, signal conditioning and readout capabilities for the closed-loop testing system. The power supply for hydraulic servovalve was capable of generating a maximum table acceleration of 3 g's (3000 gals) and the actuator was capable of a maximum stroke of ± 3 inches (7.62 cms).

An external program source was utilized for those tests conducted with a band-limited white noise signal (stage three). The program source used was an IBM/PC XT microcomputer with a LabMaster A/D - D/A expansion board, which converted a stored digital acceleration time history into a 12-bit analog ± 10 volt excitation simulating pink noise.

3.3 Sample Test Chamber

The location of the instrumentation in the sample test chamber, the rubber membrane and pressurization system utilized in all three stages of experimental testing were identical to those discussed in detail by Amato [1] and shown in Figure 3.2. The sample test chamber allowed for a

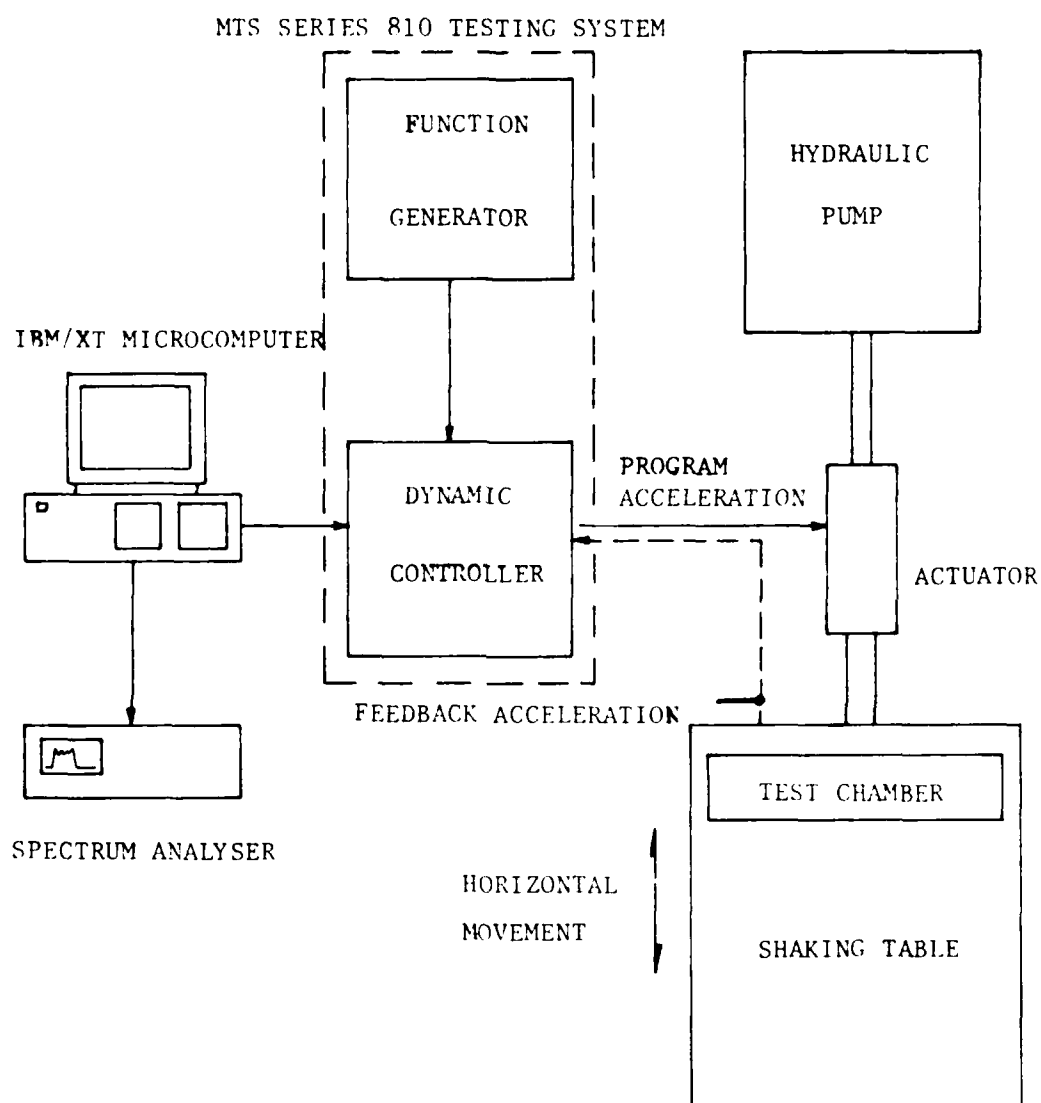


FIGURE 3.1 LARGE SCALE LABORATORY TESTING SYSTEM

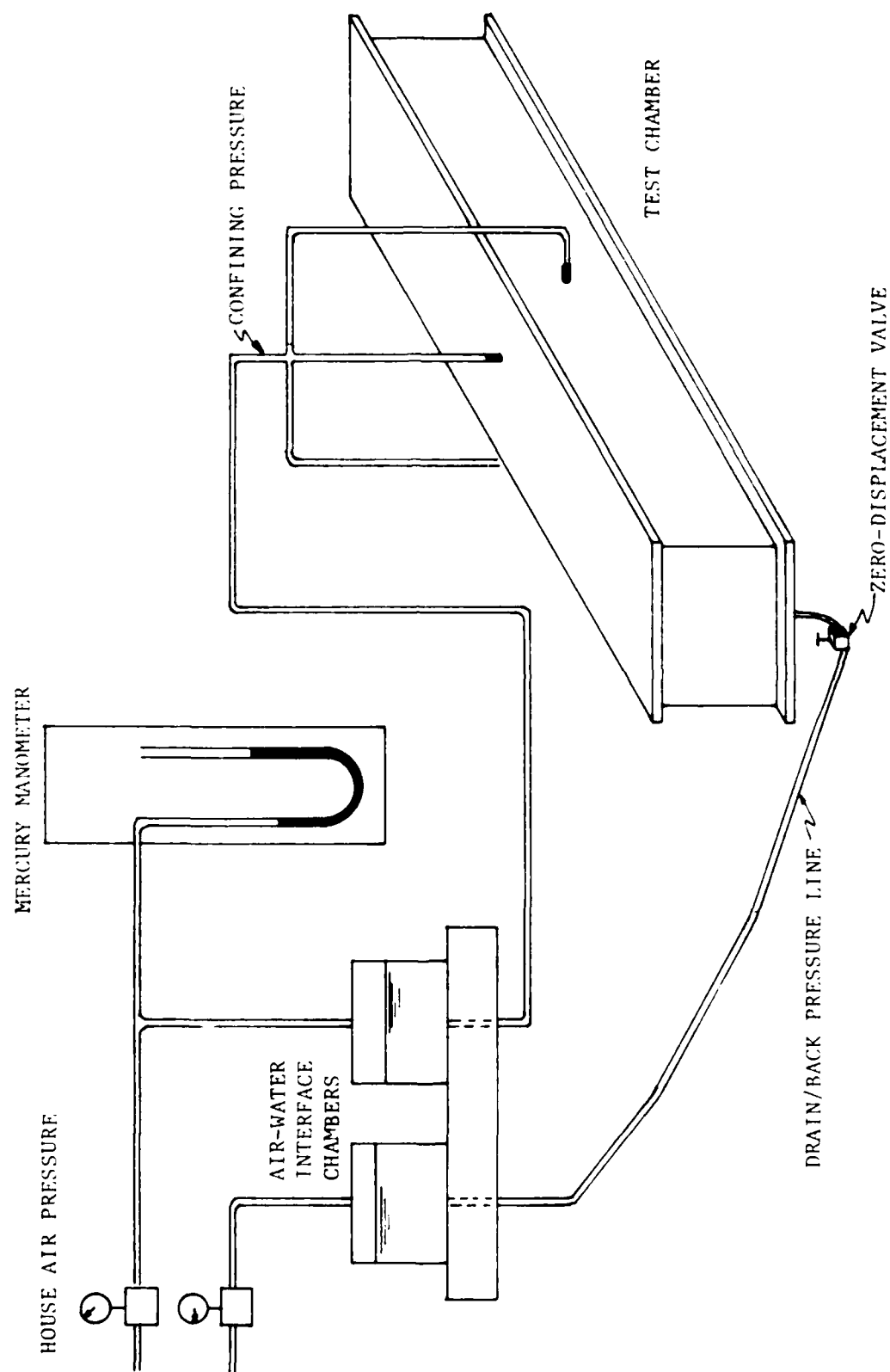


FIGURE 3.2 SAMPLE TEST CHAMBER

maximum soil sample of 48 inches (121.92 cms) long by 6 inches (15.24 cms) wide by 6 inches (15.24 cms) high, or a length-to-height ratio of 8.0:1. The sample test chamber and soil sample construction enabled " free-field " and plane strain conditions to exist in the center and the boundary of the soil sample respectively.

Only a minor modification was made to the aforementioned sample test chamber since the work completed by Amato [1]. This was the addition of a zero displacement shut-off valve (shown in Figure 3.2) located on the drainage/back pressure line as close as possible to the sample to ensure undrained conditions during pressurization and testing. This also allowed for the calculation of the amount of static sample consolidation before testing without the removal of the drainage/ back pressure line.

3.4 Instrumentation

The same National Semiconductor Corporation LX0503A type pressure transducers and Entran Devices Incorporation model EGAL3-125-5D $\pm 5g$ accelerometers were utilized as in previous liquefaction experiments at The Ohio State University with one slight modification of the pore water pressure instrumentation. A section of 200-gauge mesh was cut and formed in the shape of a cylinder to fit snugly around the tip of the hypodermic needle to prevent sand grains from plugging the needle's orifice during testing as

shown in Figure 3.3. Calibration tests showed no effect on the measurement of pore water pressure caused by the addition of these caps.

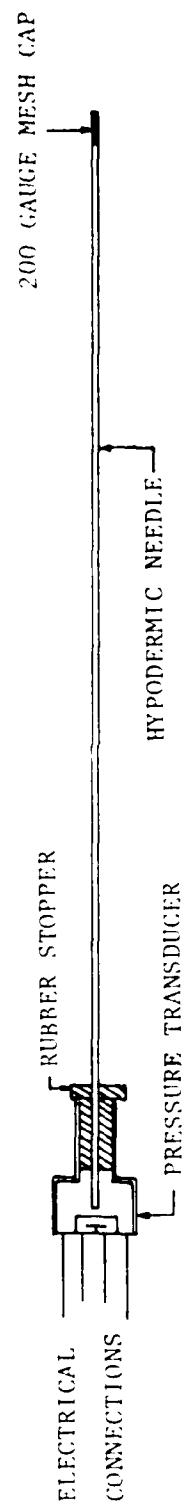


FIGURE 3.3 PORE WATER PRESSURE MEASUREMENT SYSTEM

CHAPTER IV

TESTING PROCEDURE

4.1 Introduction

The liquefaction testing procedure followed during each of the three testing stages was essentially the same as that described by Amato [1]. This was accomplished to verify the test results by Mason [22] and Amato [1], and thereby expanding the data base used for comparison with results from tests by DeAlba et al [9] and the pink noise excitation testing described in Chapter V. One modification to Amato's testing procedure was made during the second testing stage and a second was made during the third testing stage; both are described in this chapter.

4.2 Sand Sample Preparation

In order to provide a basis for comparison between large-scale liquefaction tests conducted at The Ohio State University and those reported by De Alba et al [9], the second stage testing procedure was modified from that described by Amato [1] by reducing the height of sand sample and replacing an equivalent height reaction mass. The reaction mass consisted of a ballast of steel grit and

had a flexible base to provide uniform seating on the sand sample but a rigid lateral resistance. After the sand sample was built to the desired height it was leveled with a device that was described by Amato [33] but modified to construct 4 inch (10.08 cms), 5 inch (12.60 cms) or 5 1/2 inch (13.87 cms) uniform high samples. After placement of an accelerometer on top of the sand sample and syphoning of excess water, a rectangular rubber membrane, the same material as the bottom membrane, was placed atop the sand sample. GE Silicon Rubber Adhesive Sealant (IS 808) was used to seal the middle membrane to the bottom membrane. All air between the middle membrane and the top of the sand sample was squeezed out by placing the steel grit, making up the reaction mass, from one end of the sample to the other while unrolling the middle membrane. The steel grit was placed such that the total sand/grit height was always equal to 6 inches (15.24 cms). The variable height leveling device was adjusted to level the top of the reaction mass to ensure uniformity of the entire sand/grit sample. The top membrane was then placed in the same manner as the first testing stage to separate the vertical confining fluid and steel grit. This allowed for isotropic pressurization of the entire 6 inch (15.24 cm) sample. A typical cross-section of the reaction mass and sand sample immediately before testing is shown in Figure 4.1.

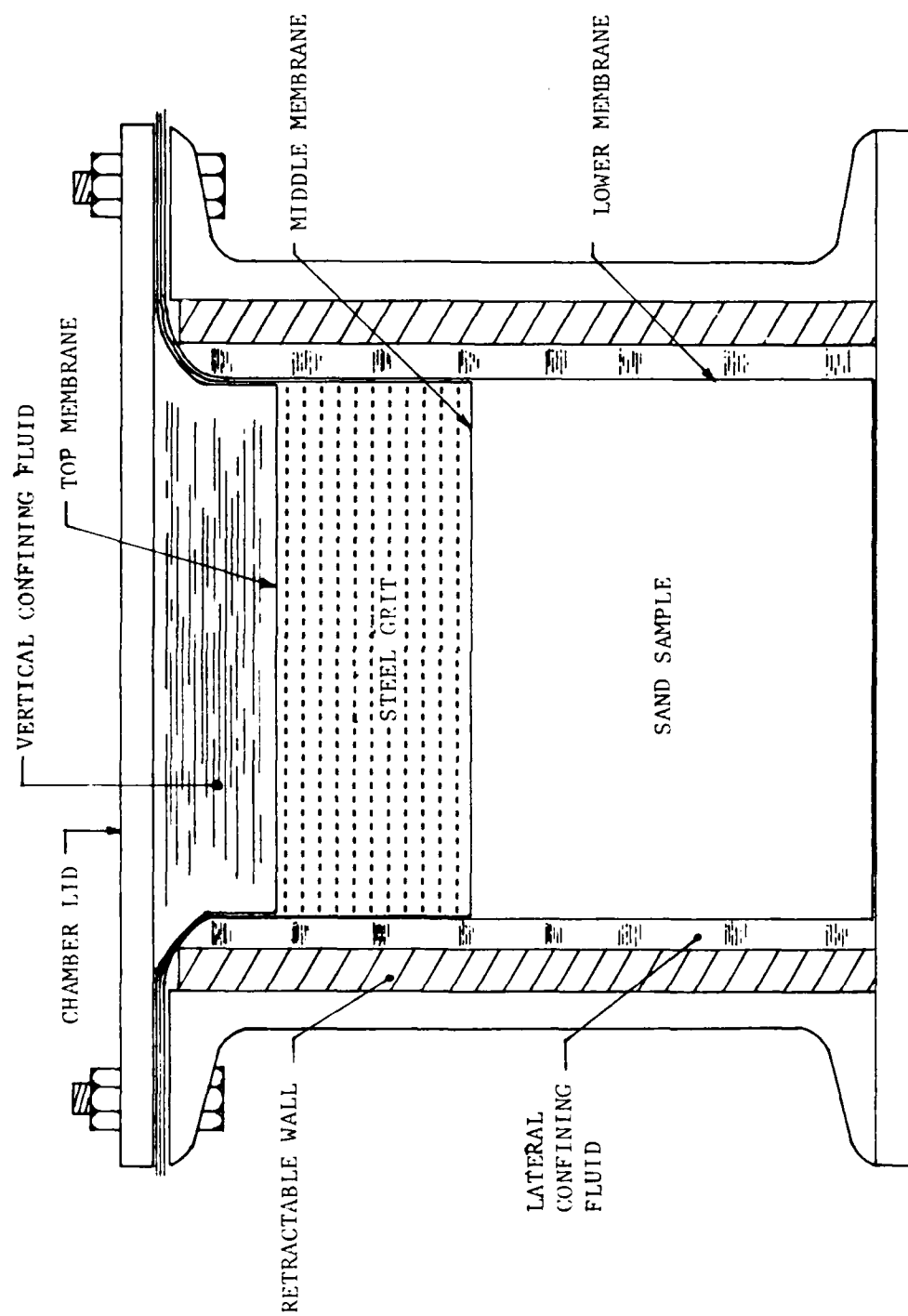


FIGURE 4.1 SECOND STAGE SAMPLE PREPARATION

4.3 Membrane Penetration

During the third testing stage, after the sample was pressurized to the test conditions and before the internal supporting walls were retracted, the test chamber was attached to a volume change measuring device as shown in Figure 4.2. With the isotropic confining pressure constant on the saturated sand sample, the back pressure valve was opened and the back pressure incrementally raised to simulate generation of an increase in pore water pressure during actual dynamic testing. Membrane penetration could be measured as movement of the membrane out from between the sand grains and recorded in the form of volume change on the manometer.

4.4 Data Collection

During each stage of the testing program, data from the accelerometers and pressure transducers were collected at a rate of one data point every 1.6×10^{-3} seconds. A detailed description of the data collection procedure is described by Wolfe et al [38]. Data collection was always begun before input accelerations were supplied to the testing system in order to collect initial conditions of acceleration and pore water pressure. During all testing stages, discrete data points were collected at a rate 64 times faster than the harmonic frequency of the first two

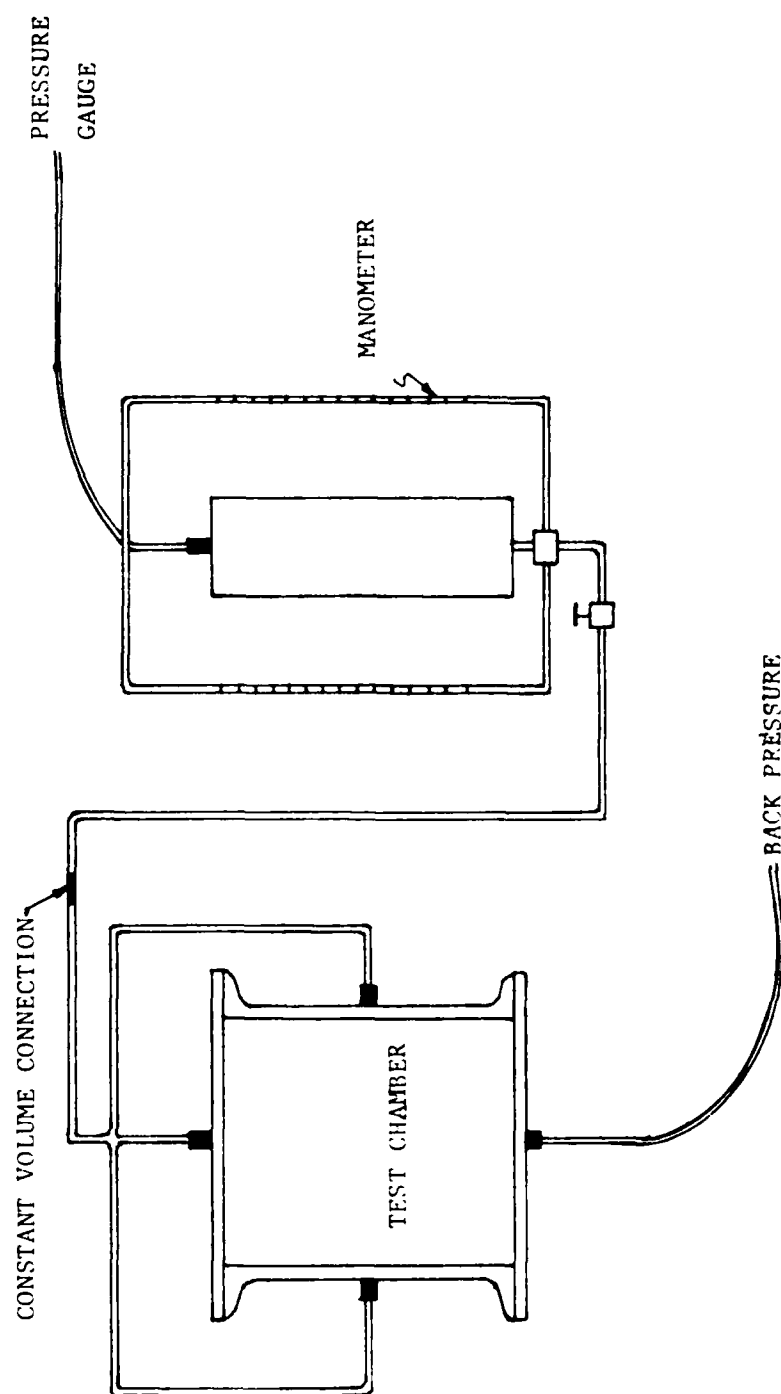


FIGURE 4.2 MEMBRANE PENETRATION TESTING

testing stages and 42 times faster than the highest dominant frequency of the third testing stage.

CHAPTER V

LIQUEFACTION TEST RESULTS

5.1 Introduction

In order to provide representative data on the behavior of in-situ soils excited by an earthquake force, large scale shaking table tests were conducted on saturated Ottawa sand. Shaking table tests were chosen because time varying shear stresses can be applied to soil samples which are large enough to not be adversely effected by implanted measuring devices. Three stages of liquefaction experiments were conducted and the results of the tests are presented in this chapter. The first stage was performed to verify results obtained by Mason [22] and Amato [1] under isotropic conditions. In verifying their results it is proposed that the testing apparatus described in Chapter III was shown to be capable of producing consistent and reproducible data on liquefaction potential. Additional isotropic testing was conducted during the second stage to investigate the effect of a heavy reaction mass on pore water pressure generation, and to provide a comparison of liquefaction potential results with those of De Alba et al

[9]. To extend the data base, a third testing stage was performed on an isotropically consolidated sand sample subjected to pink noise excitation. Specific conditions under which each stage of testing was conducted is described along with the presentation and analysis of representative results.

5.2 Sample Saturation

To ensure that each sample was fully saturated, Skempton's pore water pressure parameter (B) was determined prior to testing. According to Black and Lee [4], values of B equal to 1.0 signify full saturation of samples of low relative density. A value for B greater than 0.95 signifies an acceptable degree of saturation for sand samples having high degrees of relative density. Considering the relative densities used in this study, a B value greater than or equal to 0.98 was considered indicative of full saturation. The B value was measured by incrementally applying an isotropic confining pressure ($\Delta\sigma_c$) to the sand sample under undrained conditions. Immediately after application of the confining pressure, the induced rise in pore water pressure (Δu) was measured via pressure transducers inserted into the soil sample. The B value was then calculated as the ratio of the change in pore water pressure in the sample to the change in applied isotropic confining pressure. Care was taken to avoid

applying an effective pressure greater than the final design consolidation pressure in order to avoid overconsolidating the sample. The back pressure at test conditions was always at least 1 psi (6.89 KN/m²) to ensure the efficient operation of the pore water pressure transducers [38].

5.3 Testing Material

Uniform Ottawa sand was used in all tests conducted during each stage of the experimental program. In addition, steel grit was used in the second stage to serve as a reaction mass. The material properties of the Ottawa sand have been quantified by Wolfe et al [38] who found the minimum and maximum density to be 89.27 pcf (14.03 KN/cm³) and 101.76 pcf (15.99 KN/cm³) respectively.

The steel grit had a grain size distribution similiar to that of the Ottawa sand, see Figure 5.1, but with a specific gravity of 7.21.

5.4 Shear Stress Ratio

Following the procedure of De Alba et al [9], the results of the first two stages of testing from this study are compared with the isotropic results obtained by Mason [22], Amato [1], and De Alba et al [9]. Following the method described by De Alba et al [9], shear stresses acting on the base of the sample (τ) were calculated by

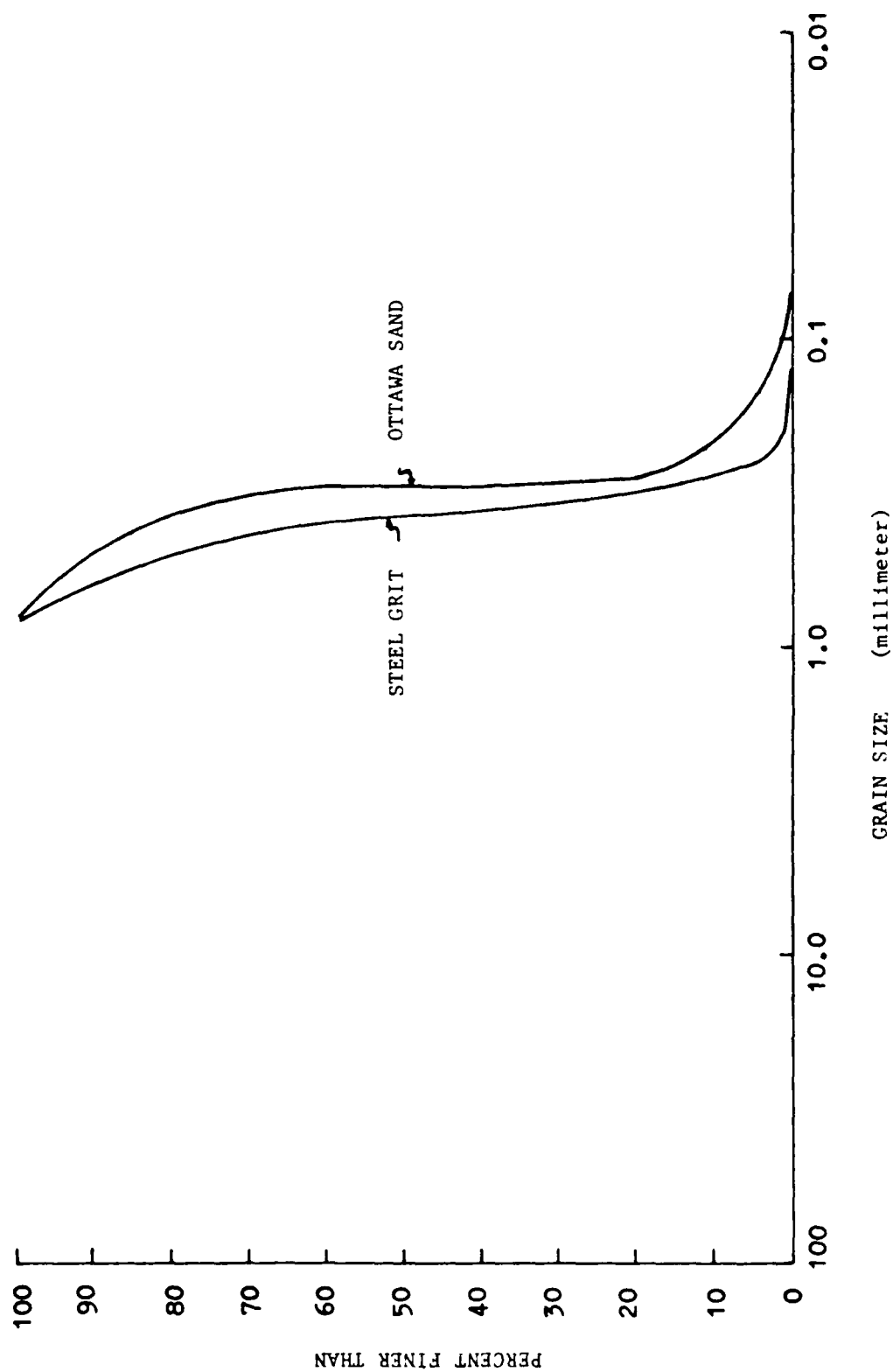


FIGURE 5.1 GRAIN SIZE DISTRIBUTION CURVE

assuming the cyclic shear stress was proportional to the sample mass and the maximum table acceleration. Sample mass was taken to be the weight per unit length of sample divided by the force of gravity (g). For stage one and stage three of this study, the weight per unit length was calculated by multiplying the saturated unit weight of the sample (γ_{sat}) by its height (h). The weight per unit length exerted on the sand sample by the reaction mass (ωb) during the second stage of this study was included in the total mass. The parameter used to characterize input motion was the maximum acceleration (A_{max}) applied to the base of the sample. The applied shear stress at the base of the sand sample was found to be:

$$\tau = (\gamma_{sat} * h + \omega b) * A_{max} / g \quad (5.1)$$

All shear stress ratios (τ / σ'_1) were calculated by dividing the applied shear stress at the base of the sample by the effective confining pressure of the sample.

5.5 First Testing Stage Results

5.5.1 Results

The results from the first testing stage of this study (Test A) are presented to demonstrate the ability of the testing apparatus and procedure to deliver consistent results. The applied conditions and results for this stage

TABLE 5.1 APPLIED ISOTROPIC TEST CONDITIONS AND RESULTS

RESEARCHER	Dr (%)	σ'_1 (psf)	τ/σ'_1	Amax (g)	N _L	B
MASON []	61.1	2.0	0.274	1.2	1530	-
	56.0	-	0.378	-	304	0.97
	53.9	-	0.666	-	85	-
AMATO []	21.0	1.7	0.48	2.0	74	0.97
	25.0	0.9	0.92	2.0	35	0.94
THIS STUDY TEST A (21 JUL 86)	29.0	0.9	0.78	2.0	41	0.98

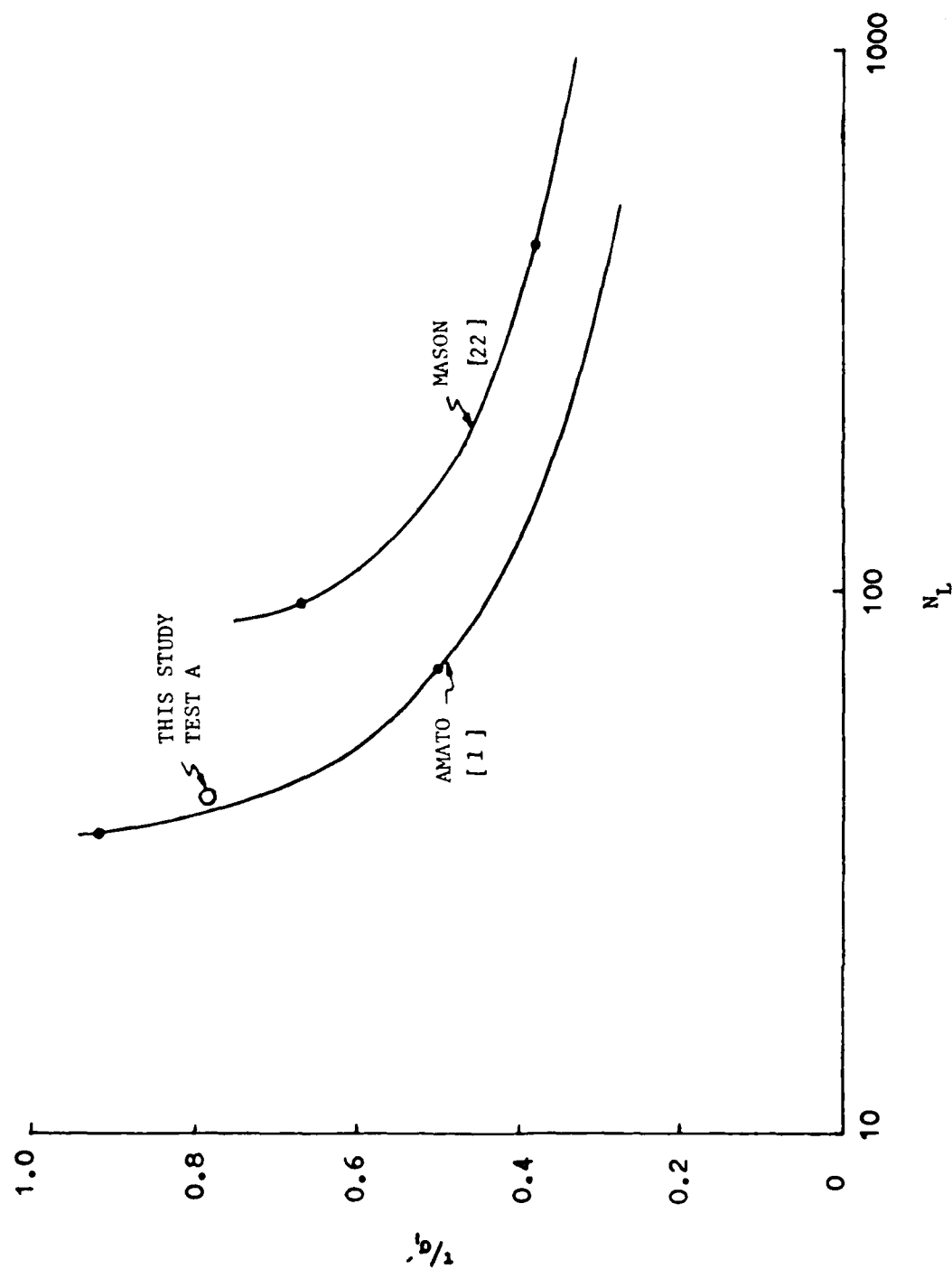


FIGURE 5.2 COMPARISON OF FIRST STAGE RESULTS WITH OTHER ISOTROPIC TESTS

pressure remained at the level of the initial effective confining pressure.

5.5.3 Table excitation

Table excitation time histories for this testing stage before, during and after initial liquefaction can be found in Appendix B. As was observed by Mason [22] and Amato [1], the 10 Hz table excitation (as shown in the appendix) did not completely reach the design acceleration until approximately two seconds had elapsed. Therefore a presentation of resistance to liquefaction strictly in terms of number of cycles to liquefaction versus peak acceleration somewhat overestimates strength and a more correct representation requires an average input to be computed for the initial excitation. Recalculating the stress ratio with this average applied input excitation according to Amato [1] resulted in an adjustment in the recorded data. The corrected plot is located adjacent to the renormalized isotropic curve presented by Amato [1] as shown in Figure 5.3.

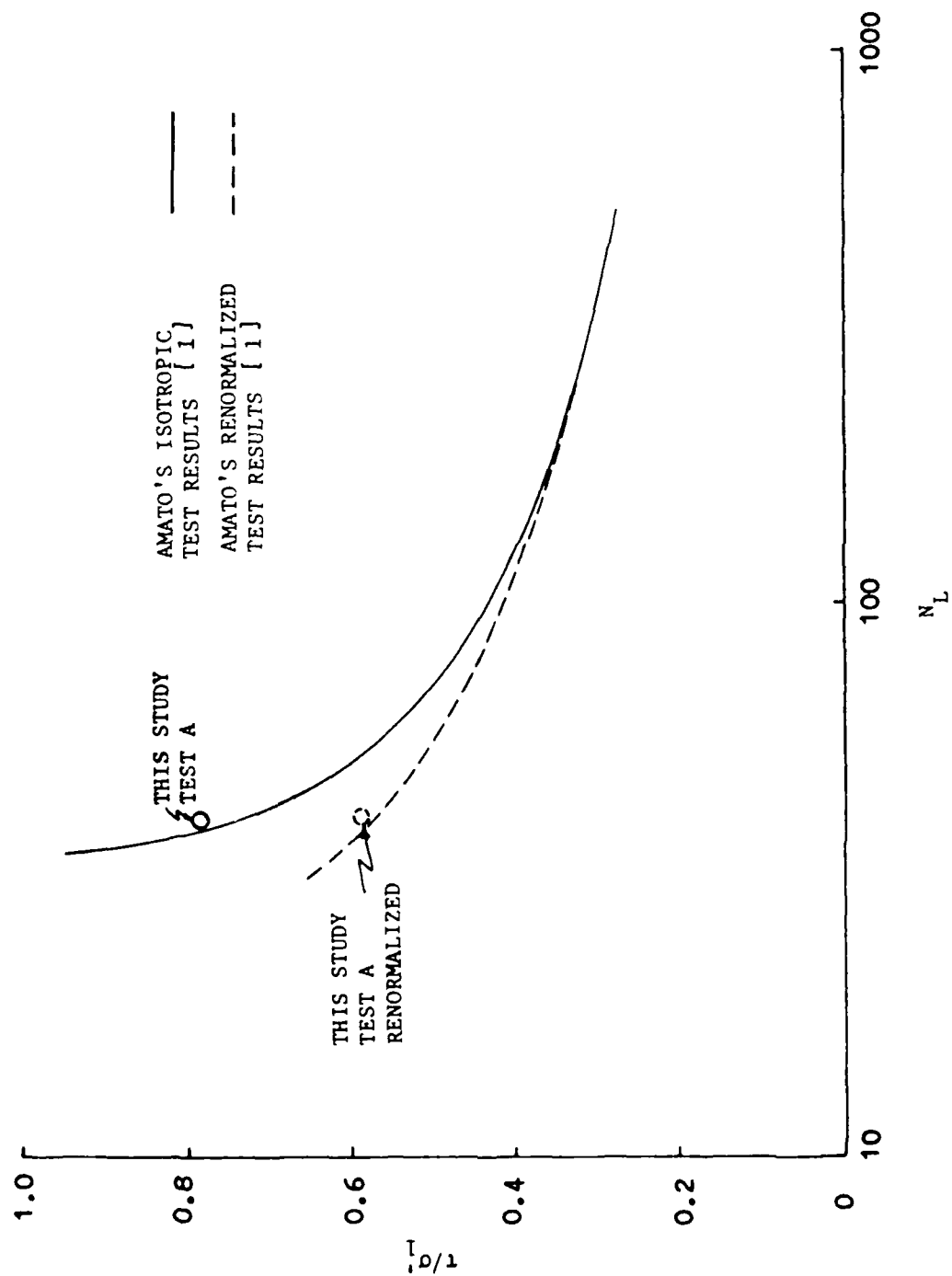


FIGURE 5.3 COMPARISON OF RENORMALIZED RESULTS

5.6 Second Testing Stage

5.6.1 Results

The results presented by De Alba et al [9] have been used as a reference and bench mark for many investigators in the study of soil liquefaction. Figure 5.4 presents the tests performed by Mason [22], Amato [1] and the first stage of this study along with the De Alba et al [9] results. It can be seen the tests conducted on The Ohio State University device consistently resulted in less conservative estimates of liquefaction potential than those presented by De Alba et al [9]. In order to study whether or not the difference could be explained by the way De Alba et al [9] constructed their sand sample the Phase B tests were conducted. In the Phase B tests a reaction mass, similiar to that reported by De Alba et al [9], was placed on top of the sample.

The test conditions and results for this stage of testing along with those which could be determined from De Alba et al [9] are presented in Table 5.2. The height of the reaction mass (H) used for each test is noted. The results are plotted as the shear stress ratio versus cycles to liquefaction in Figure 5.5. Because the addition of the reaction mass resulted in anisotropic conditions being applied to the sand sample, the confining pressure applied to the sides of the sand sample was increased to restore an isotropic state to the sand sample prior to testing. This

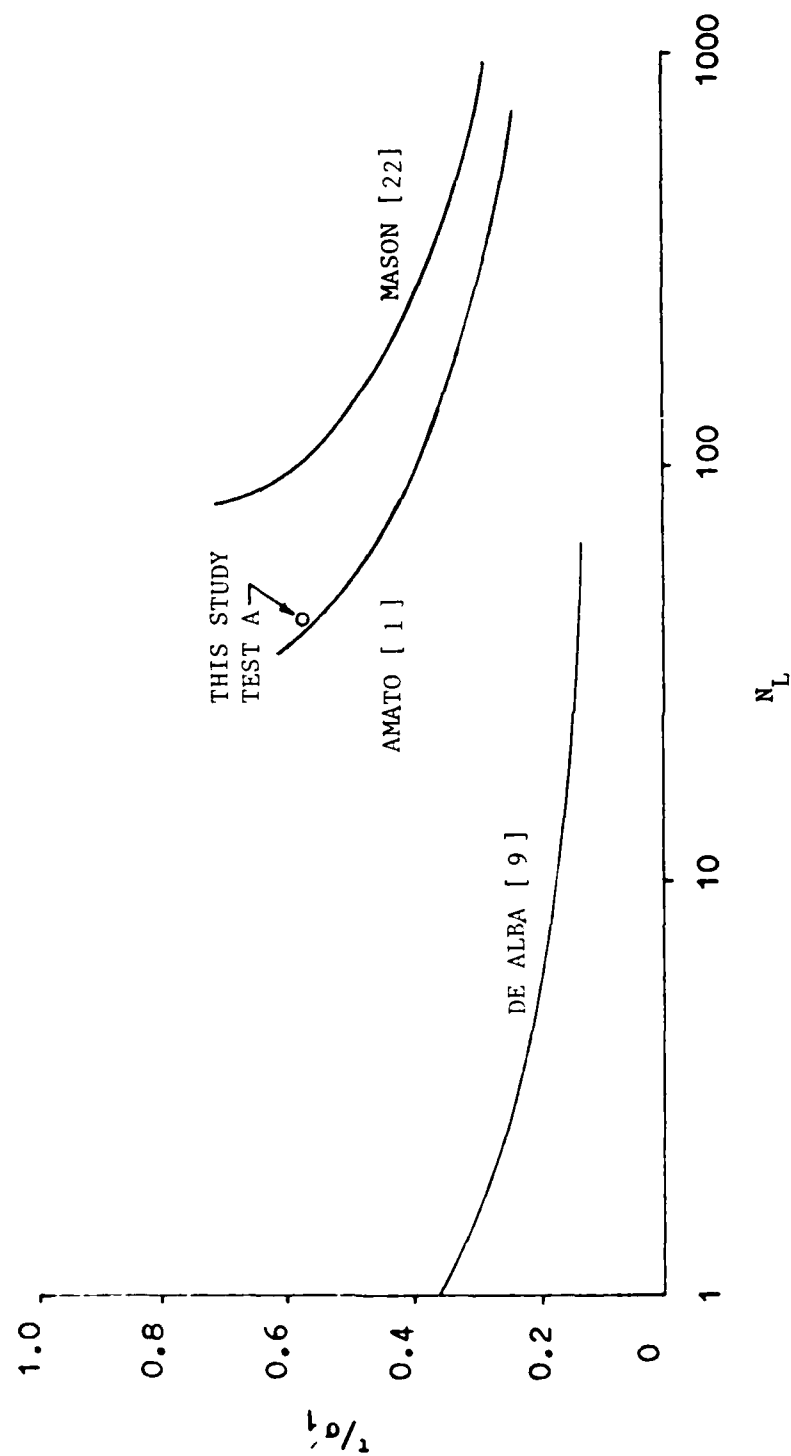


FIGURE 5.4 COMPARISON OF LIQUEFACTION POTENTIAL TEST RESULTS

TABLE 5.2 TEST CONDITIONS AND RESULTS FROM REACTION MASS TESTING

RESEARCHER	Dr (%)	σ'_1 (psi)	τ/σ'_1	H (in)	N_L	B
DE ALBA []	54	8.0	0.319	2.0	1.5	0.982
	54	8.0	0.240	2.0	3.0	0.990
	54	8.0	0.207	2.0	8.0	0.997
	54	8.0	0.195	2.0	12.5	0.976
	54	8.0	0.185	2.0	16.0	1.001
	54	8.0	0.148	2.0	63.0	0.981
<u>THIS STUDY</u>						
TEST B1 (26 AUG 86)	30.7	1.00	0.45	0.5	78.0	0.983
TEST B2 (15 SEP 86)	30.0	1.28	0.57	2.0	62.0	0.981

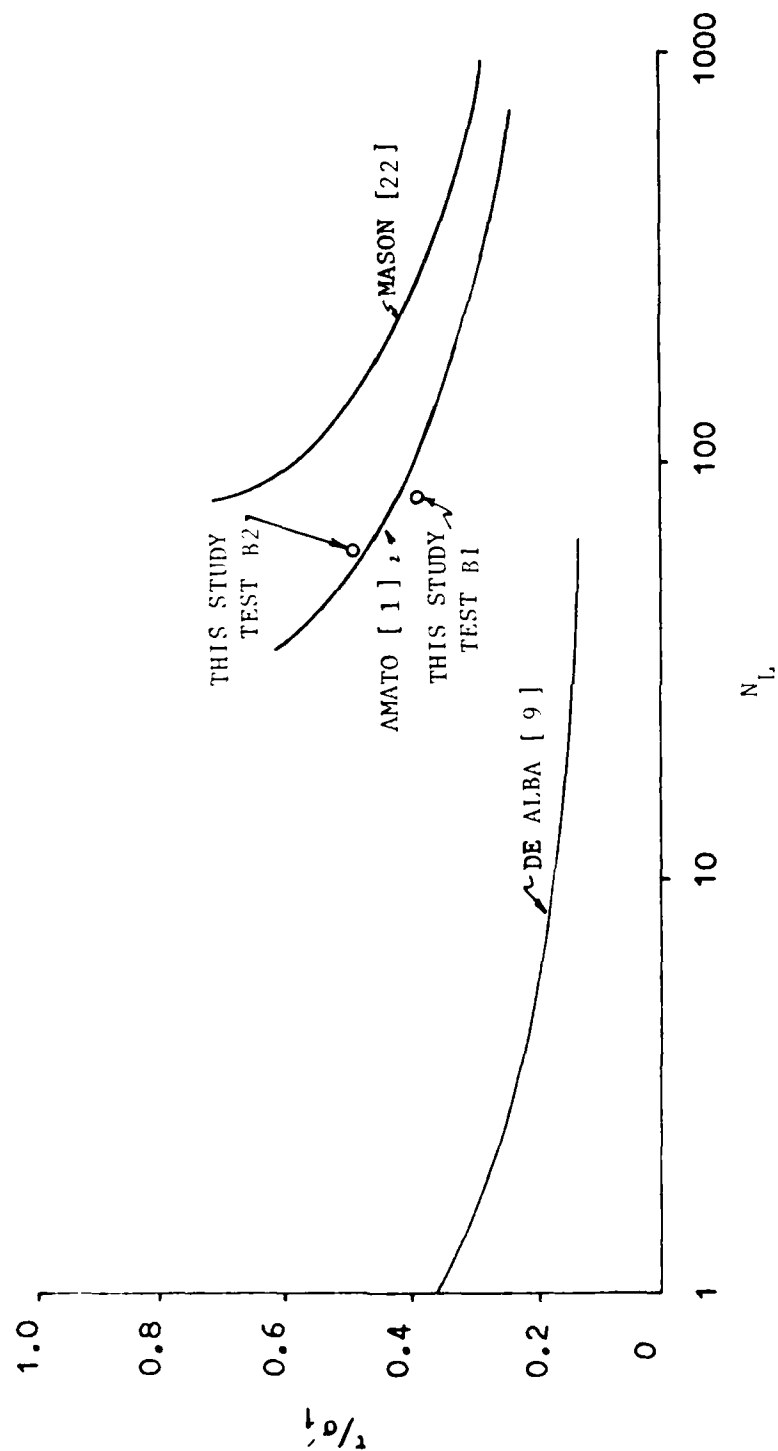


FIGURE 5.5 COMPARISON OF SECOND STAGE RESULTS WITH OTHER INVESTIGATORS

was accomplished for two reasons: first, because it enabled the results to be compared with previous isotropic tests and second, the tests conducted by De Alba et al [9] were also nearly isotropically consolidated (K_0 approximately equal to 0.98). The first test in this stage (Test B1) was conducted with a reaction mass consisting of half an inch of steel grit while the second test (Test B2) utilized two inches of steel grit. The purpose was to investigate how various heights (and thereby various weights) of reaction mass affected liquefaction potential. Both tests produced plots very close to the graph of isotropic results as presented by Amato [1]. This would indicate that the method used in this study of the reaction mass (regardless of height) had little effect on the liquefaction potential of the sand sample.

5.6.2 Pore water pressure generation

The response of the pore water pressure transducers which collected data throughout the entire course of the test are contained in Appendix A. Much like the results reported in section 5.5.2, the pressure change commenced immediately upon applying table excitation. Figure 5.6 shows a typical graph of the pore water pressure change during this stage of testing. The figure also shows once initial liquefaction was achieved, sample pore water pressures remained at a relative constant level. This is in

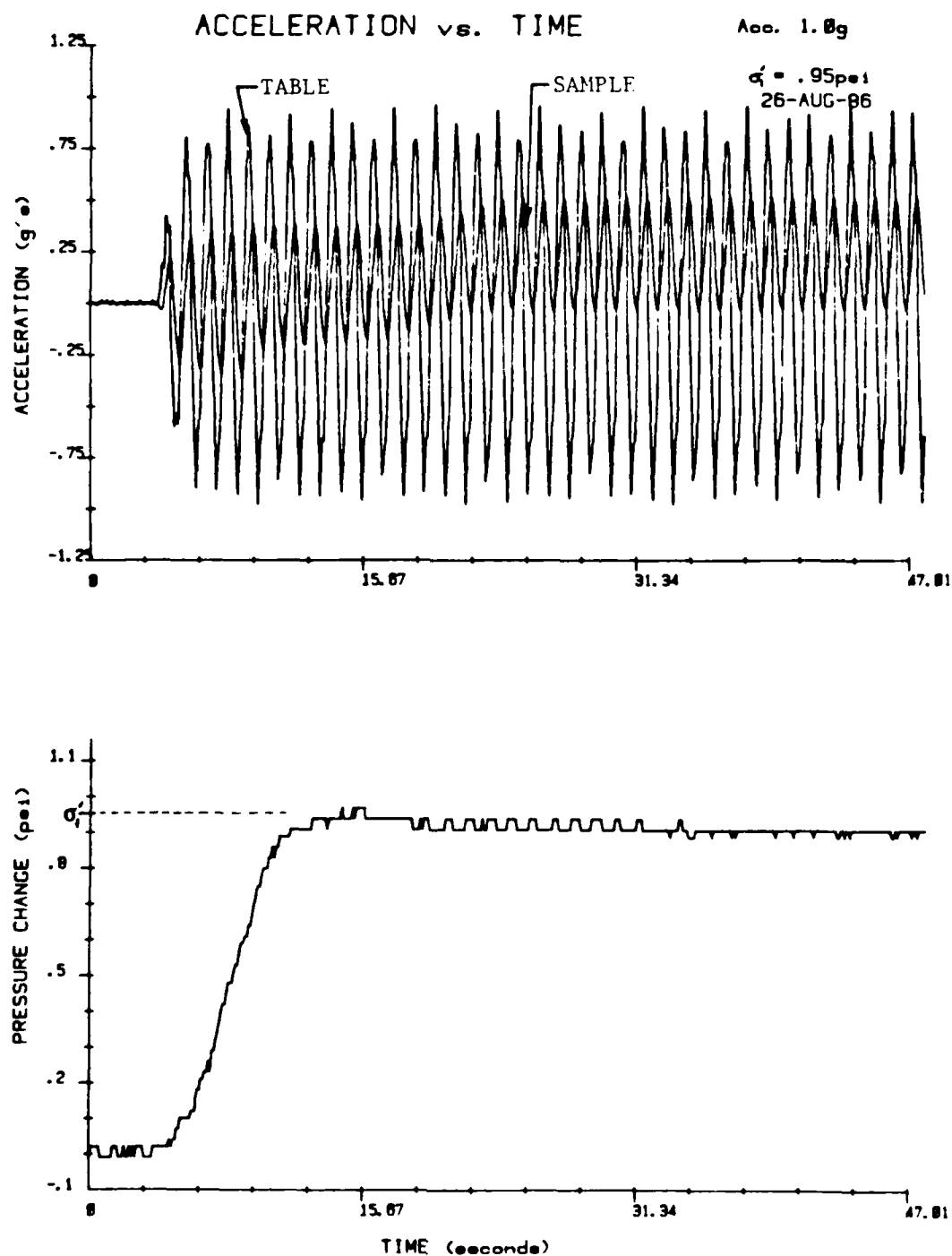
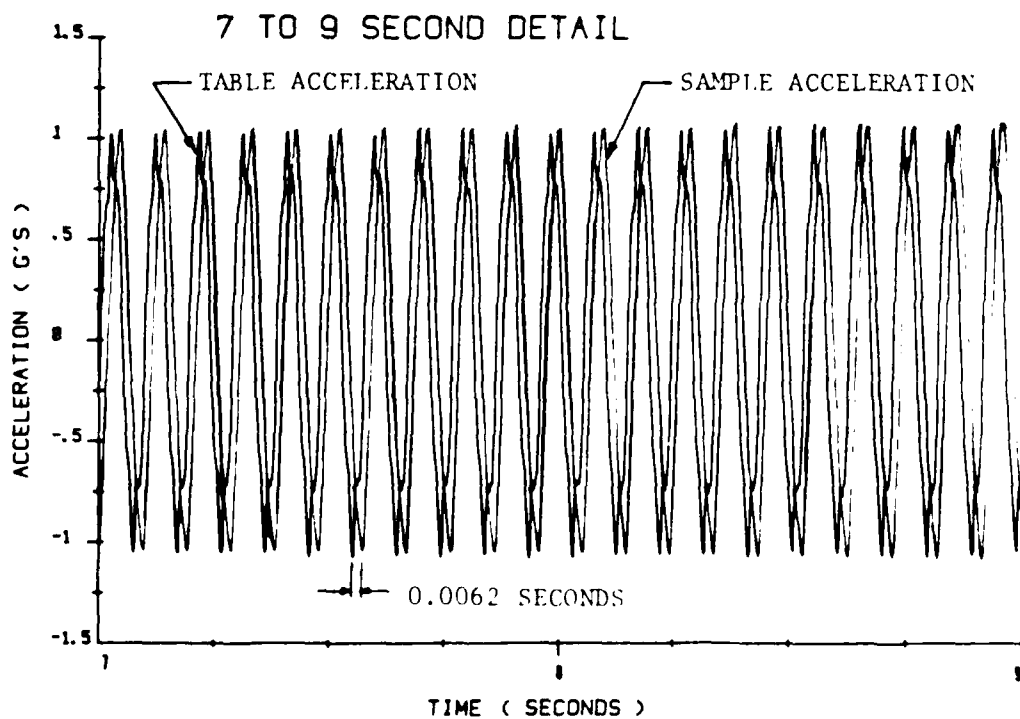
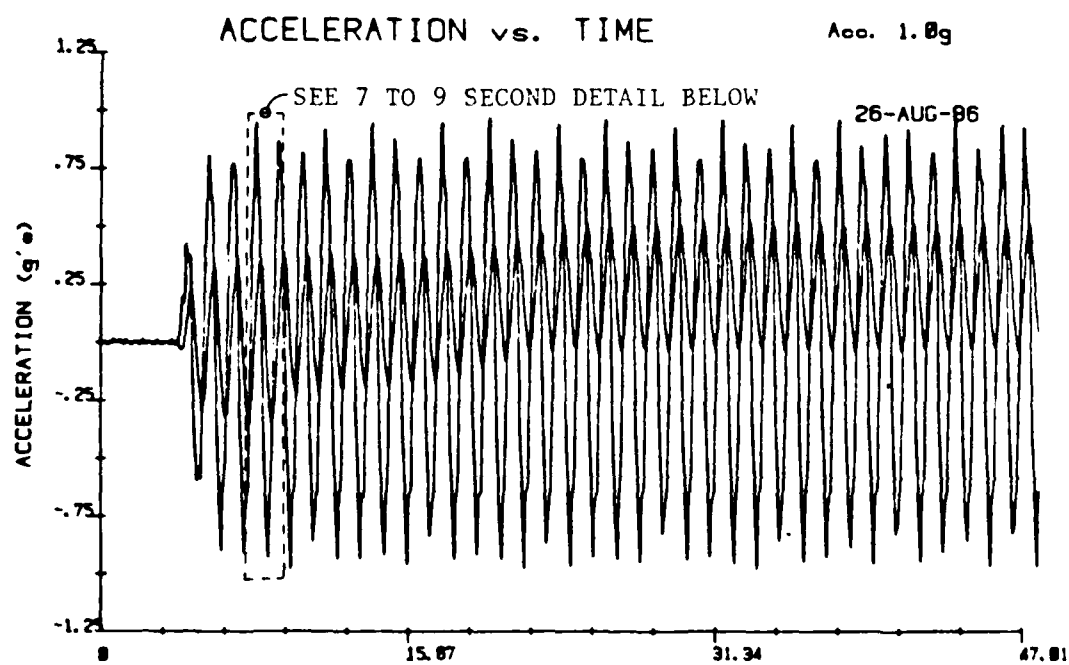


FIGURE 5.6 TYPICAL STAGE TWO TEST RECORD

agreement with the sample pore water pressure development presented by Amato [1] during his isotropic tests.

5.6.3 Table and sample excitation

The 10 Hz acceleration time histories for both tests from the second stage of this study are contained in Appendix B. Only the table acceleration was obtained for Test B2, therefore, only the table acceleration is plotted. Since the amplitude and frequency remain constant (after the initial 1.2 seconds as mentioned earlier) only the first 3.96 seconds of data collection are presented. The acceleration time histories from Test B1 also illustrate the transient and steady state responses of the table acceleration and can be found in Appendix B. The acceleration time history presented in Figure 5.6 presents the sample and table accelerations superimposed. To facilitate the comparison between the time histories, the magnitude of the sample acceleration was graphically reduced by one-fourth. After correcting for the difference in collection times between each acceleration, the sample acceleration is shown to have a time lag of approximately 6 milliseconds from the table acceleration throughout the course of the test (see Figure 5.7 for a more detailed illustration of a portion of the time history). This time lag is equal to the amount of time required for shear waves to propagate upward from the base. Although only every



twelfth cycle is represented, the graph nevertheless illustrates the change in sample acceleration amplitude and departure from its zero axis of orientation as initial liquefaction was approached. This probably is a result of the loss of strength in the sand sample which allowed the sample accelerometer to rotate about its axis.

5.7 Third Testing Stage

5.7.1 Input Motions

A standard method of illustrating the frequency content of an acceleration time history is by means of a Fourier amplitude spectrum. The Fourier spectrum is an indication of the final energy in the excitation as a function of frequency. In the context of the liquefaction tests, the peaks of the spectrum represent frequencies at which relatively large amounts of energy were supplied to the shaking table/sand system. The Fourier amplitude spectrum for the input excitation is presented in Figure 5.8. The spectra show the dominant frequencies of the pink noise input to be between 6 to 15 Hz and slightly offset from the S00E component of the 1940 El Centro earthquake. This frequency range was constructed with a combination of a high and low pass filter, and was selected for three reasons: first, it is within the range of frequencies observed for the majority of recorded strong motion earthquake frequency spectra; secondly, it symmetrically

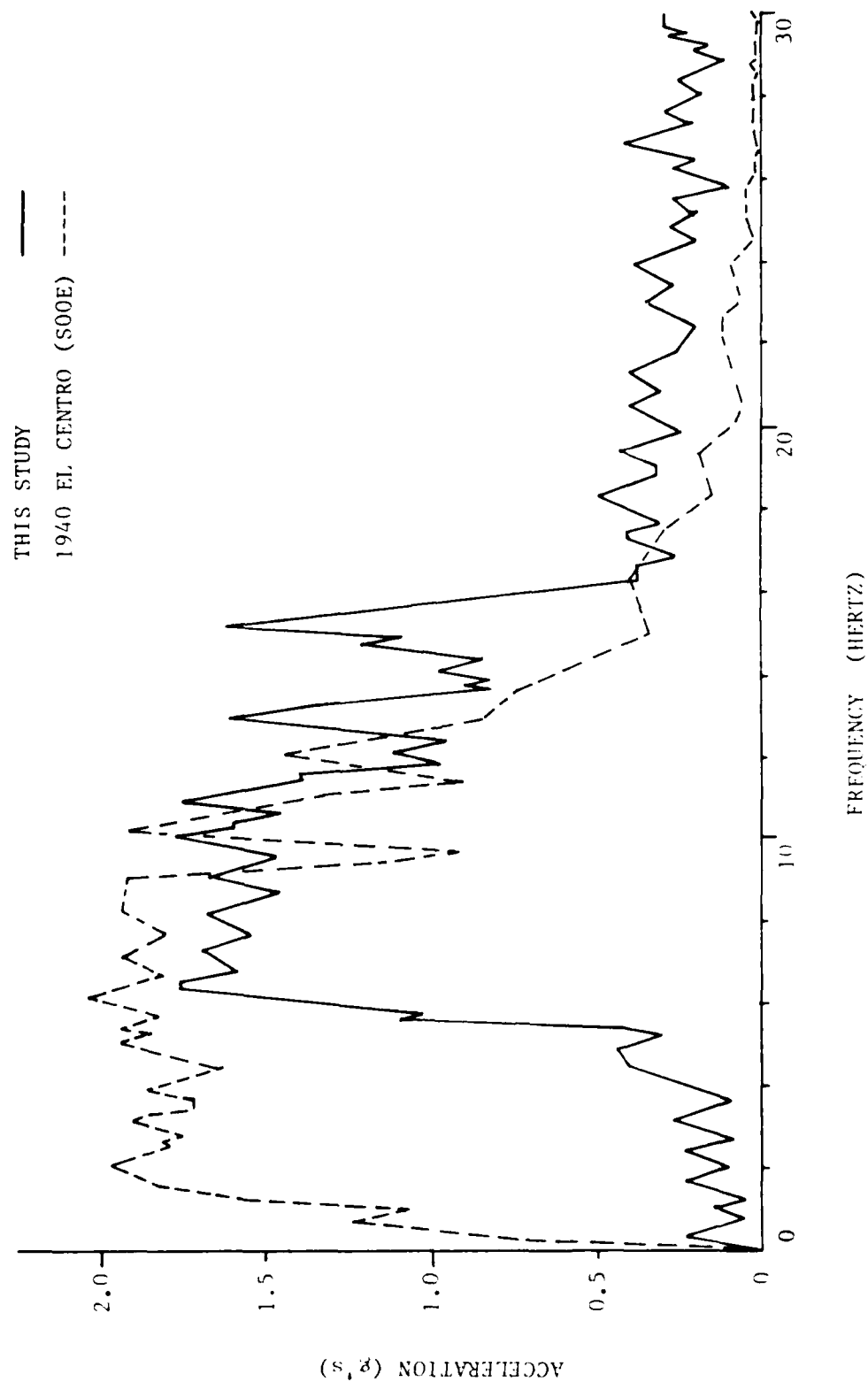


FIGURE 5.8 FOURIER SPECTRA OF STAGE THREE STUDY AND 1940 EL CENTRO EARTHQUAKE

brackets previous harmonic liquefaction potential testing described in section 5.5 and; lastly, the displacement capabilities of the hydraulic actuator prevented the input of lower excitation. Any frequencies greater than approximately 15 Hz represent unsolicited noise which was not eliminated during filtering. High and low pass filters causing abrupt truncation of the frequency spectrum will produce an undesirable side effect of ripples (referred to as Gibbs phenomenon) near where the amplitudes change rapidly. Through the use of small side lobes visible on the input spectrum, this phenomenon was avoided. The input excitation frequency spectrum was derived from data generated on an IBM/PC XT microcomputer and shows an essentially constant amplitude in the desired frequency range.

5.7.2 Results

While the vast majority of previous laboratory tests on soil liquefaction potential utilized uniform cycles of loading, the time history of shear stress during an earthquake is quite random. As mentioned in section 2.3, pink noise is then possibly a more appropriate laboratory representation of strong earthquake induced ground accelerations in liquefaction studies. Two pink noise acceleration time histories were used in this final stage of testing on isotropically consolidated saturated sand

samples. Test C2 and Test C4 were conducted with pink noise having dominant frequencies between 6 and 15 Hz (see Figure 5.9). Test C1 and Test C3 were conducted with pink noise composed with the same frequency range as above, with a large amplitude acceleration spike added during the first second of testing (see Figure 5.10). The test conditions and results for this stage are presented in Table 5.3. The amount of time required to liquefy each sample is designated as T_l .

Figures 5.11 through 5.14 present typical records for each of the four tests conducted during the third stage of this study. A complete collection of pore water pressure change and acceleration time histories can be found in Appendices A and B respectively.

Both pink noise acceleration time histories were capable of producing liquefaction conditions in each of the sand samples. Figure 5.15 presents a normalized comparison of each test conducted during this stage on a plot of pore water pressure ratio versus time to initial liquefaction. The spiked pink noise acceleration time history (Tests C1 and C3) is shown to induce initial liquefaction at a much earlier time than did the non-spiked time history (Tests C2 and C4). Also, while the spiked pink noise time history induced a sudden and continuous rise in the pore water pressure ratio, the non-spiked pink noise is shown to cause the rise to be more gradual and occurring in a stepped

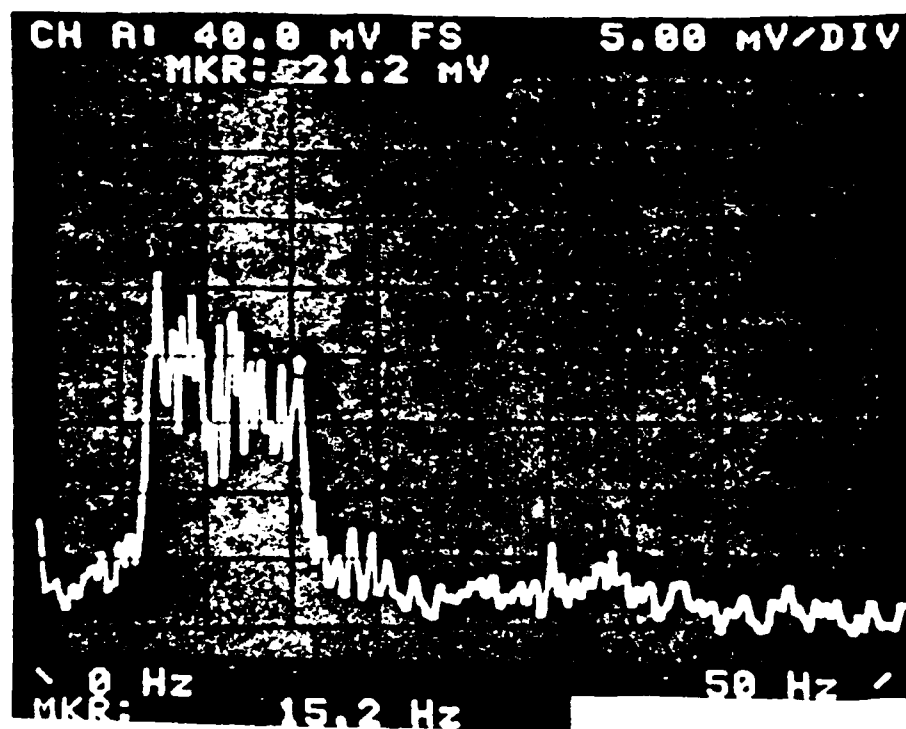
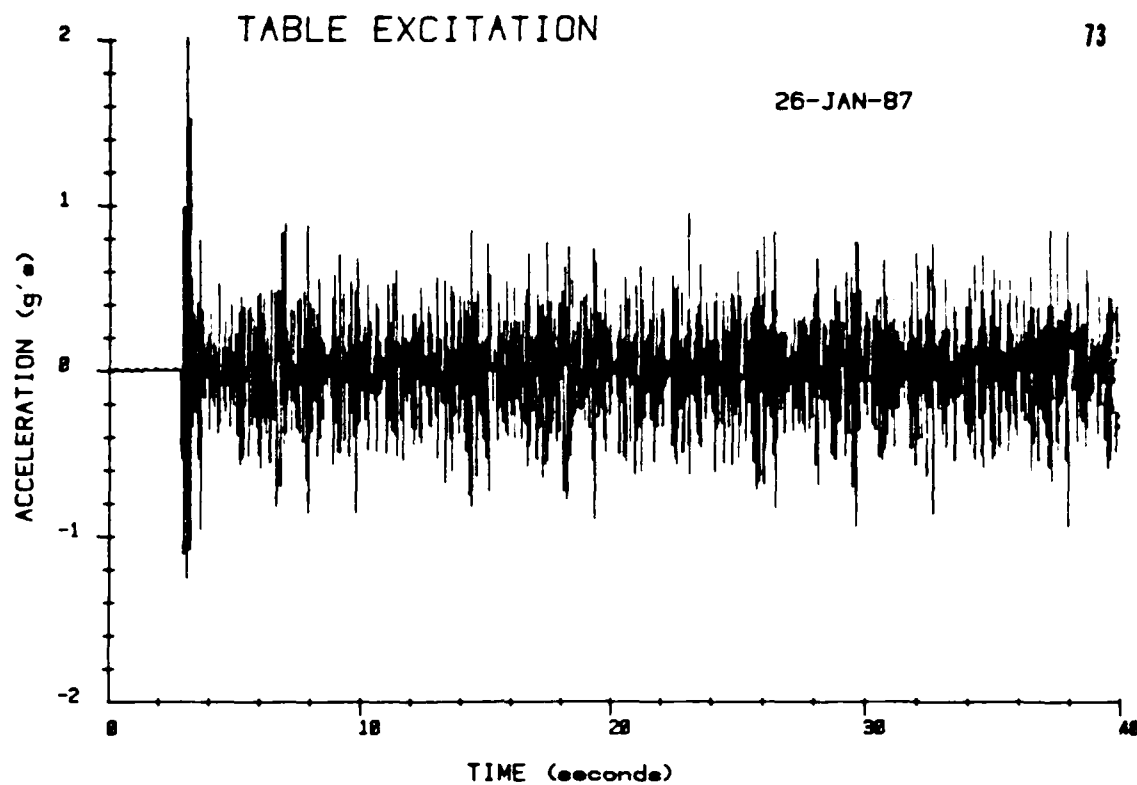


FIGURE 5.9 TYPICAL SPIKED ACCELERATION TEMPORAL AND FREQUENCY RECORD

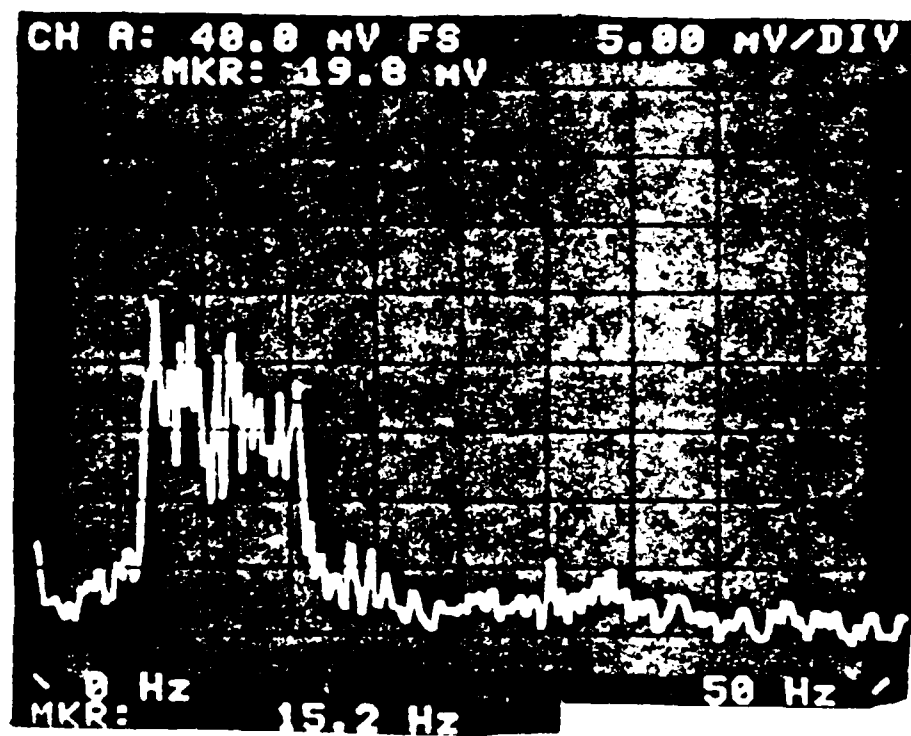
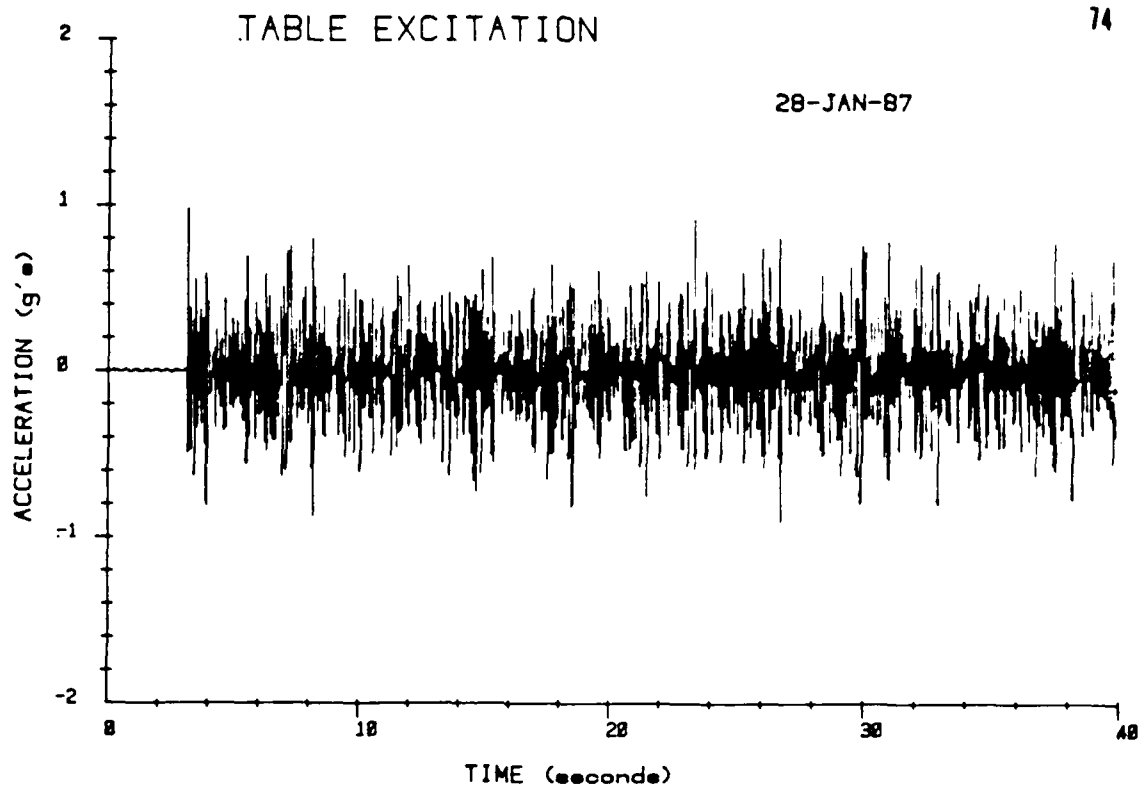


FIGURE 5.10 TYPICAL NON-SPIKED ACCELERATION
TEMPORAL AND FREQUENCY RECORD

TABLE 5.3 TEST CONDITIONS AND RESULTS FROM PINK NOISE EXCITATION TESTING

TEST	Dr (%)	σ'_1 (psi)	$(\tau/\sigma'_1)_{\max}$	Amax (g)	T_L (sec)	B
TEST C1 (21 JAN 87)	20.7	0.8	1.08	2.19	0.71	0.98
TEST C2 (24 JAN 87)	19.8	2.0	0.19	0.94	27.65	0.98
TEST C3 (26 JAN 87)	21.6	1.6	0.56	2.19	4.92	0.99
TEST C4 (28 JAN 87)	20.9	1.1	0.37	0.97	15.21	0.99

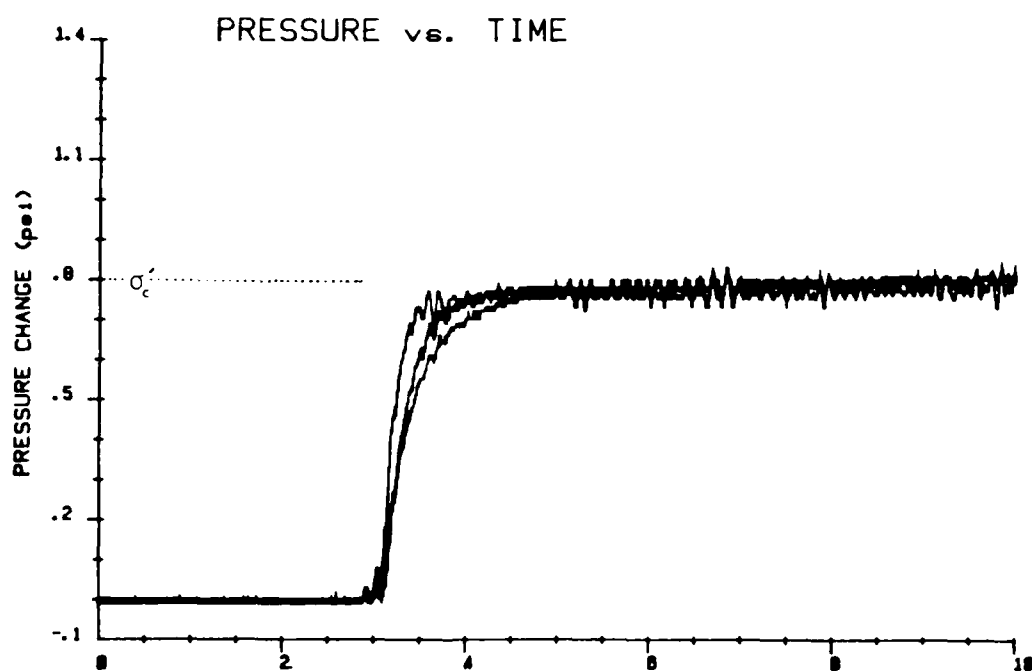
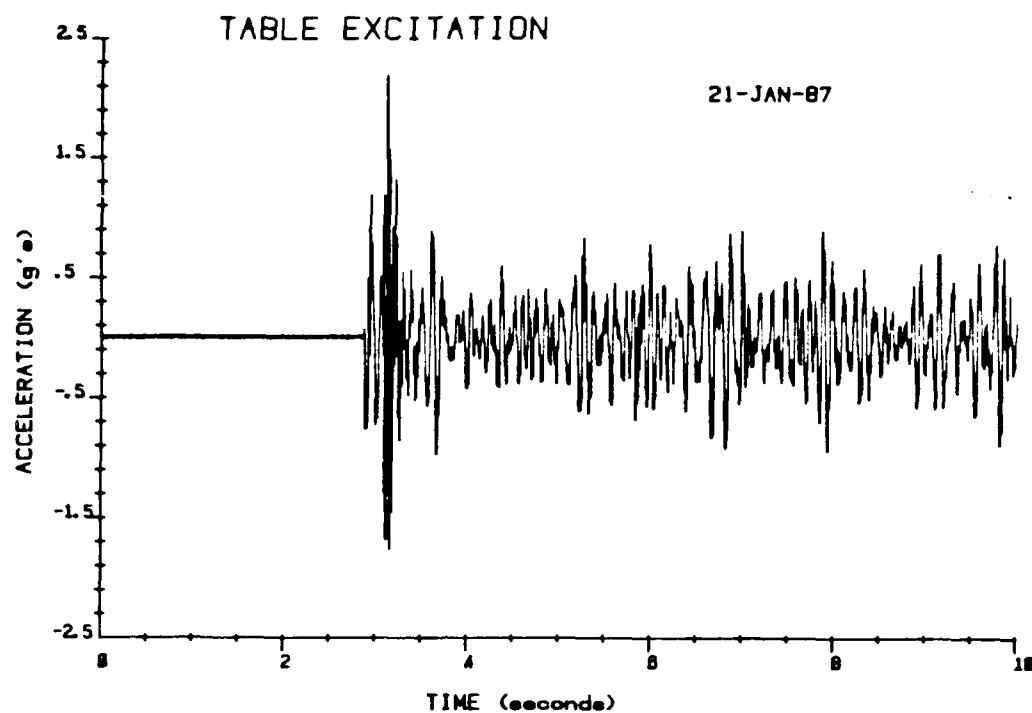


FIGURE 5.11 TEST C1 RECORD

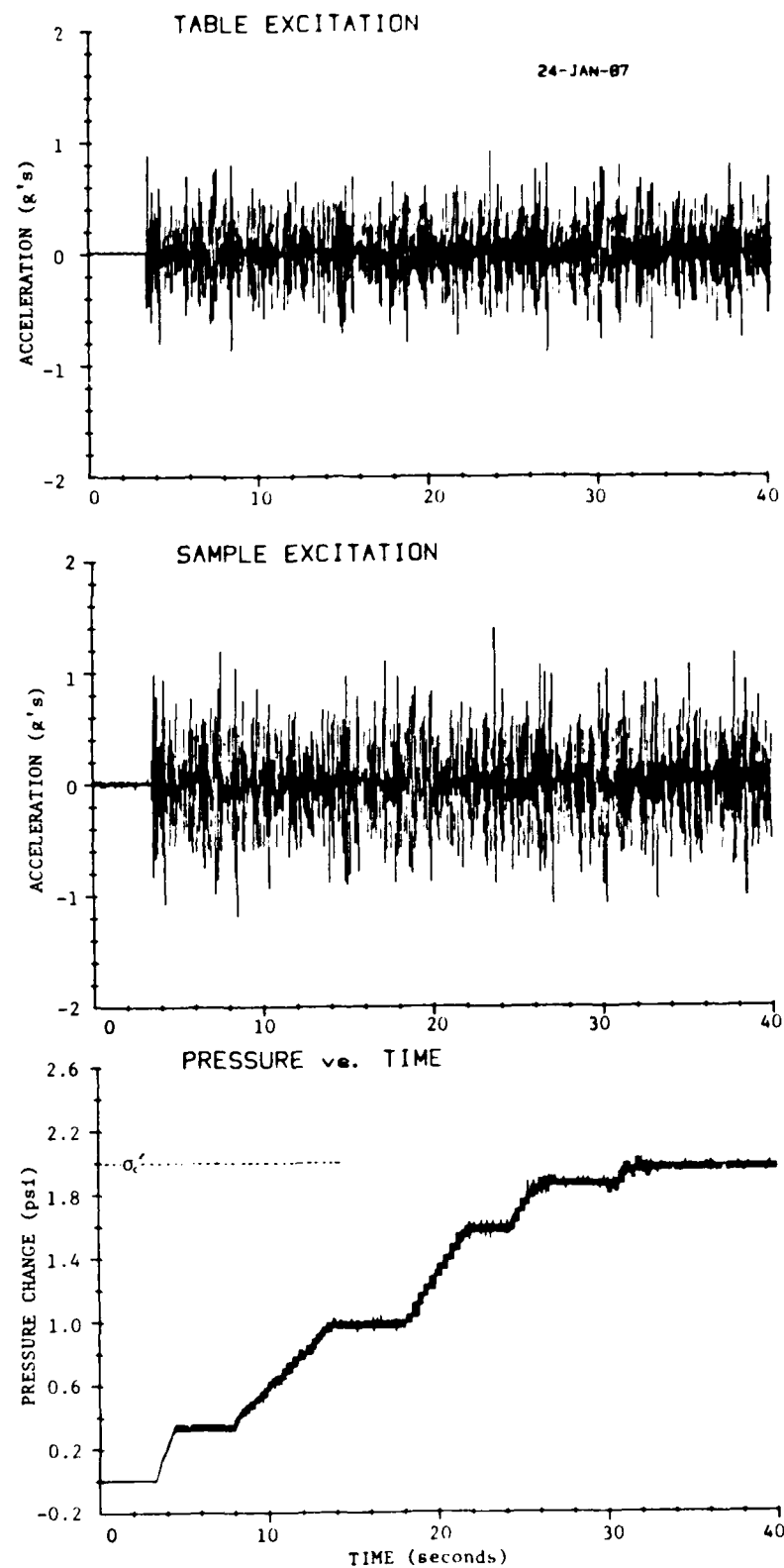


FIGURE 5.12 TYPICAL TEST C2 RECORD

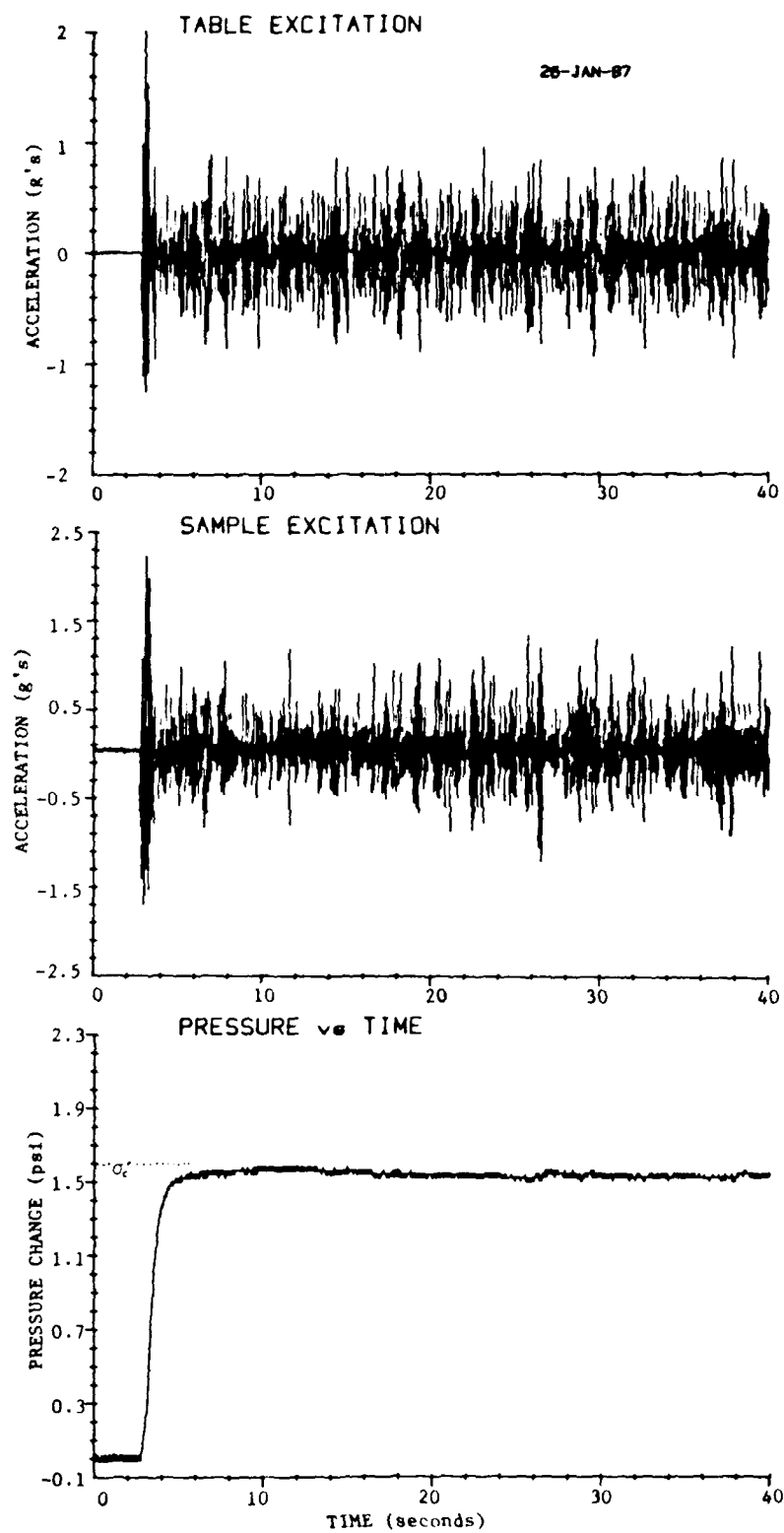


FIGURE 5.13 TYPICAL TEST C3 RECORD

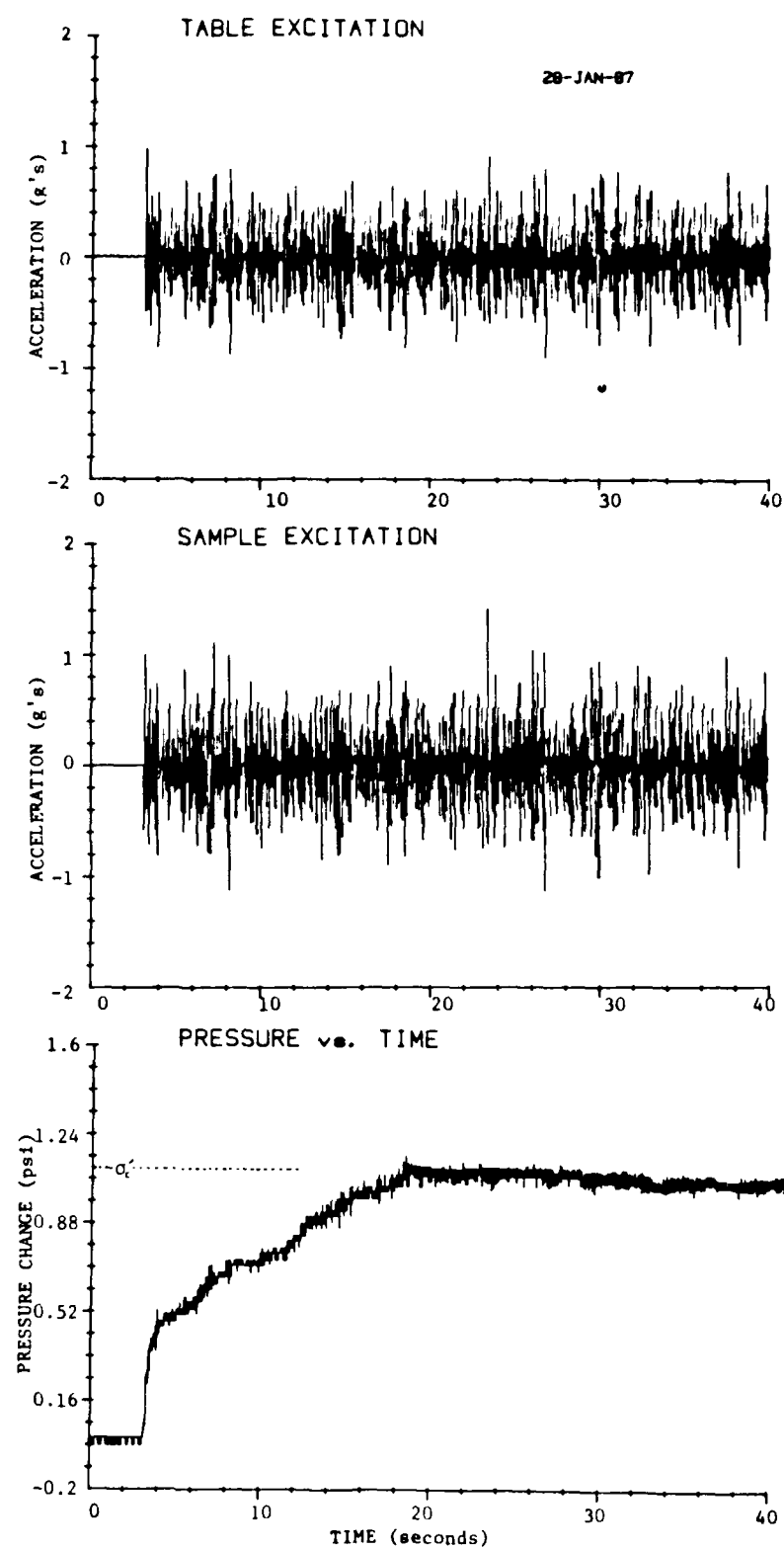


FIGURE 5.14 TYPICAL TEST C4 RECORD

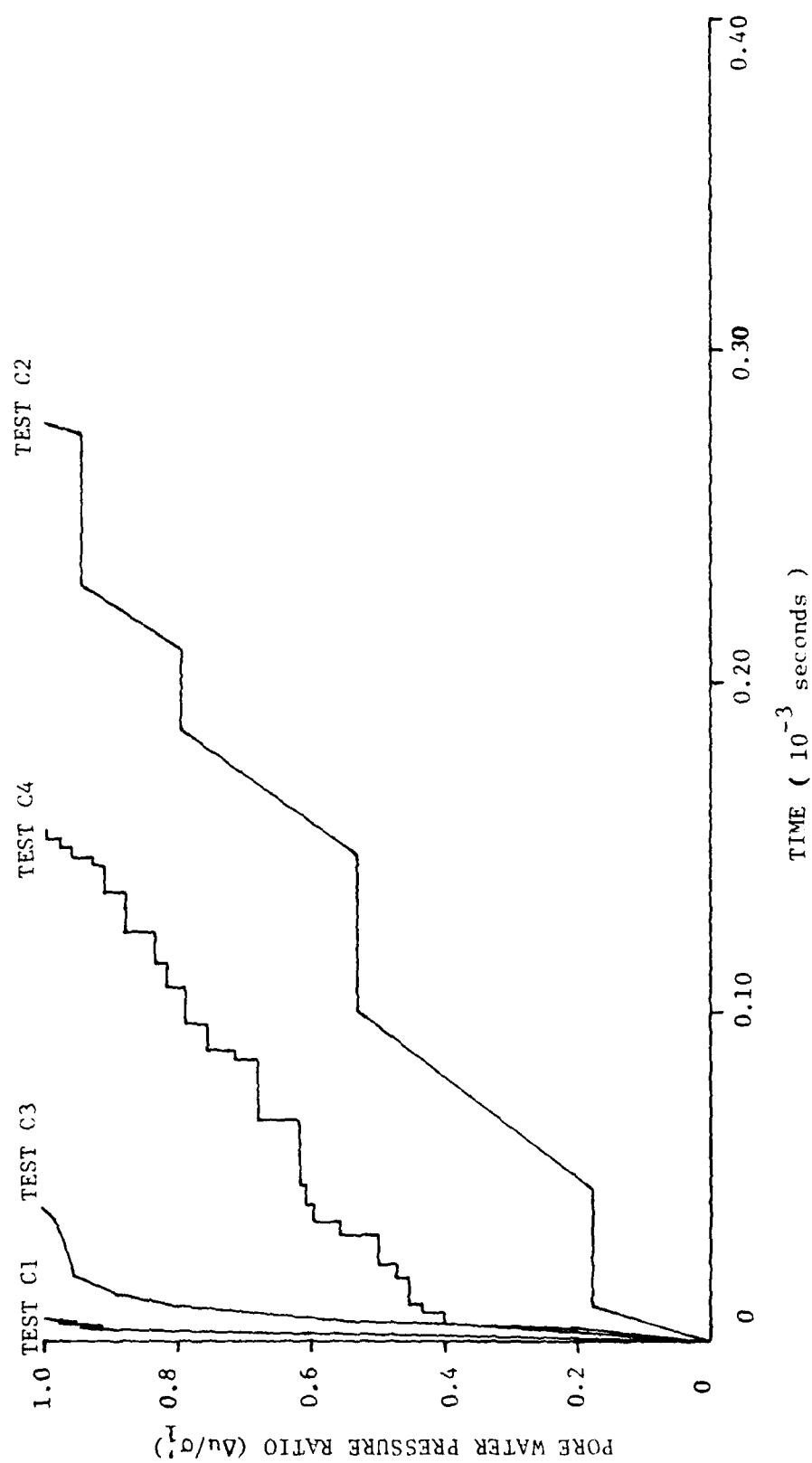


FIGURE 5.15 COMPARISON OF TIME TO LIQUEFACTION FOR STAGE THREE RESULTS

manner. Tests conducted with the same pink noise acceleration time histories (C1, C3 and C2, C4) differ only in the initial effective confining pressure applied to the sand sample. Figure 5.15 shows that those tests confined at a lower initial effective pressure and thereby subjected to a higher stress ratio liquefied in a shorter amount of time than tests with higher initial effective confining pressures. This same observation was cited in section 2.2 for uniform, harmonically loaded cohesionless samples. The large acceleration spike alone produced an increase in the pore water pressure ratio of 0.5 in Test C1 and a ratio of 0.25 in the Test C3. This implies the remainder of the pore water pressure increase for these tests were the result of subsequent, relatively smaller acceleration peaks.

The results obtained during this stage of testing along with those obtained by other investigators [1,22] are plotted (see Figure 5.16) as the maximum shear stress ratio, $(\tau/\sigma'_v)_{\max}$, versus time to liquefaction. The spiked acceleration test results (Tests C1 and C3) plot on a curve which is simply an extension of the isotropic curve presented by Amato [1]. The plot from Test C3 is very close to the isotropic curve while the plot from Test C1 smoothly extends the isotropic curve upward and to the left because of the higher shear stress ratio applied to the sand sample. The results of the non-spiked acceleration tests

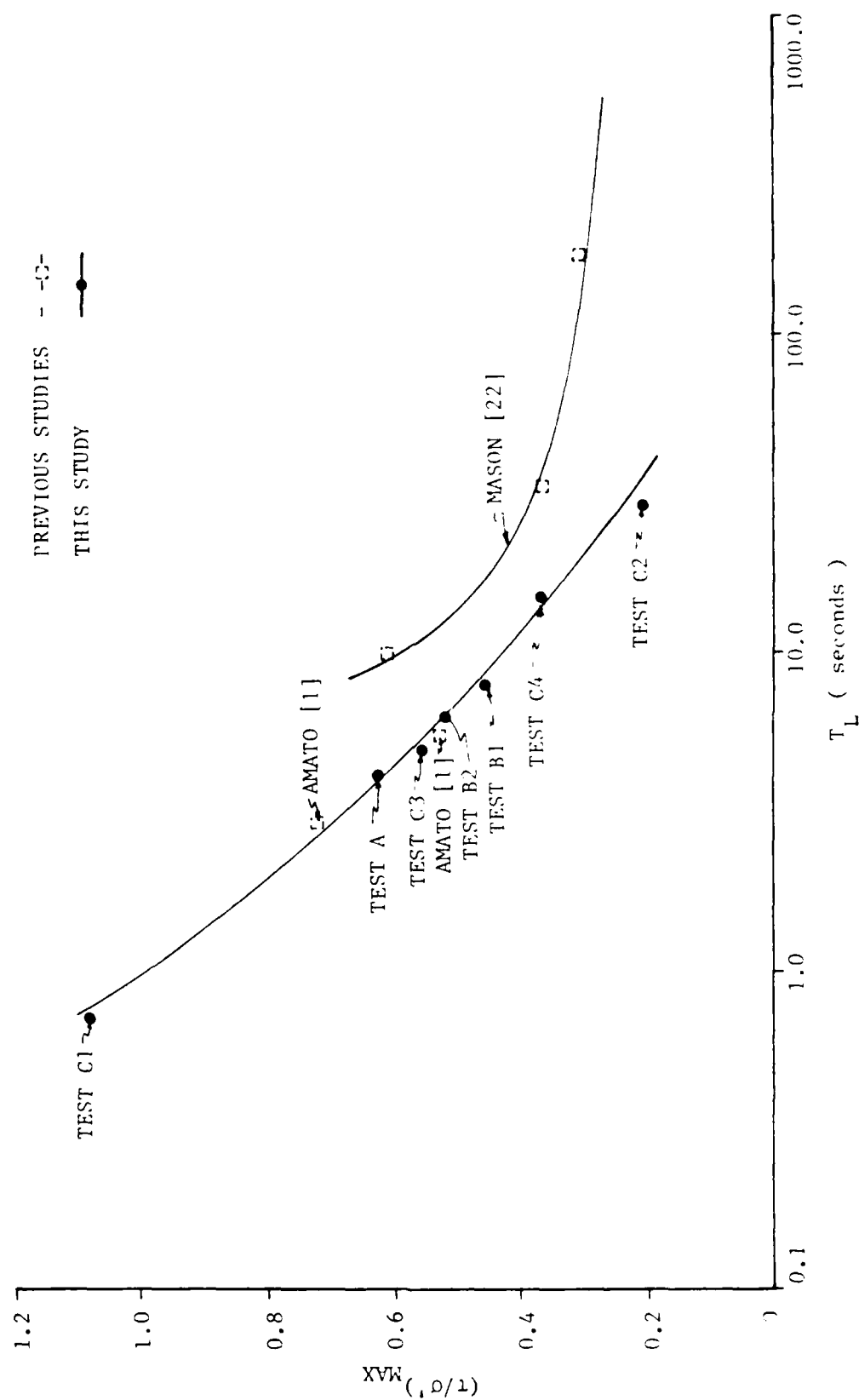


FIGURE 5.16 COMPARISON OF RESULTS FROM THIS STUDY WITH OTHER INVESTIGATORS

(Tests C2 and C4) are also shown in the Figure 5.16. The plot for Test C4 is also located on the isotropic curve presented by Amato [1]. Test C2, however, plots somewhat below the curve proposed by Amato [1]. Figure 5.16 also illustrates that all test results from this study plot within a narrow range around the isotropic curve presented by Amato [1].

Figures 5.11 through 5.14 present typical records for each of the four tests conducted during the third stage of this study. A complete collection of pore water pressure change and acceleration time histories can be found in Appendices A and B respectively.

5.7.3 Table and sample excitations

The magnitudes of the excitations measured at the top of the sand sample appear to be amplified when compared to their respective table excitation. This phenomenon occurred regardless of what type of table excitation was applied to the base of the sand sample, the initial effective confining pressure, or the pore water pressure ratio reached. Additionally, the sample excitation record lags the table excitation (see Figure 5.17) in the same manner (approximately 5 milliseconds) as the second testing stage of this study as discussed in section 5.6.3.

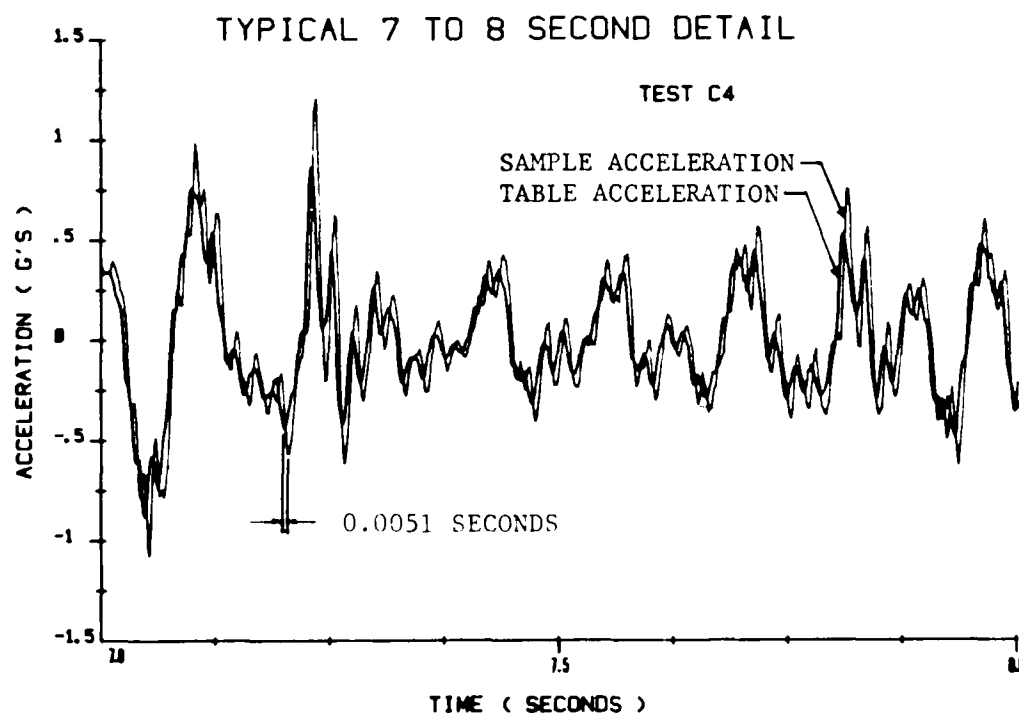
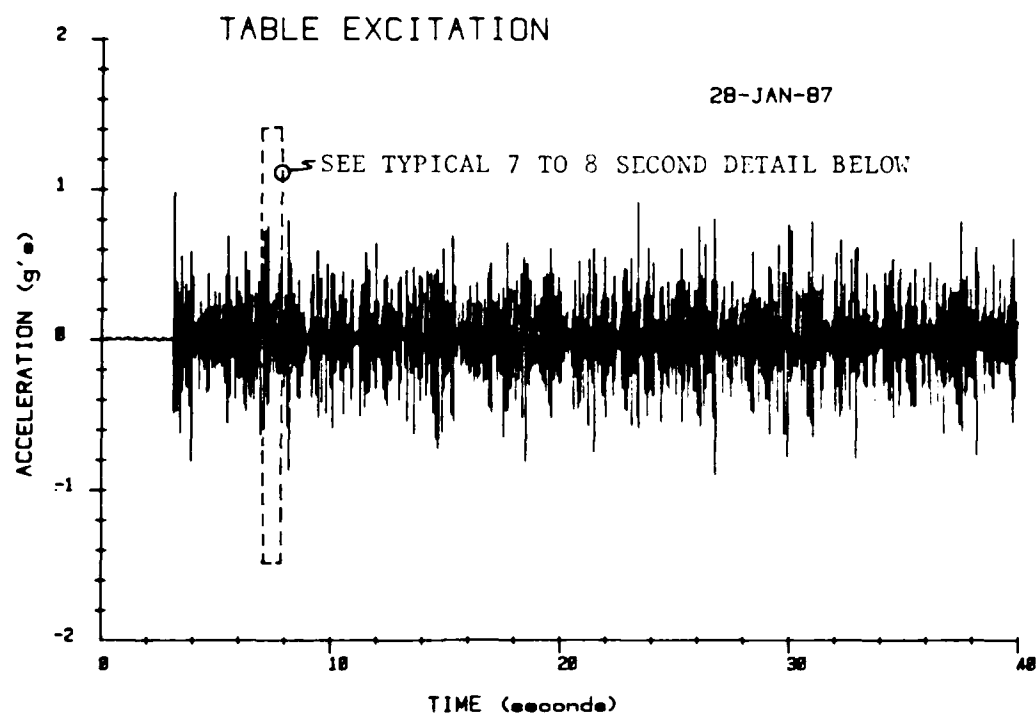


FIGURE 5.17 COMPARISON OF TYPICAL STAGE THREE
TABLE AND SAMPLE ACCELERATION TIME HISTORY

5.7.4 Spectrum analysis

Fourier amplitude spectra for the large spiked pink noise table and sample excitations, and non-spiked pink noise table and sample excitations are contained in Appendix C. Each spectrum shows the dominant frequencies of the resulting excitations remained within the 6 to 15 Hz range throughout the course of the test.

Comparison of the spiked and non-spiked excitations shows the former to have had the effect of slightly increasing the amplitude of the frequency spectrum while still maintaining its dominant frequency range. Within each particular pink noise acceleration time history, the amplitude of the frequency spectrum of the sample response was slightly higher than the table spectrum throughout the dominant frequency range. This amplification of sample excitations confirms previous observations.

5.7.5 Pore water pressure generation

Typical pore water pressure records for each test are shown in Figures 5.11 through 5.14 in relation to their respective acceleration time histories. As mentioned in section 5.7.1, the large spiked accelerations were responsible for generating 50 to 25 percent of the total pore water pressure change in their respective test. Subsequent peaks of lower amplitude in acceleration were necessary to completely liquefy the sand sample. In those

tests conducted without a large spike at the beginning of the test, the first dominant acceleration spike also induced immediate pore water pressure generation. However, the increase was less than 10 percent and numerous other relatively dominant acceleration spikes were needed to liquefy the sand sample. In addition to the difference in confining pressures, the non-spiked excitation records differ in that the Test C4 has slightly greater accelerations at the beginning of the time history than does Test C2. The greater accelerations and lower initial effective confining pressure resulted in approximately twice as much initial pore water pressure generation in the first second of data collection. After this point in time, the pore water pressures increased at nearly the same rate in both tests as shown in Figure 5.15, with the more highly confined sample having a slightly flatter slope.

CHAPTER VI

CONCLUSIONS AND RECOMMENDATIONS

This study was conducted to provide a better understanding of large scale liquefaction potential testing. Through the use of a three stage testing program, definitive observations can be made and some reasonable conclusions drawn. The results of the test program presented in this thesis are considered to have generated valuable information and expanded the database for the study of sand liquefaction.

The first stage test results showed the apparatus is capable of operating successfully and providing consistent results. Isotropic tests conducted by Mason [22], Amato [1] and during this test program were plotted together to illustrate this conclusion. The small offset between the point plotted from this study and the curve presented by Amato [1] can be explained by observing that the test from this study was conducted with a soil sample of slightly higher relative density. Because the test from this study had a slightly higher relative density it is to be expected that a few additional cycles of the same shear stress ratio

would be required before the sample liquefies.

It was shown in the second testing stage that tests conducted with the same testing apparatus continued to provide consistent results even with the addition of a reaction mass. Figure 5.5 shows the results from this stage of testing are again in close proximity to the isotropic curve presented by Amato [1]. Therefore, the boundary conditions imposed on the top of the sand sample by this reaction mass cannot be the explanation as to why the testing apparatus used in this study consistently gives much different results for liquefaction potential when compared with the results presented by De Alba et al [9]. Other boundary conditions must exist in their samples which we have not been able to reproduce with the apparatus used in this study. Membrane penetration was measured during the third stage of tests to determine if this factor was responsible for the greater number of cycles to liquefaction, since a large amount of penetration of the membrane between the grains of the sand sample would have resulted in slower changes in pore water pressure [22]. The amount of membrane penetration measured was consistently less than 1.75×10^4 percent of the sample volume. This amount of penetration was considered negligible.

The third testing stage utilized a band limited (or pink) noise excitation to provide the same an isotropically consolidated sample.

NO-A185 232

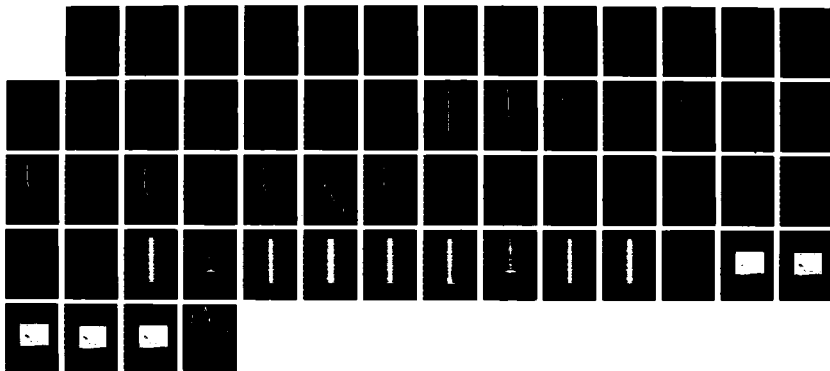
THE EFFECTS OF BAND-LIMITED WHITE NOISE EXCITATION ON
LIQUEFACTION POTENTIAL IN LARGE-SCALE TESTS(U) AIR
FORCE INST OF TECH WRIGHT-PATTERSON AFB OH
D L JASINSKI 1987 AFIT/CI/NR-87-58T

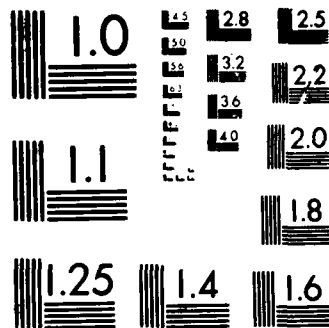
2/2

UNCLASSIFIED

F/G 8/10

NL





MICROCOPY RESOLUTION TEST CHART
 NATIONAL BUREAU OF STANDARDS 1963 A

reports available to the author, it is believed that these were the first such tests conducted on a large scale sample. Two distinct time histories were used to produce different results. Depending upon the hydraulic servovalve compensation rate setting, a spiked or a non-spiked acceleration time histories could be produced. Both acceleration time histories contained the same dominant frequencies (6 to 15 Hz). However, the spiked accelerations are an improvement over the non-spiked acceleration in that they also incorporated a distinctive maximum acceleration at the beginning of the acceleration time history. All recorded strong earthquake acceleration time histories have possessed the same type of acceleration spike at the onset of recorded motion. It is this maximum acceleration amplitude which is used in assigning a magnitude to the earthquake. Results from the third testing stage were plotted along with results from the first two stages and those of other investigators. The curve drawn from these results shows this study produced a plot which forms extensions of the isotropic curve presented by Amato [1]. The same curve also illustrates that times to liquefaction of isotropically consolidated soil samples subjected to random excitation loadings can be plotted as a function of maximum shear stress (the numerator of the maximum shear stress ratio) along the same curve as uniformly loaded soil samples. Therefore, it is proposed

that the use of the maximum shear stress within the soil sample during cyclic loading is an appropriate method with which to characterize earthquake effects.

Another factor shown to influence the time to liquefaction of each time history used was the initial effective confining pressure (the denominator of the maximum shear stress ratio) applied to the sand sample. The time to liquefaction was shown to increase with increase in the initial confining pressure. A Fourier spectrum analysis of the sample excitation showed an increase in magnitude of the frequencies within the dominant frequency range when compared to their respective input table spectra.

Recommendations for further research can be separated into two categories: (1) improvement and modification of the testing apparatus based on this study, and (2) substantiation of the results derived from the third stage of testing and determination of the effects other factors within the capabilities of the testing system have on liquefaction potential. Specific methods of improving the testing system are:

- a) Reducing the volume of confining fluid on the sides of the sample to determine what effect that has on confinement during excitation.

- b) Mean table accelerations during the third stage of testing were set at the maximum level the present testing

system would provide. Increased mean acceleration levels are believed to only be possible through the addition of larger accumulators on the hydraulic servovalve. This would also improve the testing system response during peak flow conditions.

c) An override mechanism is necessary in order to remove the build up time at the beginning of testing.

In order to obtain a more complete database, the following is recommended:

a) Accurate determination of the natural frequency of the sand sample. Pink noise tests could then be structured around this natural frequency to determine if an account of frequency content of input excitations must be made to adequately assess the true damage potential of sand samples.

b) Additional tests with the same pink noise excitations as in stage three of this study. The results would better define the effects of relative density, initial confining pressure and anisotropic consolidation on liquefaction potential.

c) Determination what the effect the location of the largest acceleration spike has on the time to liquefaction. This may be accomplished by locating a predominantly large acceleration spike at various locations within an acceleration time history.

REFERENCES

1. Amato, V.E., "Shaking Table Tests to Determine Liquefaction Potential of Anisotropically Consolidated Saturated Ottawa Sand," Thesis presented to The Ohio State University, Columbus, Ohio, in 1986 in partial fulfillment of the requirements for the degree of Master of Science.
2. Annaki, M. and Lee, K.L., "Equivalent Uniform Cycle Concept for Soil Dynamics," Liquefaction Problems in Geotechnical Engineering, ASCE, 1976, pp. 227-254.
3. Bycroft, G.N., "White Noise Representation of Earthquakes," Journal of the Engineering Mechanics Division, ASCE, Vol. 86, No. EM2, April, 1960, pp. 1-16.
4. Black, K.D. and Lee, K.L., "Saturating Laboratory Samples By Back Pressure," Journal of the Soil Mechanics and Foundations Division, ASCE, Vol. 99, No. SM1, January, 1973, pp. 75-93.

5. Castro, G., "Liquefaction and Cyclic Mobility of Saturated Sands," Journal of the Geotechnical Engineering Division, ASCE, Vol. 101, No. GT6, June, 1975, pp. 551-569.
6. Chang, C.S., "Residual Pore Pressure and Deformation Behavior of Soil Samples Under Variable Cyclic Loading," International Conference on Recent Advances in Geotechnical Earthquake Engineering and Soil Dynamics, Edited by Prakash, S., Vol. 1, 1981, pp. 107-110.
7. Collacott, R.A., Vibration Monitoring and Diagnosis, John Wiley & Sons, New York, 1979, pp. 52-58.
8. Crandall, S.H. and Mark, W.D., Random Vibration in Mechanical Systems, Academic Press, New York 1963, pp. 36-145.
9. De Alba, P., Chan, C.K. and Seed, H.B., "Determination of Soil Liquefaction Characteristics by Large-Scale Laboratory Tests," Shannon and Wilson, Inc. and Agbabian Associates, Report prepared for the U.S. Nuclear Regulatory Commission, September, 1976.

10. Gasparini, D.A. and Sun, W.J., "Random Vibration Analysis of Finite Element Models of Earth Dams," Proceedings of the Conference on Soil Dynamics and Earthquake Engineering, Edited by Cakmak, A.S., Vol. 2, 1982, pp. 635-649.
11. Halдар, A., "Uniform Cycles in Earthquakes - A Statistical Study," International Conference on Recent Advances in Geotechnical Earthquake Engineering and Soil Dynamics, Edited by Prakash, S., Vol. 1, 1981, pp. 195-198.
12. Halдар, A. and Tang, W.H., "Statistical Study of Uniform Cycles in Earthquake Motions," Journal of the Geotechnical Engineering Division, ASCE, Vol. 107, No. GT5, May, 1981, pp. 577-589.
13. Housner, G.W. and Jennings, P.C., "Generation of Artificial Earthquakes," Journal of the Engineering Mechanics Division, ASCE, Vol. 90, No. EM1, February, 1964, pp. 113-150.
14. Housner, G.W., "Important Features on Earthquake Ground Motion," Proceedings of the 5th World Conference on Earthquake Engineering, Rome, Vol. 1, 1974, pp. CLIX - CLXVIII.

15. Ishihara, K. and Yasuda, S., "Sand Liquefaction Due to Irregular Excitation," Soils and Foundations, Vol. 12, No. 4, December, 1972, pp. 65-77.
16. Ishihara, K. and Yasuda, S., "Sand Liquefaction Under Random Earthquake Loading Condition," Proceedings of the 5th World Conference on Earthquake Engineering, Rome, Vol. 1, 1974, pp. 329-338.
17. Kanai, K., Engineering Seismology, University of Tokyo Press, Tokyo, 1983, pp. 1-249.
18. Lee, K.L. and Fitton, J.A., "Factors Affecting the Cyclic Loading Strength of Soil," Special Technical Pub. No. 450, Symposium on Vibration Effects of Earthquakes on Soils and Foundations, ASTM, 1969, pp. 71-95.
19. Lee, K.L. and Focht, J.A., "Liquefaction Potential at Ekofisk Tank in North Sea," Journal of the Geotechnical Engineering Division, ASCE, Vol. 101, No. GT1, January, 1975, pp. 1-18.
20. Martin, G.R., Finn, W.D.L. and Seed, H.B., "Fundamentals of Liquefaction Under Cyclic Loading,"

Journal of the Geotechnical Engineering Division,
ASCE, Vol. 101, No. GT5, May, 1975, pp. 423-438.

21. Martin, G.R., Finn, W.D.L. and Seed, H.B., "Effects of System Compliance on Liquefaction Tests," Journal of the Geotechnical Engineering Division, ASCE, Vol. 104, No. GT4, April, 1978, pp. 463-479.
22. Mason, S.F., "Large Scale Testing of Sand Liquefaction," Thesis presented to The Ohio State University, Columbus, Ohio, in 1982 in partial fulfillment of the requirements for the degree of Master of Science.
23. National Academy of Science, Liquefaction of Soils During Earthquakes, Committee on Earthquake Engineering, National Academy Press, Washington D.C., 1985.
24. Nigam, N.C., Introduction to Random Vibrations, MIT Press, Cambridge, 1983.
25. Oka, F. and Murase, T., "Liquefaction Analysis of Sand Deposits Based on Cyclic Elasto-Plasticity," International Conference on Recent Advances in Geotechnical Earthquake Engineering and Soil

Dynamics, Edited by Prakash, S., Vol. 1, 1981, pp. 151-154.

26. Ozgur, D. and Gulpinar, A., "A Theoretical Simulation of Earthquake Acceleration Spectra," Proceedings of the 5th World Conference on Earthquake Engineering, Rome, Vol. 1, 1974, pp. 1284-1293.
27. Penzien, J., "Applications of Random Vibration Theory," Earthquake Engineering, Robert Wiegel, editor, pp. 867-923.
28. Robson, J.D., An Introduction to Random Vibration, Edinburgh University Press, Edinburgh, United Kingdom, 1964.
29. Rucker, W., "Measurement and Evaluation of Random Vibrations," Proceedings of DSMR 77, Vol. 1, September, 1977, pp. 407-421.
30. Seed, H.B. and Idriss, I.M., "Analysis of Soil Liquefaction: Niigata Earthquake," Journal of the Soil Mechanics and Foundations Division, ASCE, Vol. 93, No. SM3, May, 1967, pp. 83-108.

31. Seed, H.B., Mori, K. and Chan, C.K., "Influence of Seismic History on Liquefaction of Sands," Journal of the Geotechnical Engineering Division, ASCE, Vol. 103, No. GT4, April, 1977 pp. 257-270.
32. Shen, C.K., Harder, L.F., Vrymoed, J.L. and Bennett, W.J., "Dynamic Response of a Sand Under Random Loadings," Proceedings of the Geotechnical Engineering Division, Specialty Conference on Earthquake Engineering and Soil Dynamics, ASCE, Vol. 2, June, 1978, pp. 852-863.
33. Sherif, M.A. and Ishibashi, I., "A Rational Theory for Predicting Soil Liquefaction," Journal of Soil Dynamics and Earthquake Engineering, Vol. 1, No. 1, 1982, pp. 20-29.
34. Shibata, T., Yokitomo, H. and Miyoshi, M., "Liquefaction Process of Sand During Cyclic Loading," Soils and Foundations, Vol. 12, No. 1, March, 1972, pp. 1-16.
35. Shinozuka, M., "Digital Simulation of Ground Accelerations," Proceedings of the 5th World Conference on Earthquake Engineering, Rome, Vol. 2, 1974, pp. 2829-2838.

36. Silver, M.L., Chan, C.K., Ladd, R.S., Lee, K.L., Tiedemann, D.A., Townsend, F.C., Valera, J.E., and Wilson, J.H., "Cyclic Triaxial Strength of Standard Test Sand," Journal of the Geotechnical Engineering Division, ASCE, Vol. 102, No. GT5, May, 1976, pp. 511-523.
37. Townsend, F.C., "A Review of Factors Affecting Cyclic Triaxial Tests," Special Technical Pub. No. 654, Symposium on Dynamic Geotechnical Testing, ASTM, 1978, pp. 356-383.
38. Wolfe, W.E., Sandhu, R.S. and Amato, V.E., "Preliminary Tests on Liquefaction of Ottawa Sand," Report to the Air Force of Scientific Research, Geotechnical Report No. 19, The Department of Civil Engineering, The Ohio State University, Columbus, Ohio, 1986.
39. Wong, R.T., Seed, H.B. and Chan, C.K., "Cyclic Loading Liquefaction of Gravelly Soils," Journal of the Geotechnical Engineering Division, ASCE, Vol. 101, No. GT6, June, 1975, pp. 571-583.

APPENDIX A
TIME HISTORIES OF SAMPLE PORE WATER PRESSURE CHANGE

The pore water pressure time histories in this appendix are presented in chronological order. Only those pore water pressure transducers which functioned throughout a particular test are included. When possible (because of the number of operative transducers or clarity of presentation) transducers from a particular test are also combined onto a single graph to facilitate comparison. The orientation of each pore water pressure transducer (PT) in the sample test chamber is illustrated below.

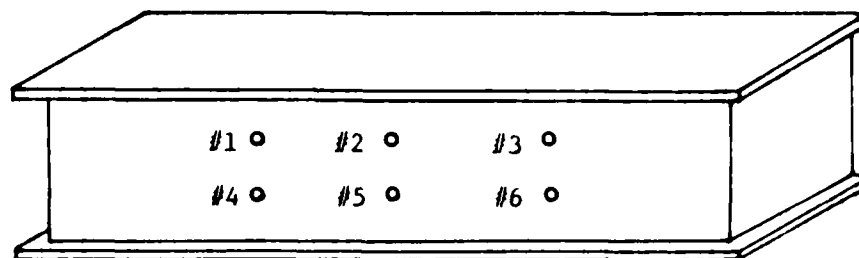
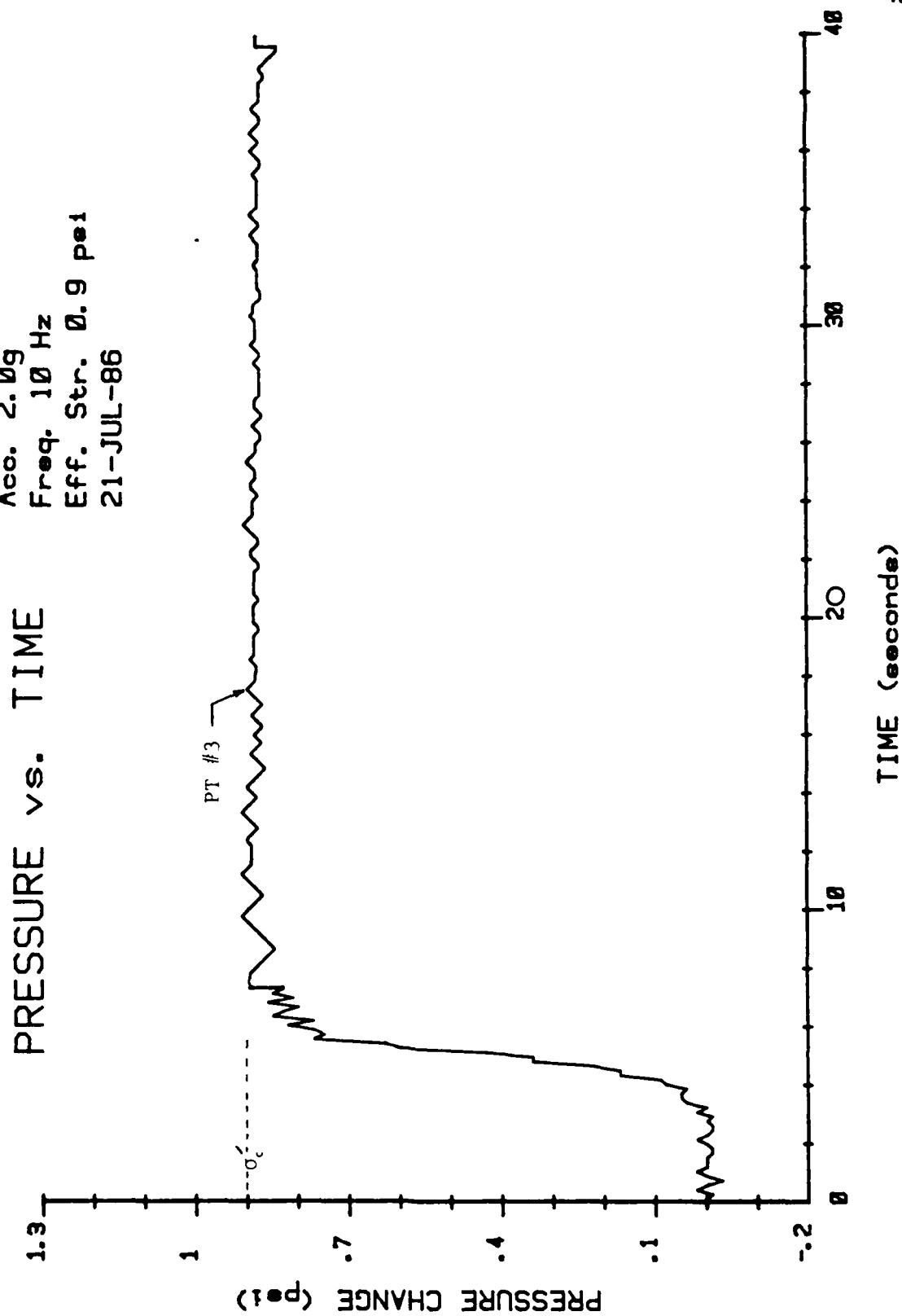


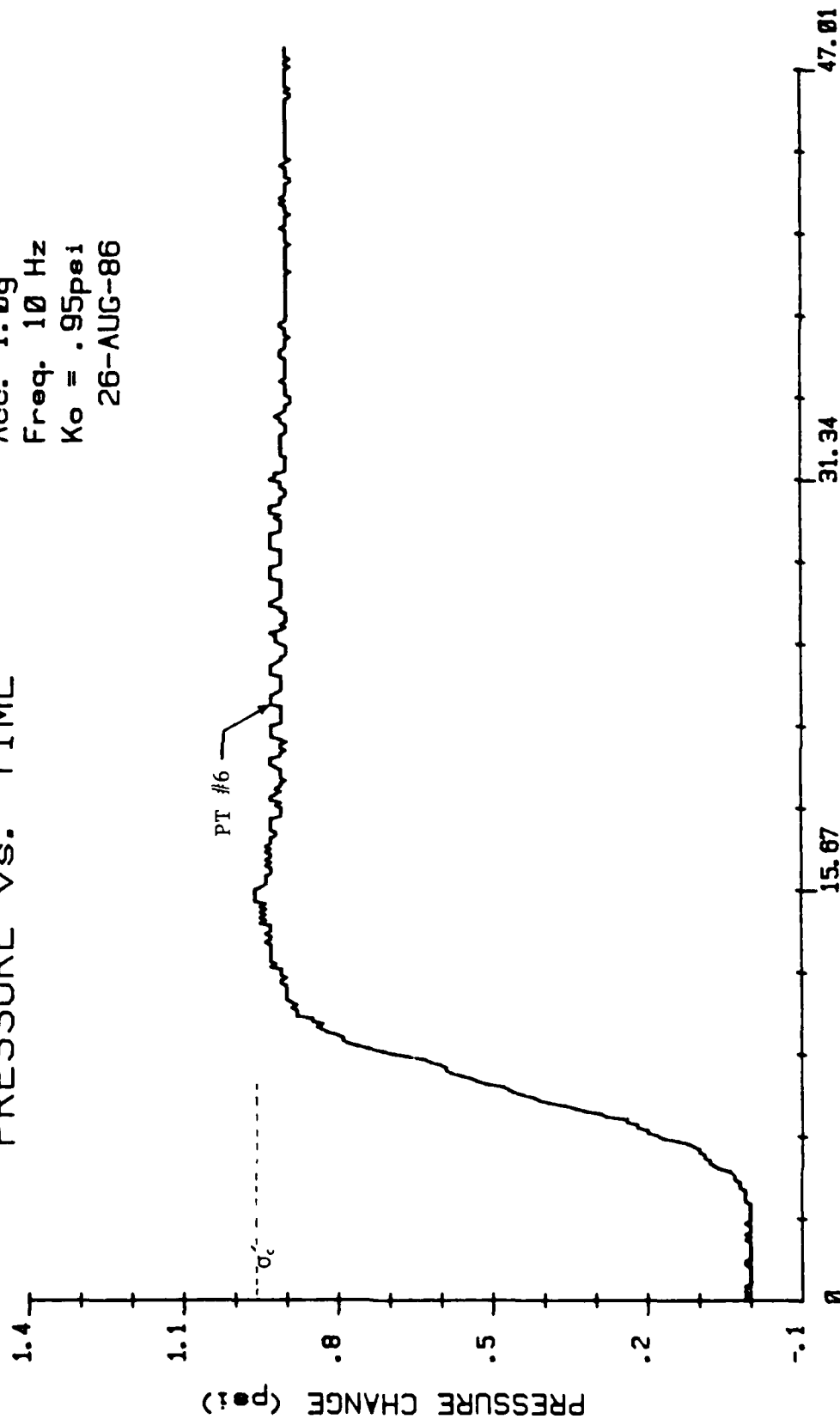
FIGURE A.1 PORE WATER PRESSURE TRANSDUCER ORIENTATION

Aco. 2.0g
Freq. 10 Hz
Eff. Str. 0.9 psi
21-JUL-86



PRESSURE vs. TIME

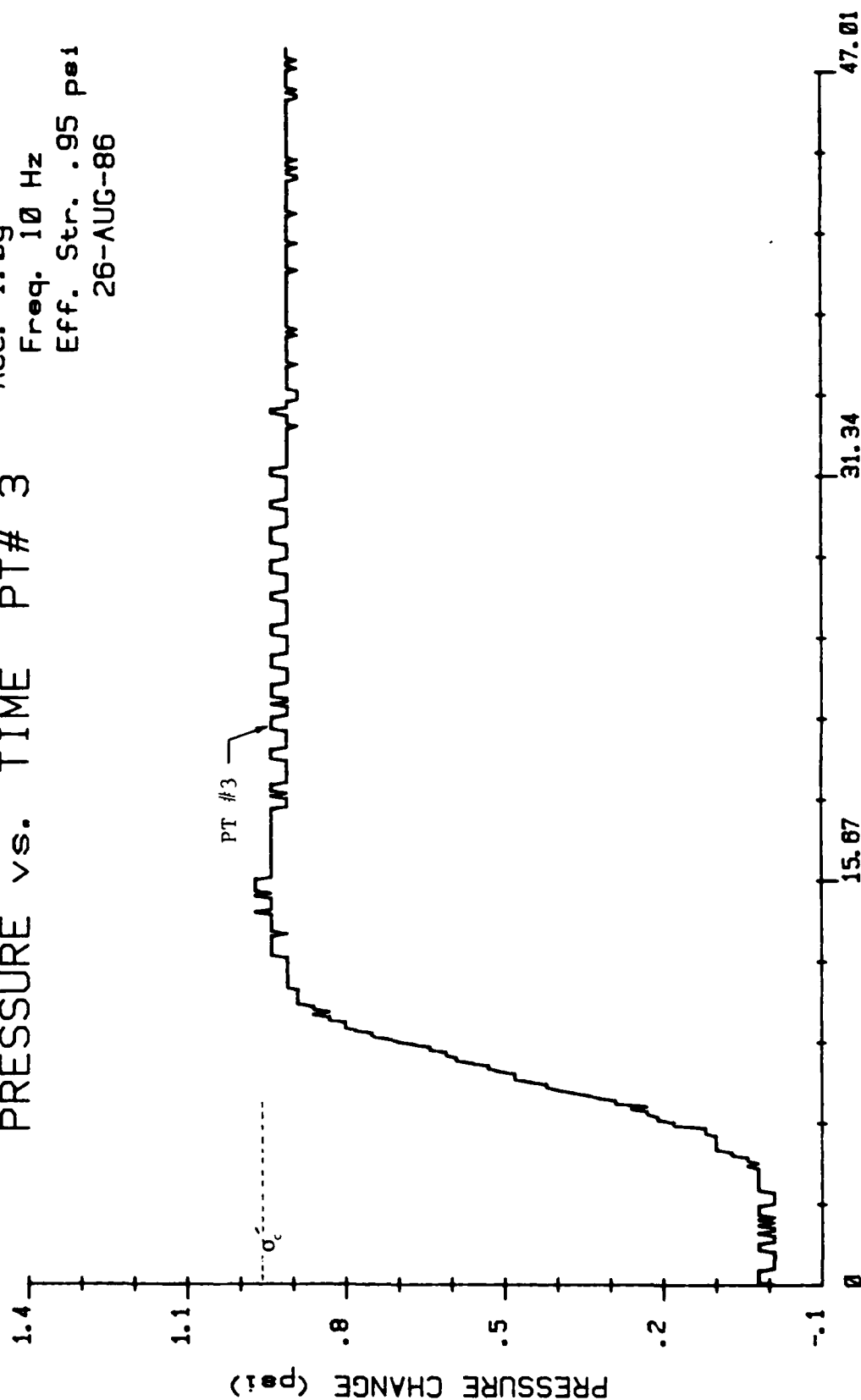
Acc. 1.0g
Freq. 10 Hz
Ko = .95pei
26-AUG-86



TIME (seconds)

Acc. 1.0g
Freq. 10 Hz
Eff. Str. .95 psi
26-AUG-86

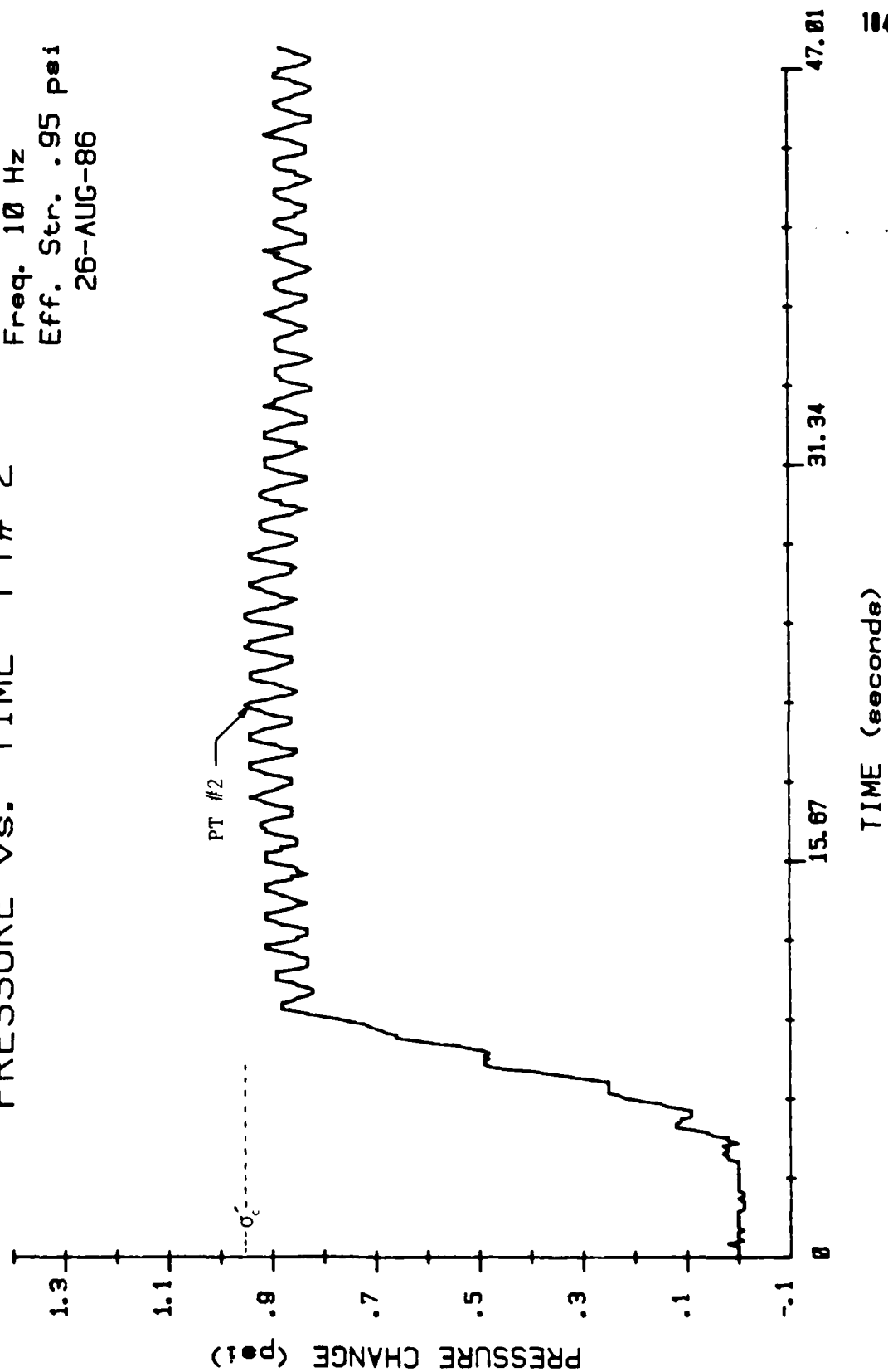
PRESSURE vs. TIME PT# 3



TIME (seconds)

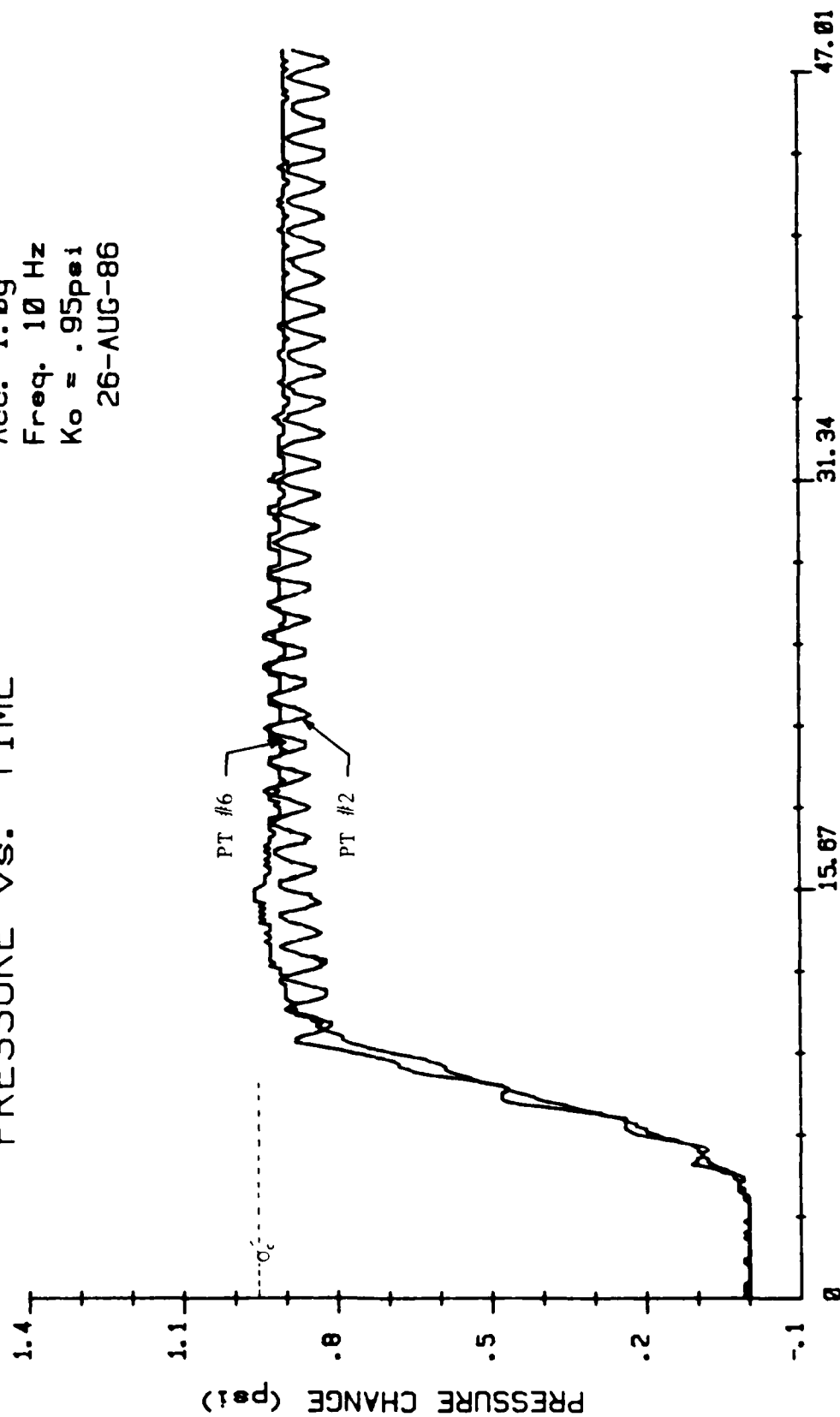
Acc. 1.0g
Freq. 10 Hz
Eff. Str. .95 psi
26-AUG-86

PRESSURE vs. TIME PT# 2



PRESSURE vs. TIME

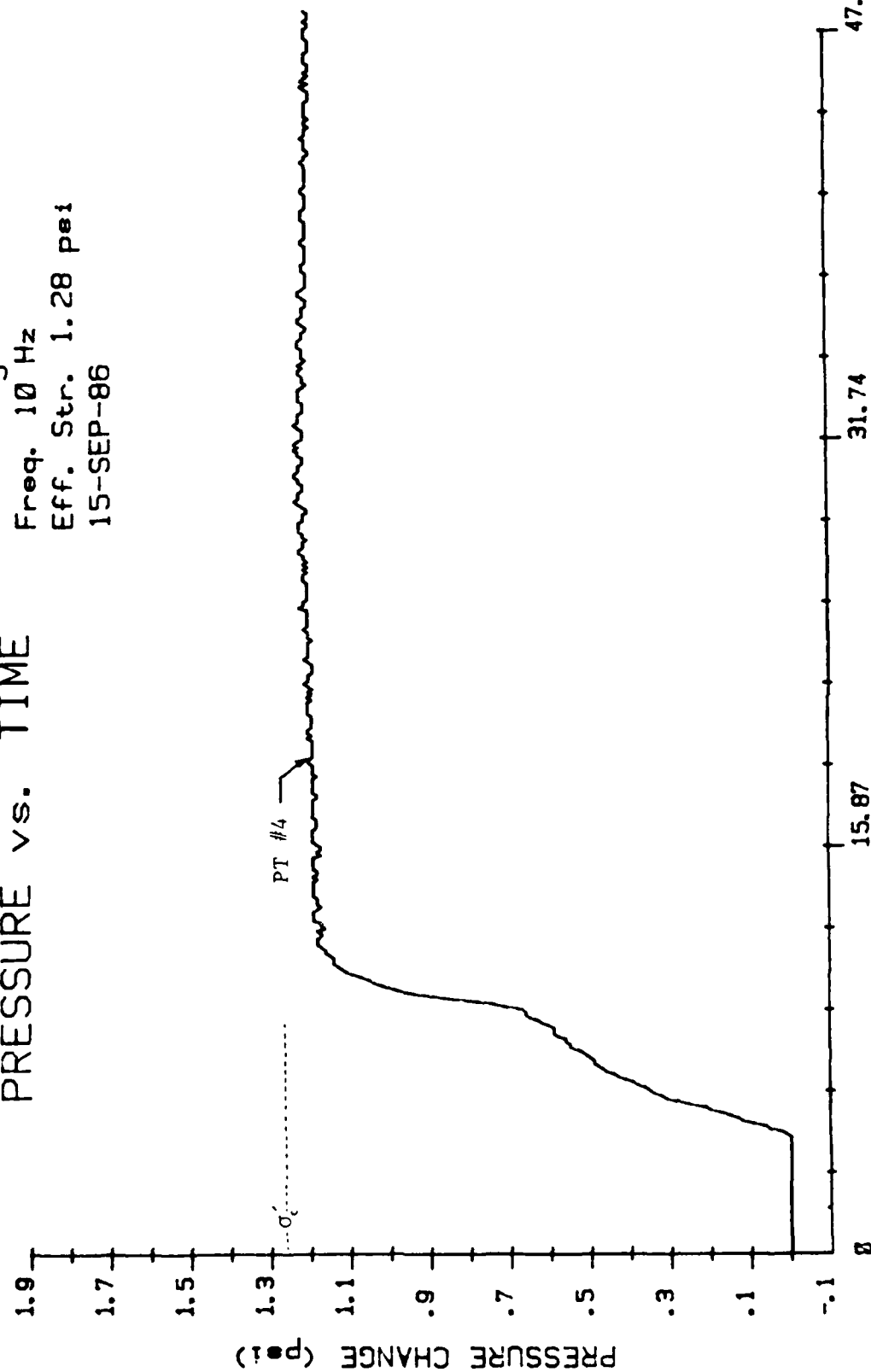
Acc. 1.0g
Freq. 10 Hz
Ko = .95psi
26-AUG-86



TIME (seconds)

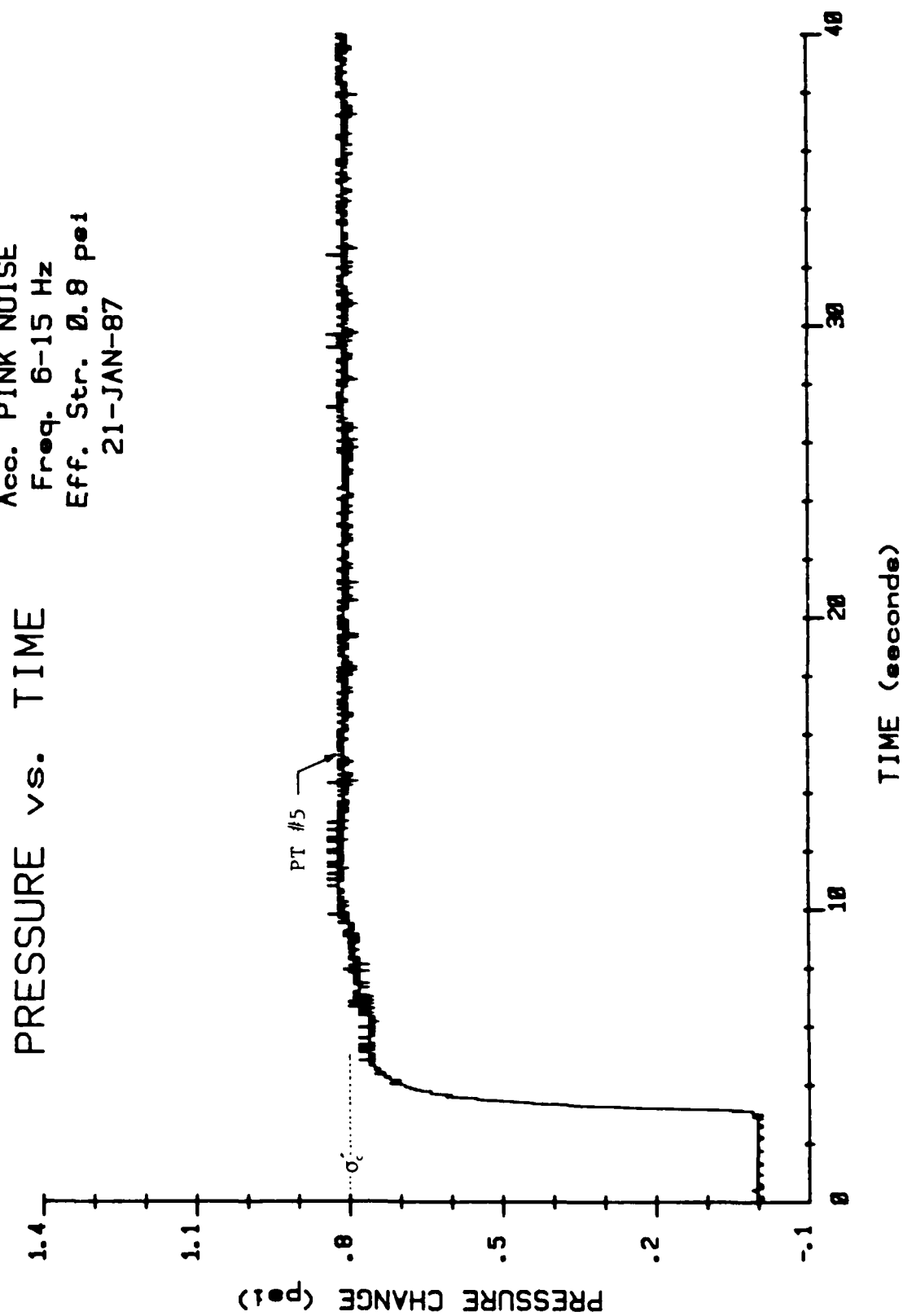
Acc. 1.3g
Freq. 10 Hz
Eff. Str. 1.28 psi
15-SEP-86

PRESSURE vs. TIME

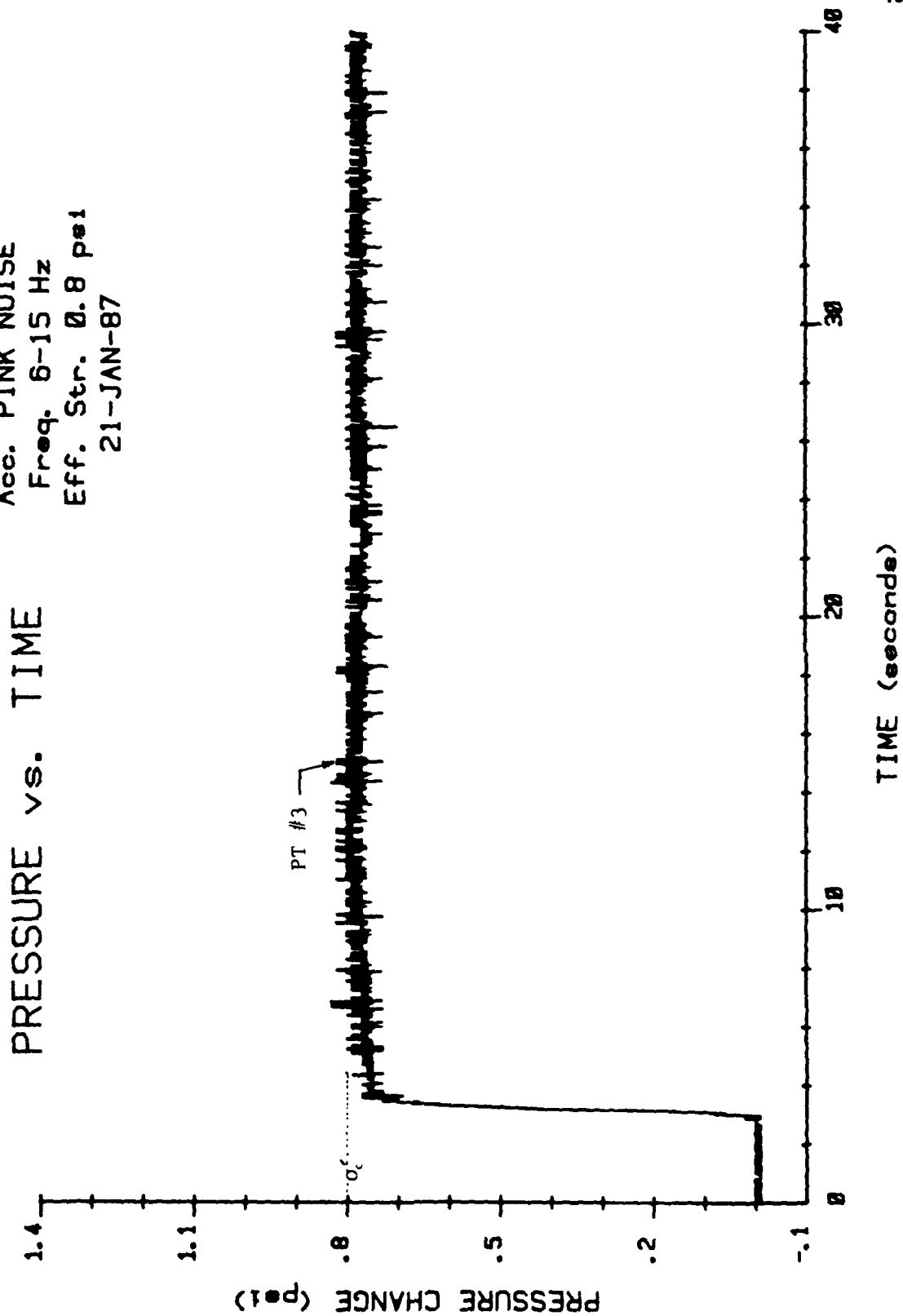


TIME (seconds)

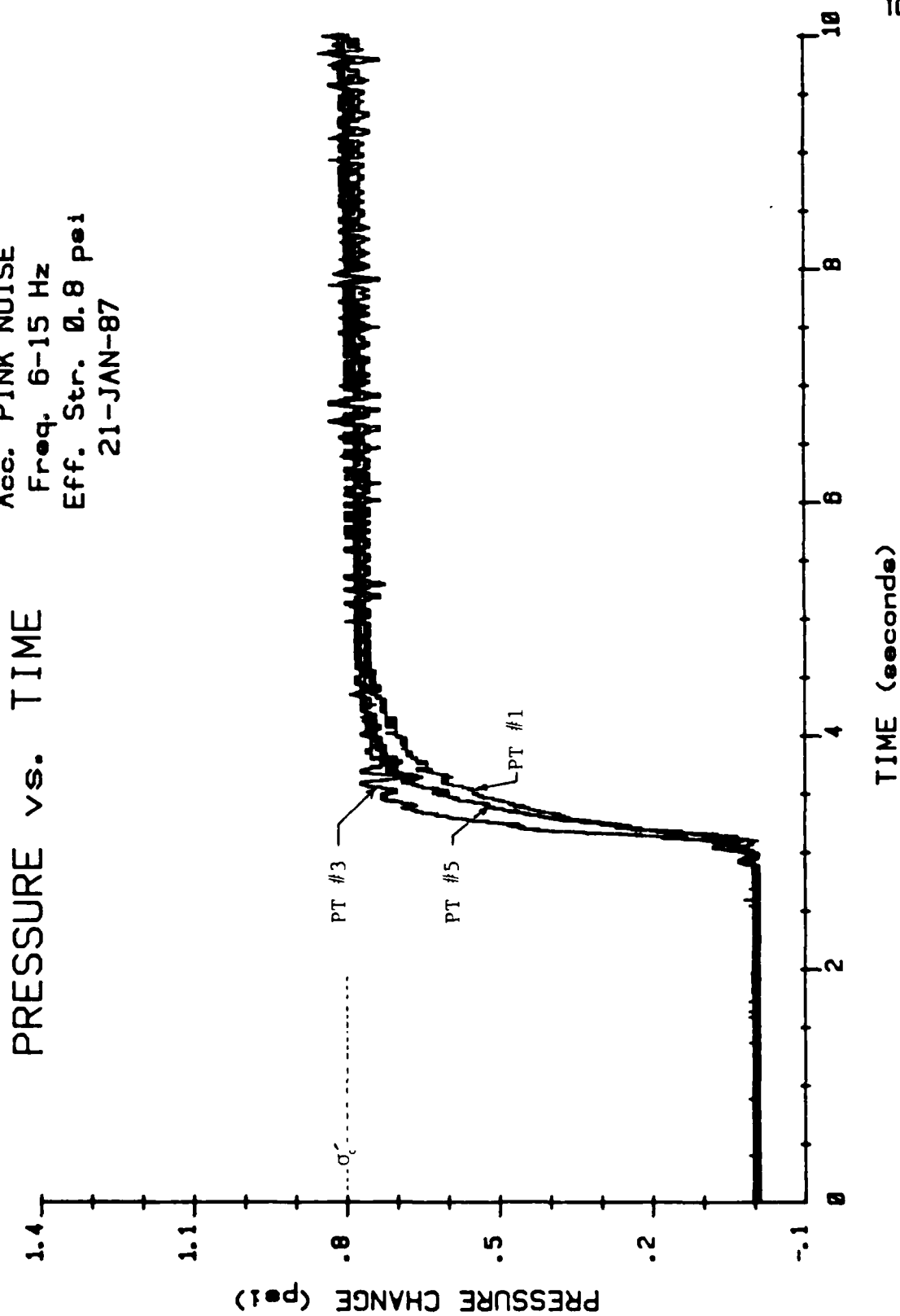
Acc. PINK NOISE
Freq. 6-15 Hz
Eff. Str. 0.8 psi
21-JAN-87



Acc. PINK NOISE
Freq. 6-15 Hz
Eff. Str. 0.8 psi
21-JAN-87

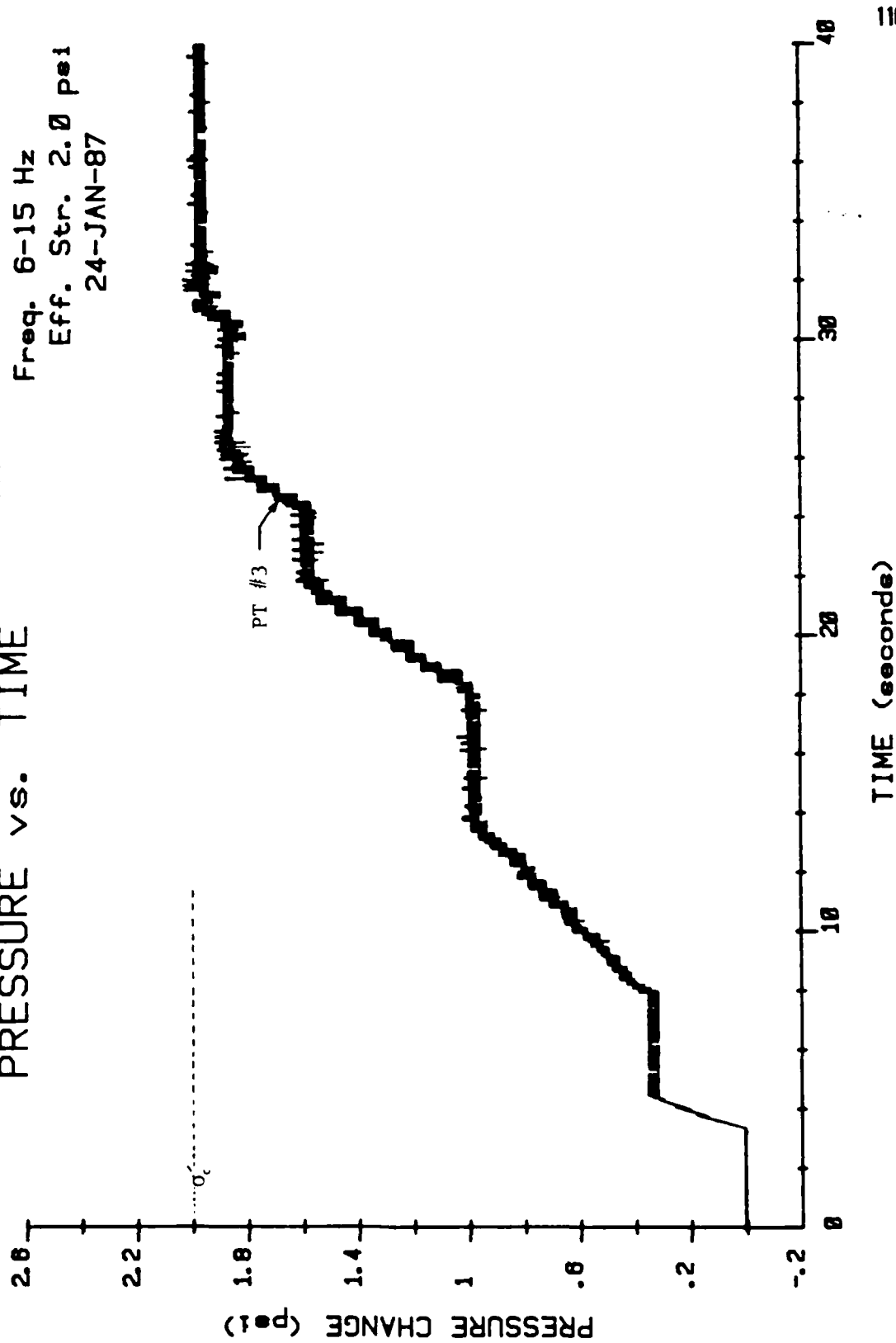


Acc. PINK NOISE
Freq. 6-15 Hz
Eff. Str. 0.8 psi
21-JAN-87

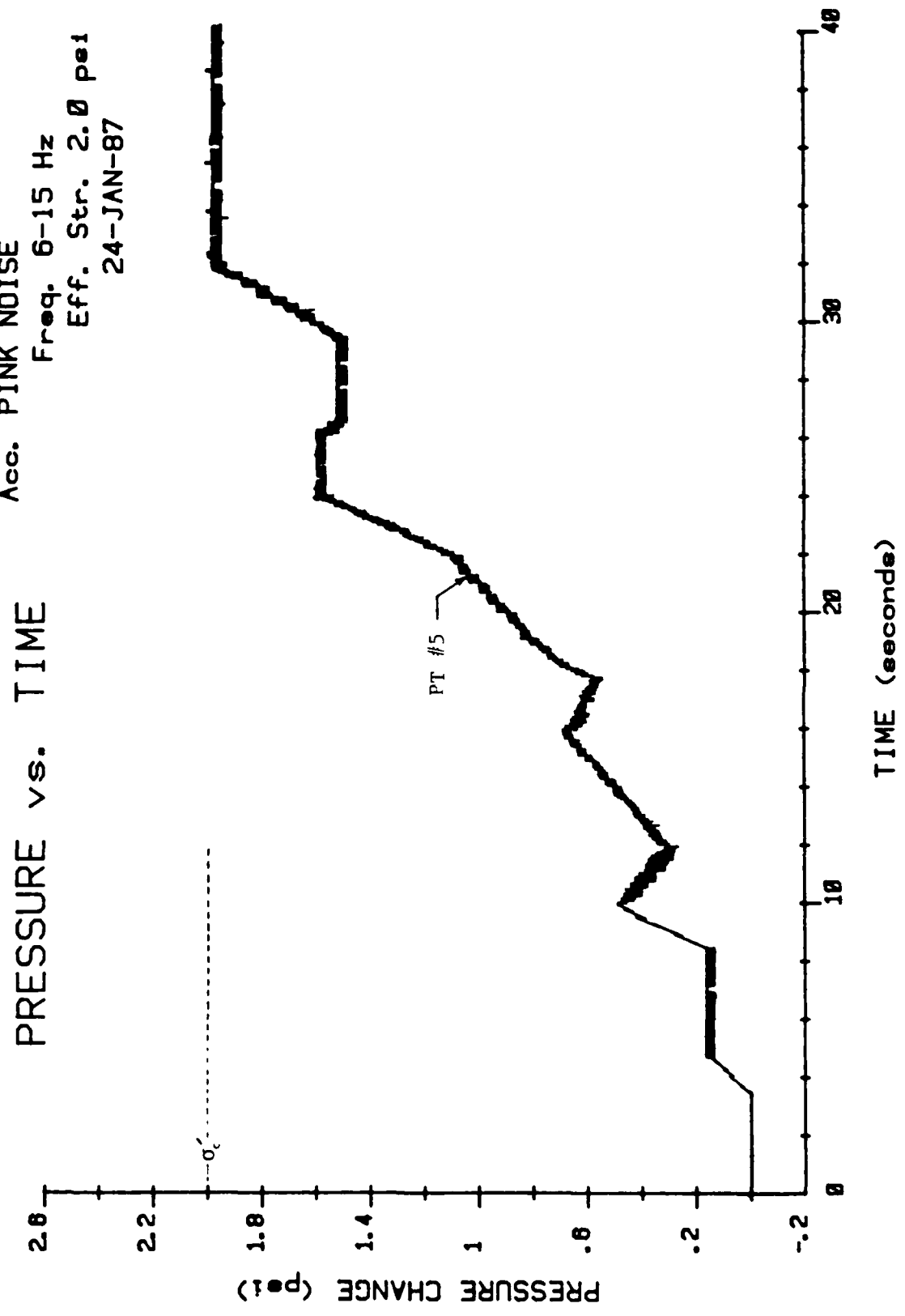


Acc. PINK NOISE
Freq. 6-15 Hz
Eff. Str. 2.0 psi
24-JAN-87

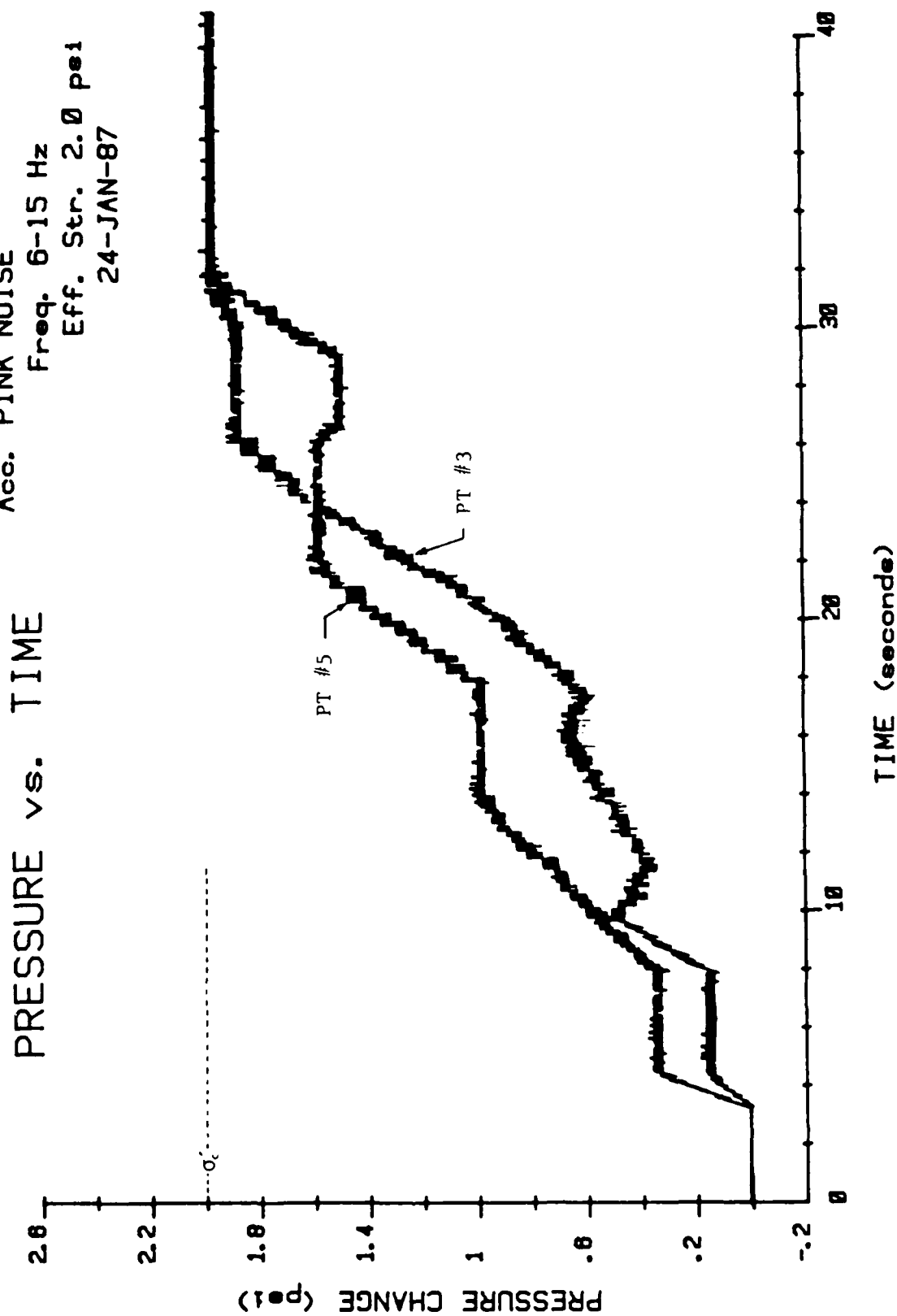
PRESSURE vs. TIME



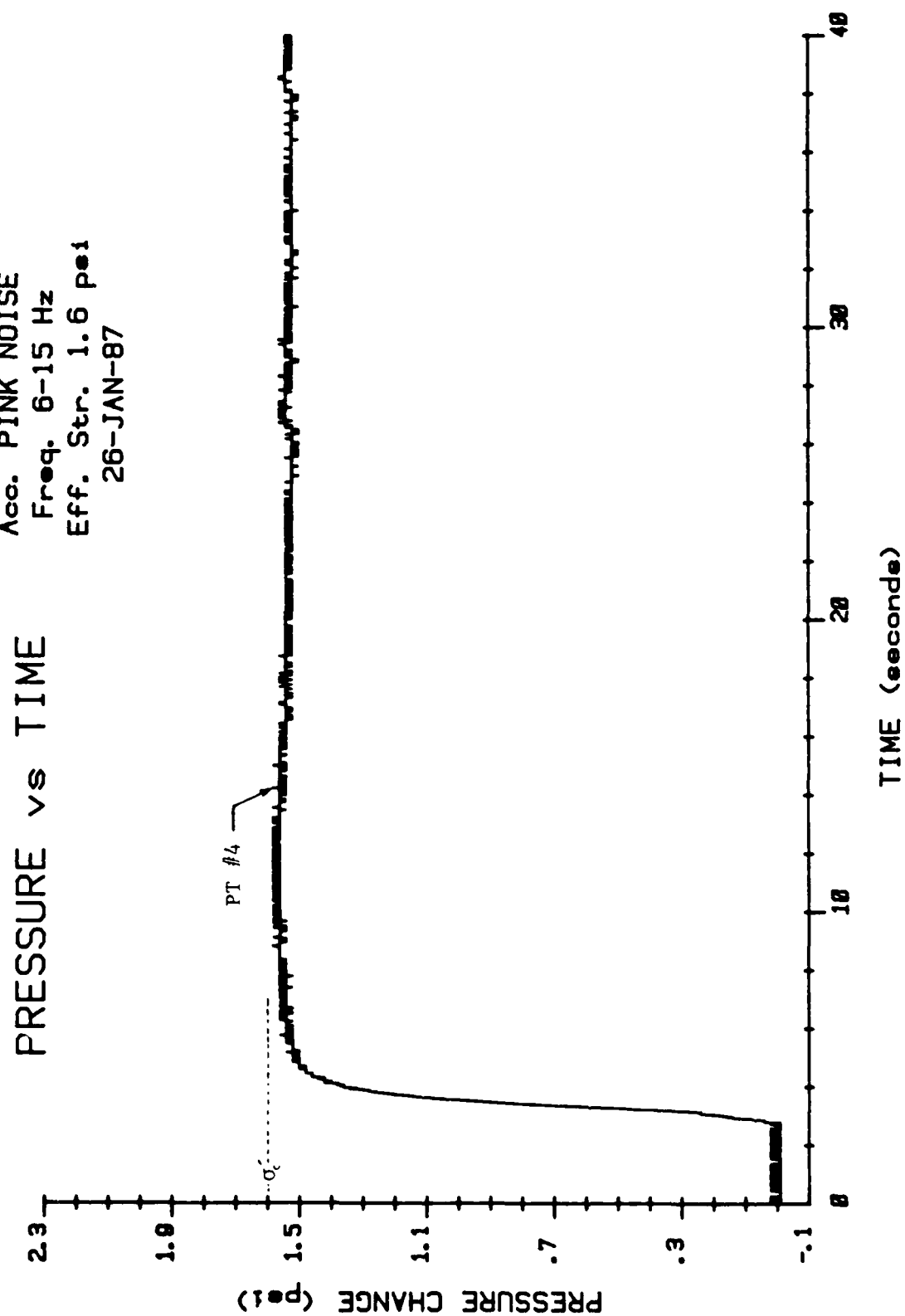
Acc. PINK NOISE
Freq. 6-15 Hz
Eff. Str. 2.0 psi
24-JAN-87

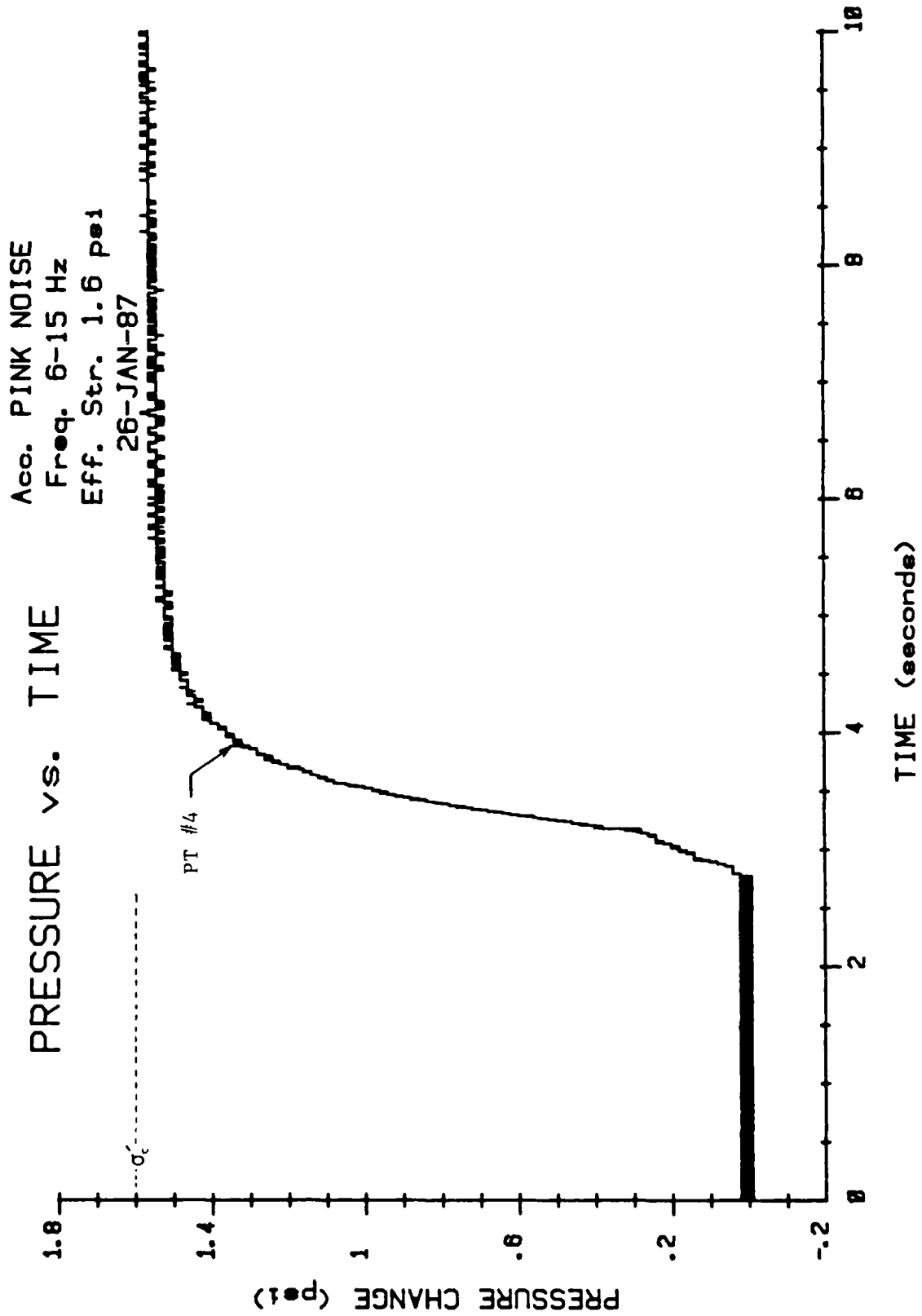


Acc. PINK NOISE
Freq. 6-15 Hz
Eff. Str. 2.0 psi
24-JAN-87

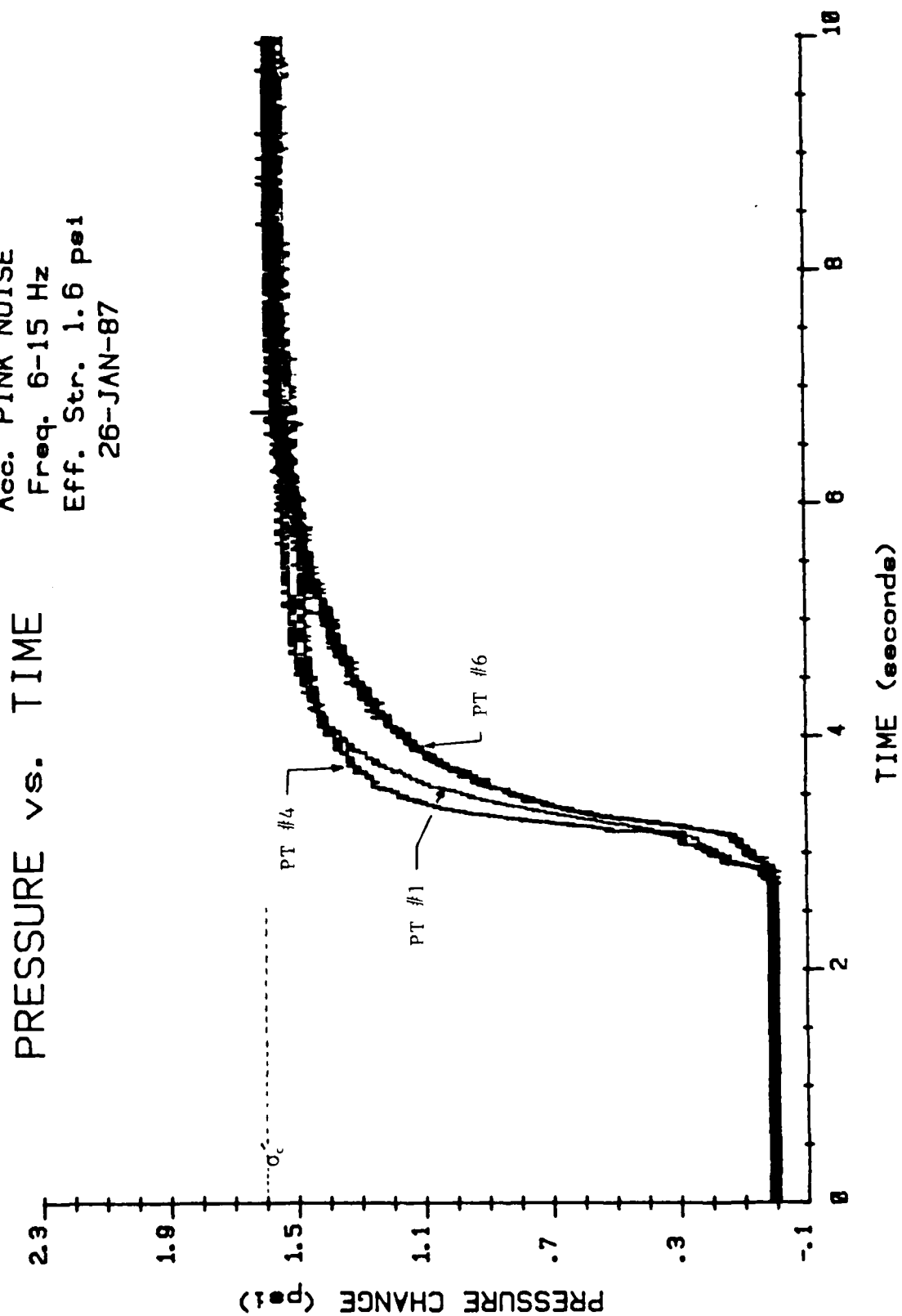


Acc. PINK NOISE
Freq. 6-15 Hz
Eff. Str. 1.6 psi
26-JAN-87



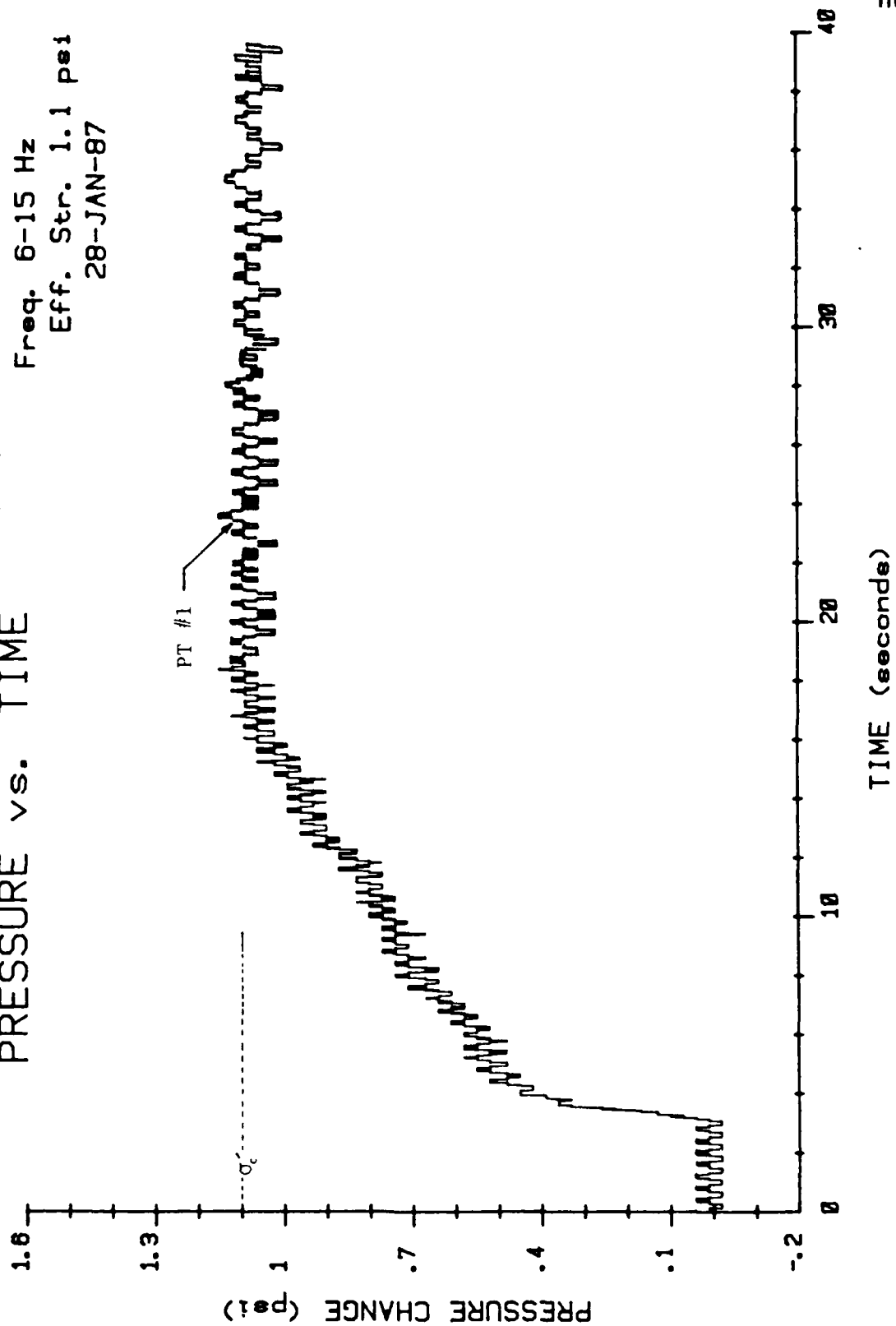


Acc. PINK NOISE
Freq. 6-15 Hz
Eff. Str. 1.6 psi
26-JAN-87

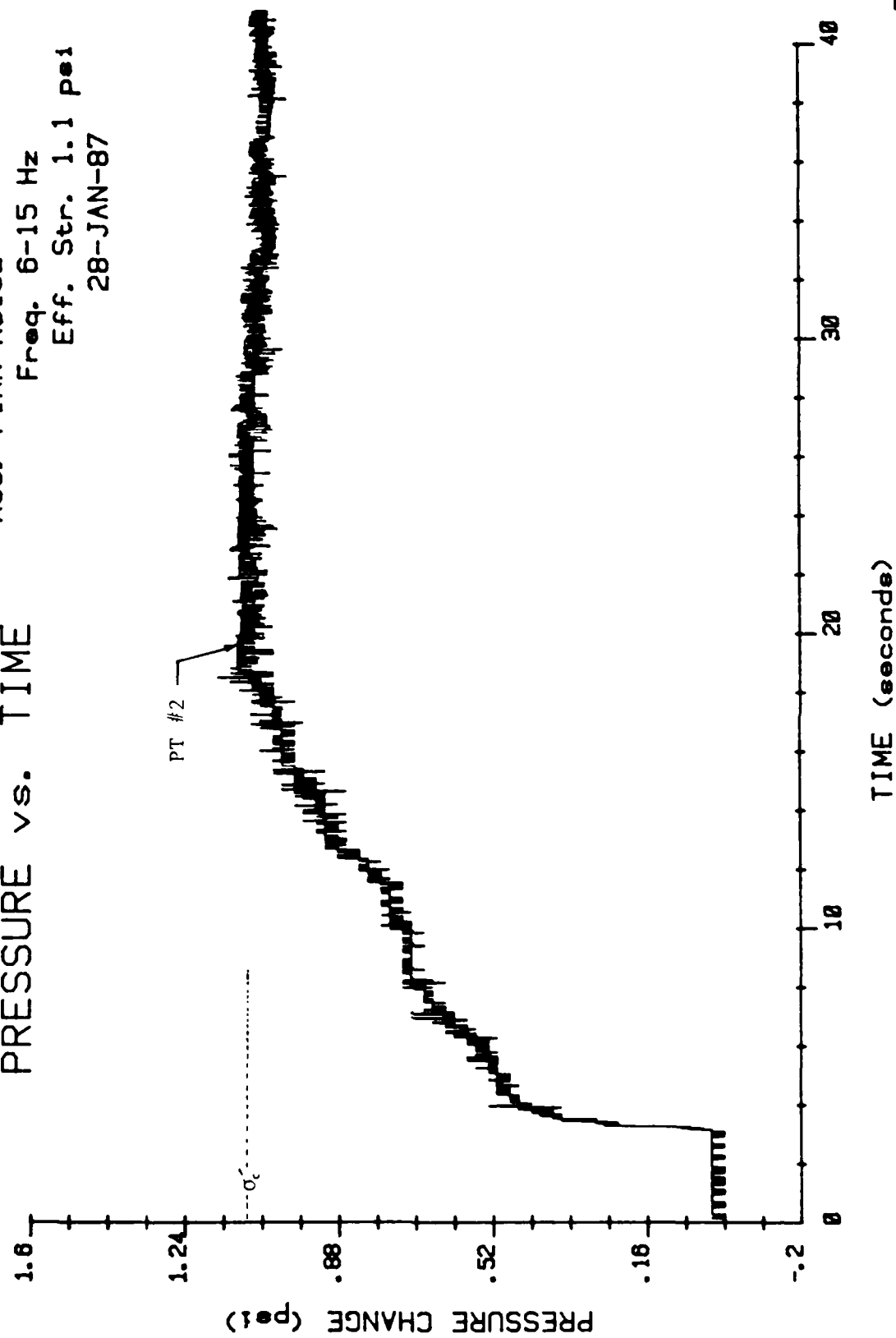


Acc. PINK NOISE
Freq. 6-15 Hz
Eff. Str. 1.1 psi
28-JAN-87

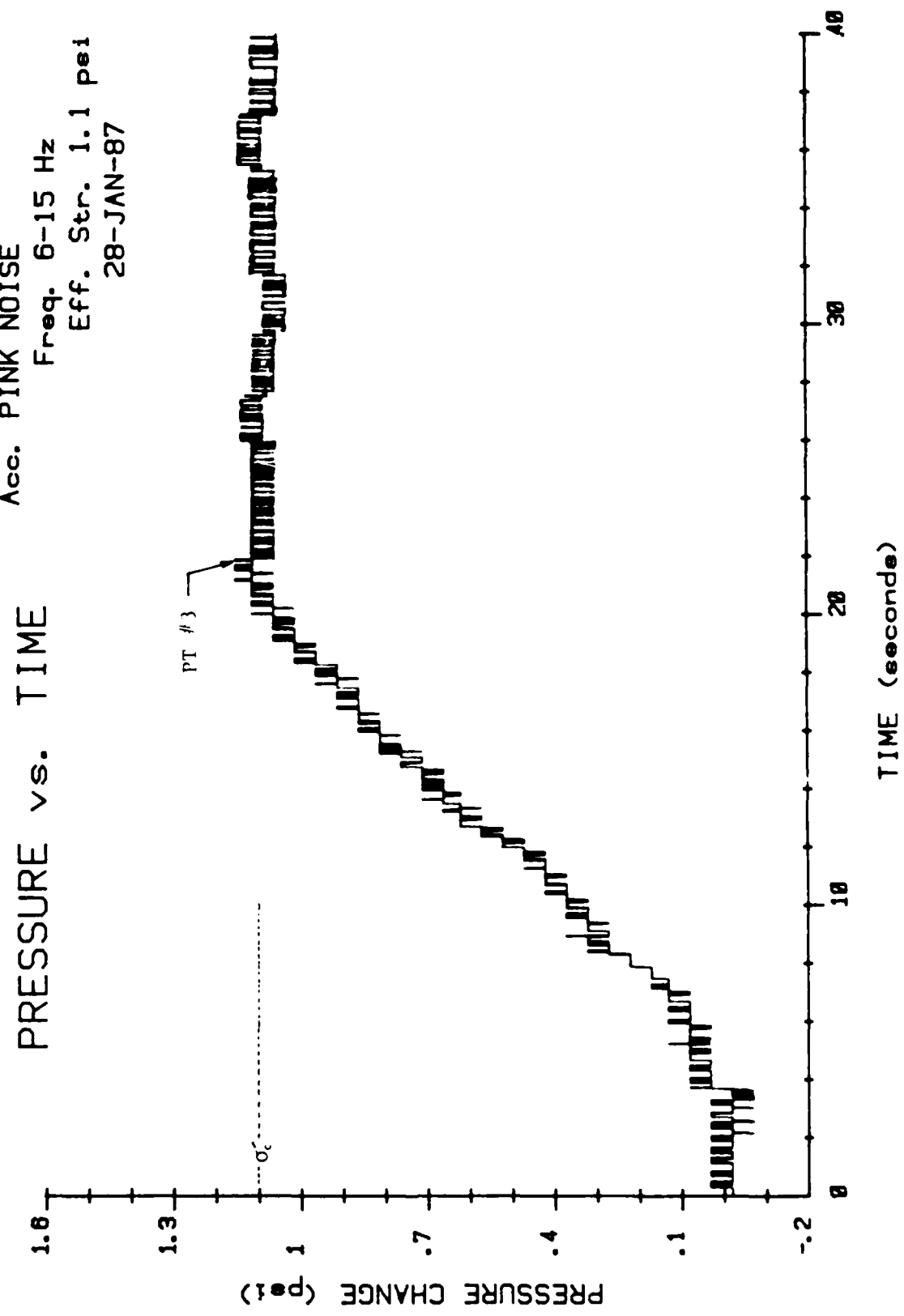
PRESSURE vs. TIME



Acc. PINK NOISE
Freq. 6-15 Hz
Eff. Str. 1.1 psi
28-JAN-87

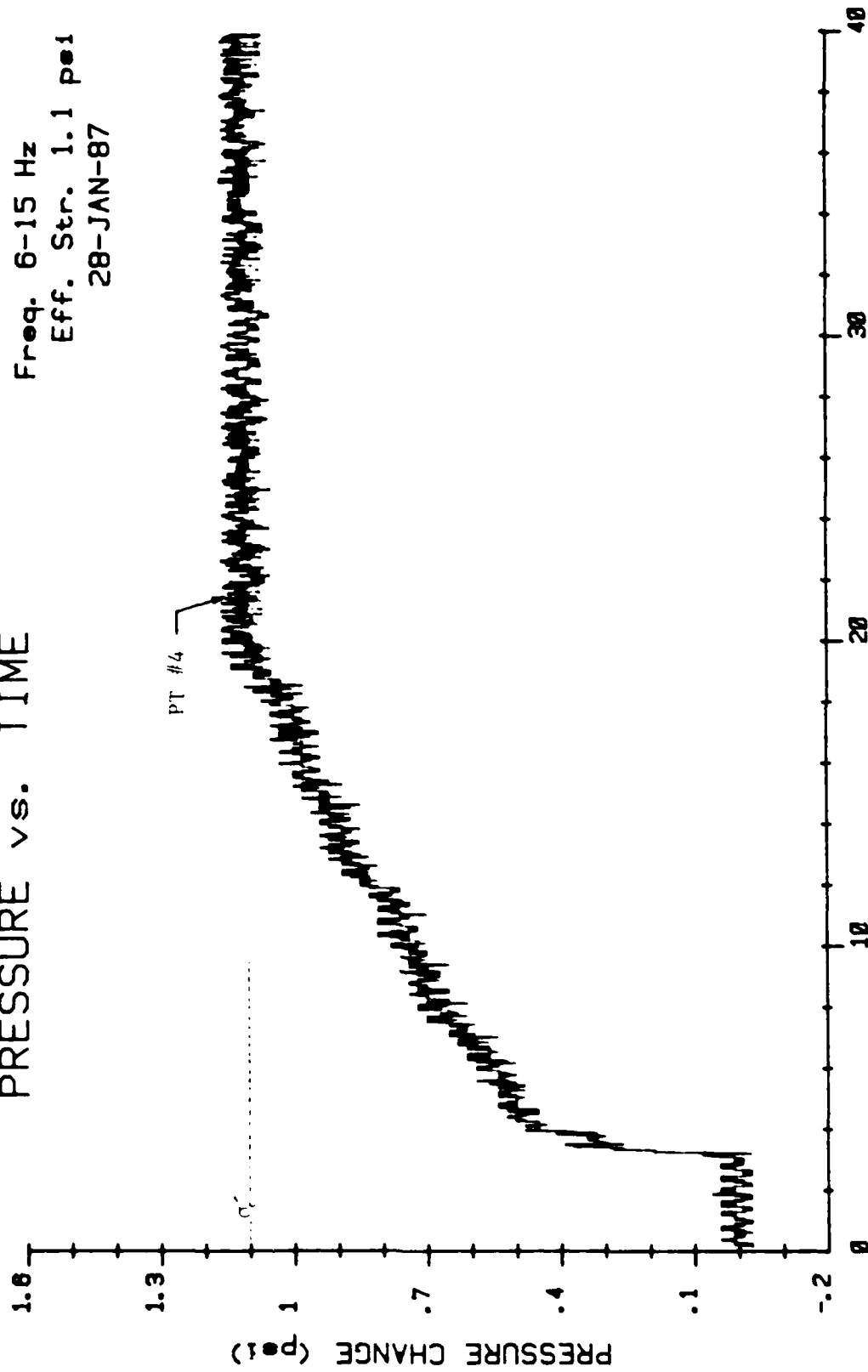


Acc. PINK NOISE
Freq. 6-15 Hz
Eff. Str. 1.1 psi
28-JAN-87



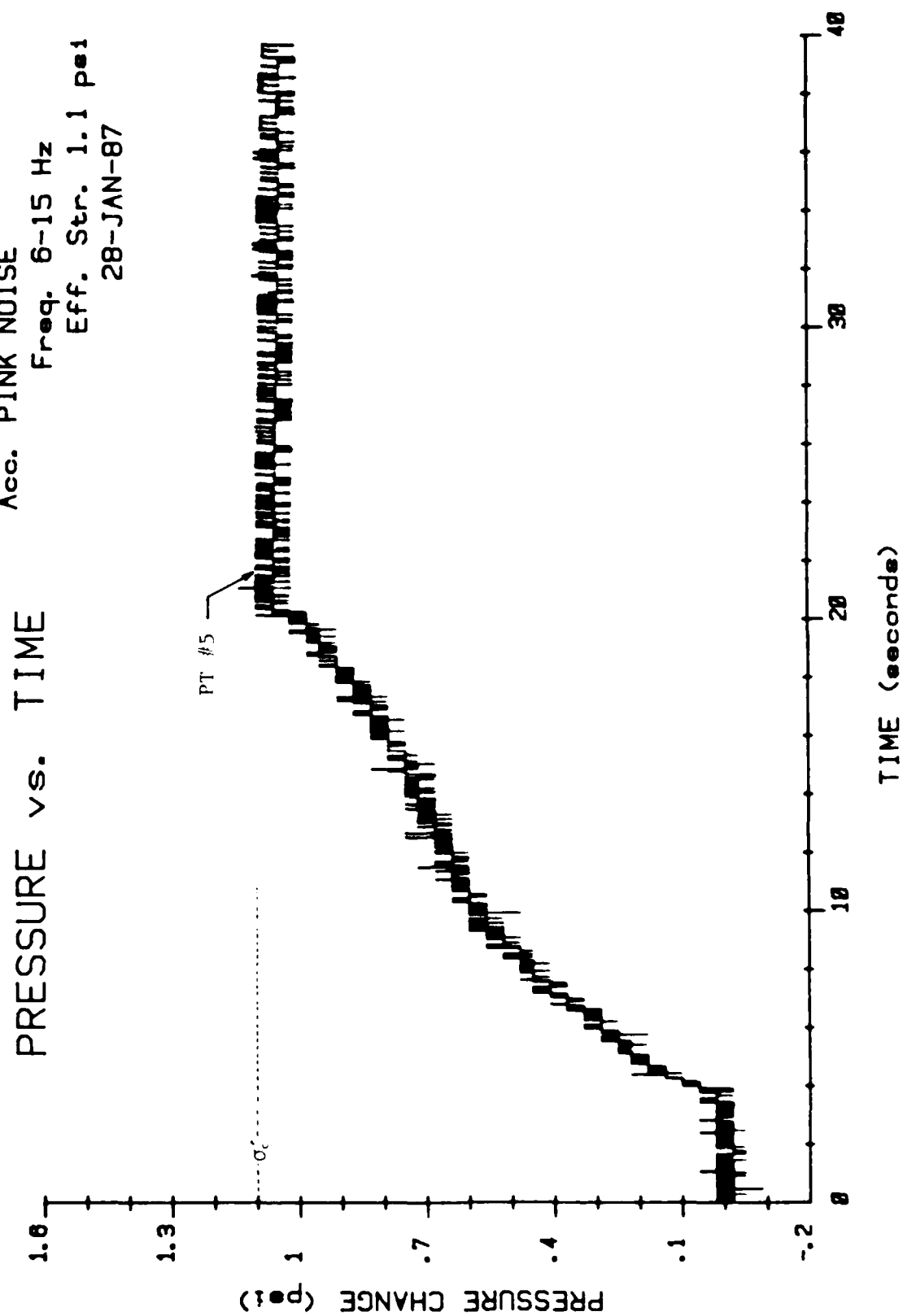
Acc. PINK NOISE
Freq. 6-15 Hz
Eff. Str. 1.1 psi
28-JAN-87

PRESSURE vs. TIME

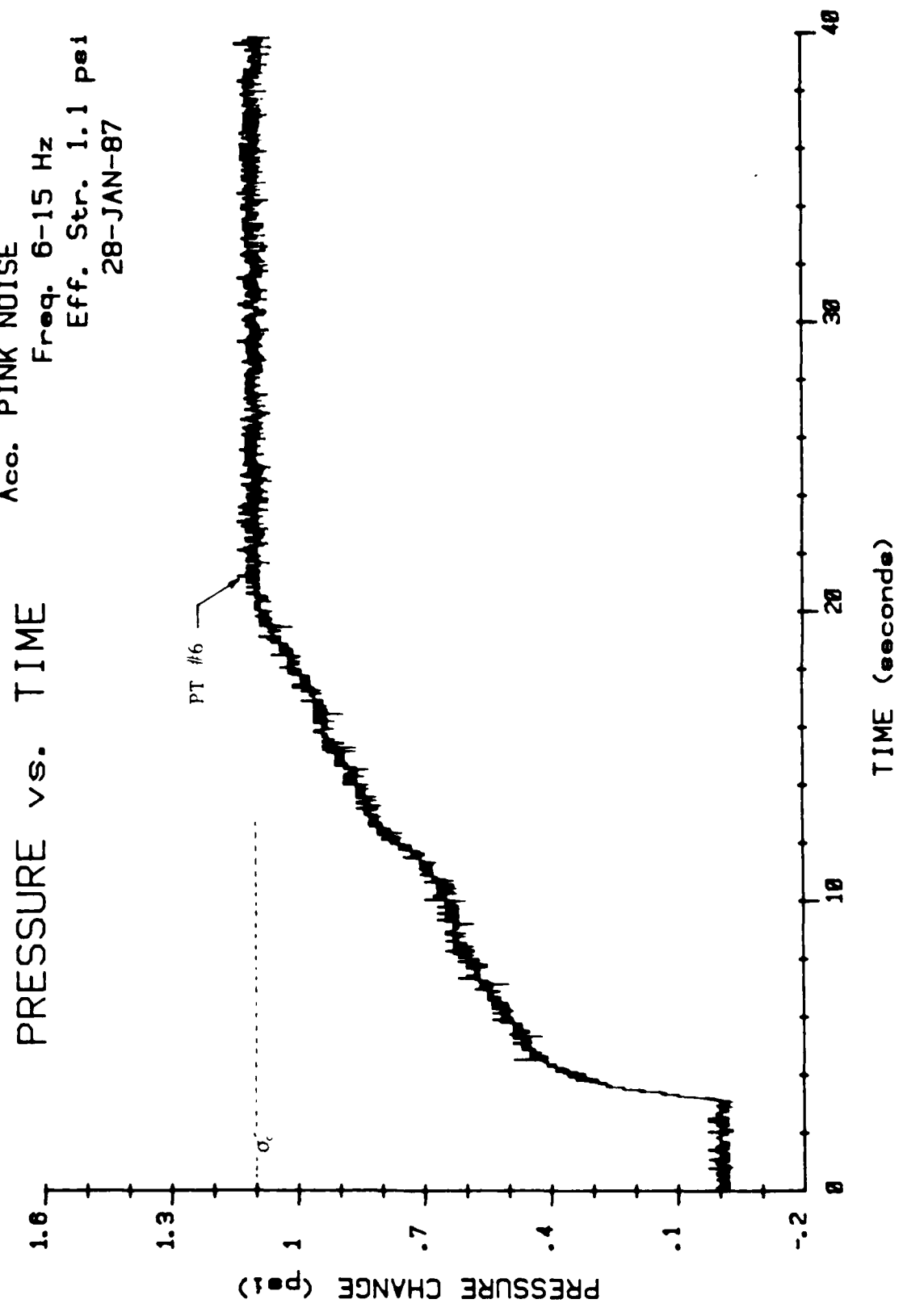


TIME (seconds)

Acc. PINK NOISE
Freq. 6-15 Hz
Eff. Str. 1.1 psi
28-JAN-87



Acco. PINK NOISE
Freq. 6-15 Hz
Eff. Str. 1.1 psi
28-JAN-87



APPENDIX B

TIME HISTORIES OF TABLE AND SAMPLE EXCITATIONS

Time histories of table excitation for every test conducted during this study are included in this appendix. Time histories of sample excitations are also included in this appendix for all tests except Tests A, B2, and C1 where the sample accelerometer failed to collect data.

TABLE EXCITATION

Acc. 2.0g
Freq. 10 Hz
Eff. Str. 0.9 psi
21-JUL-86

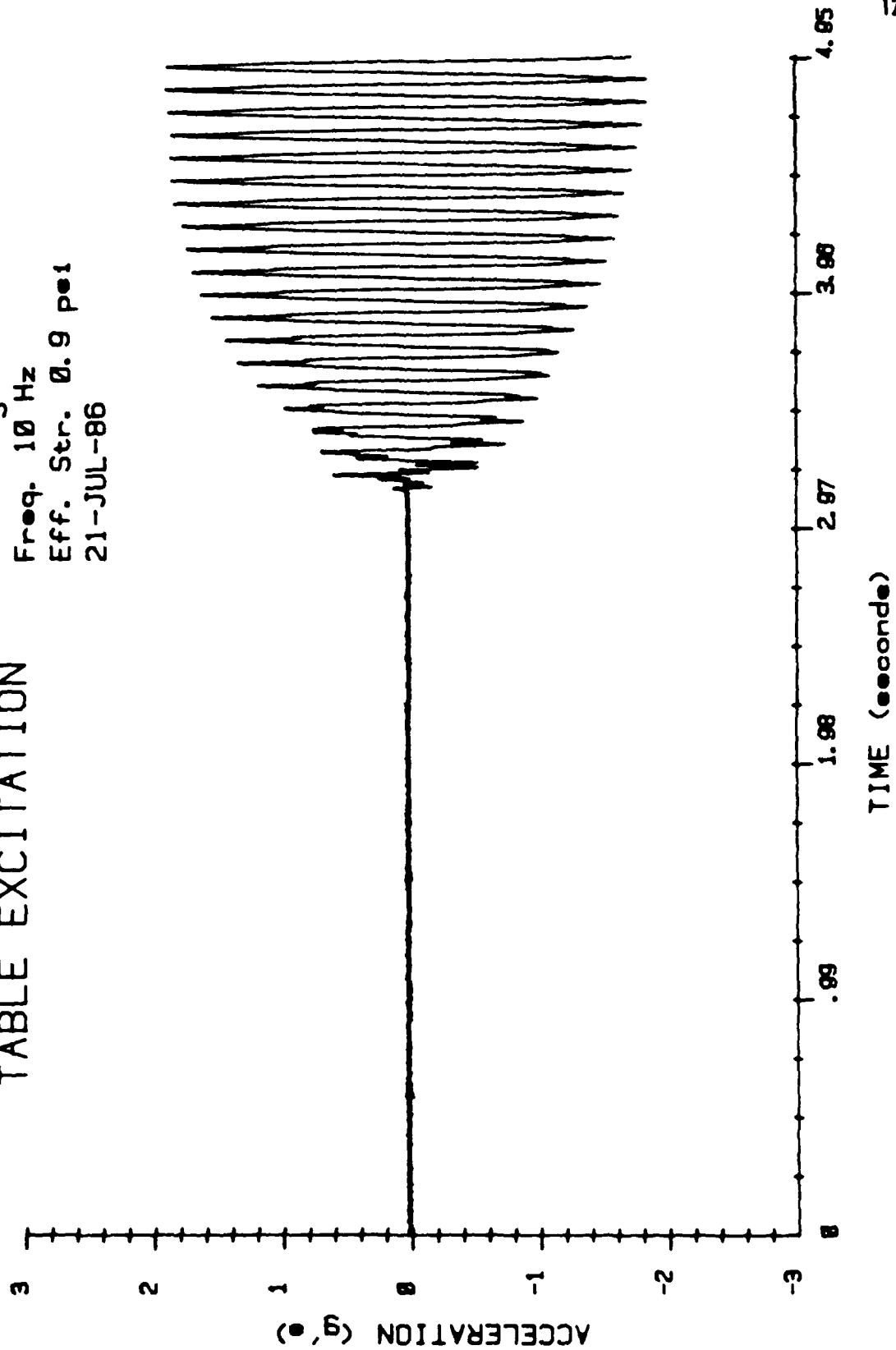


TABLE EXCITATION

Acc. 2.0g
Freq. 10 Hz
Eff. Str. 0.9 psi
21-JUL-86

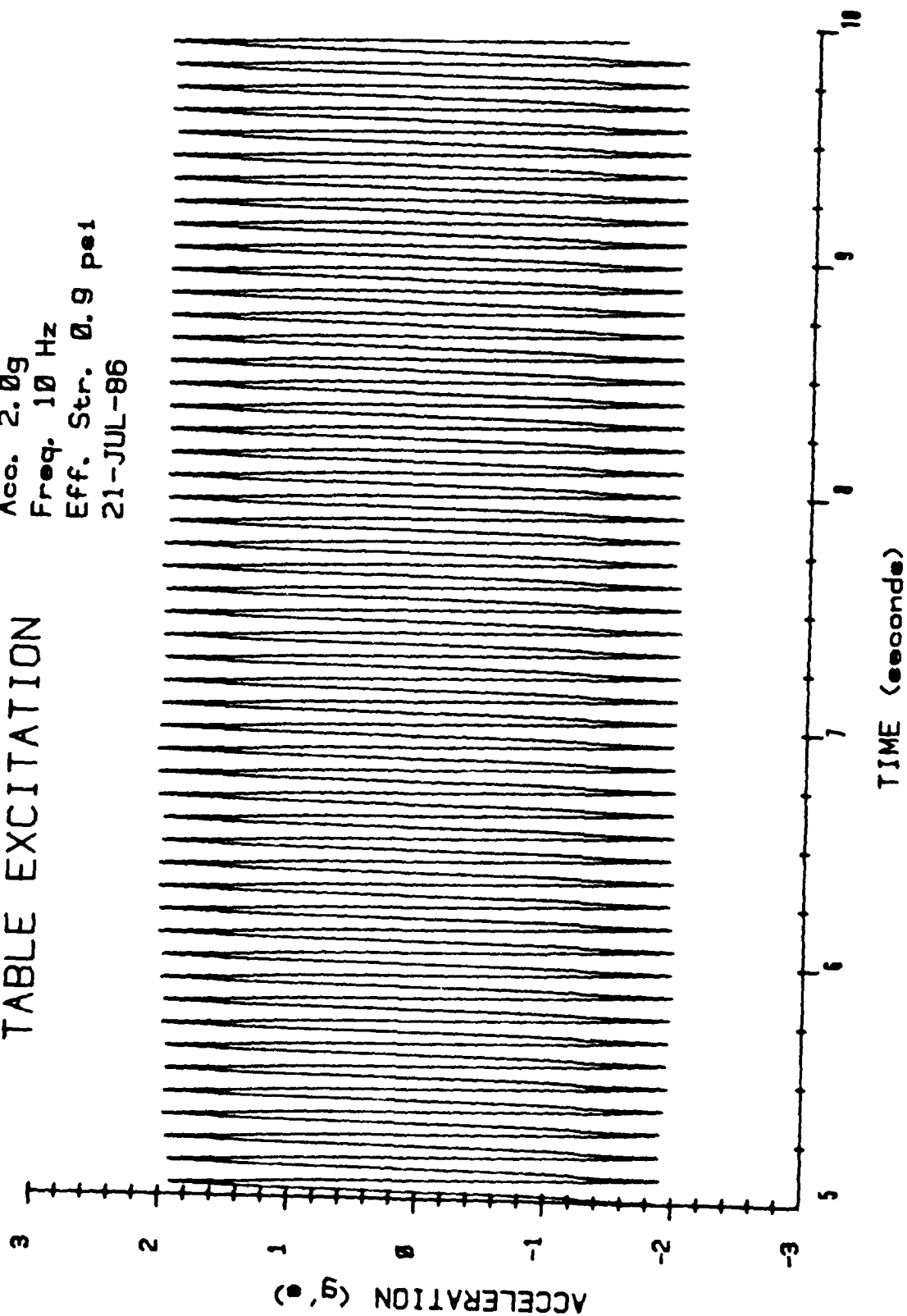
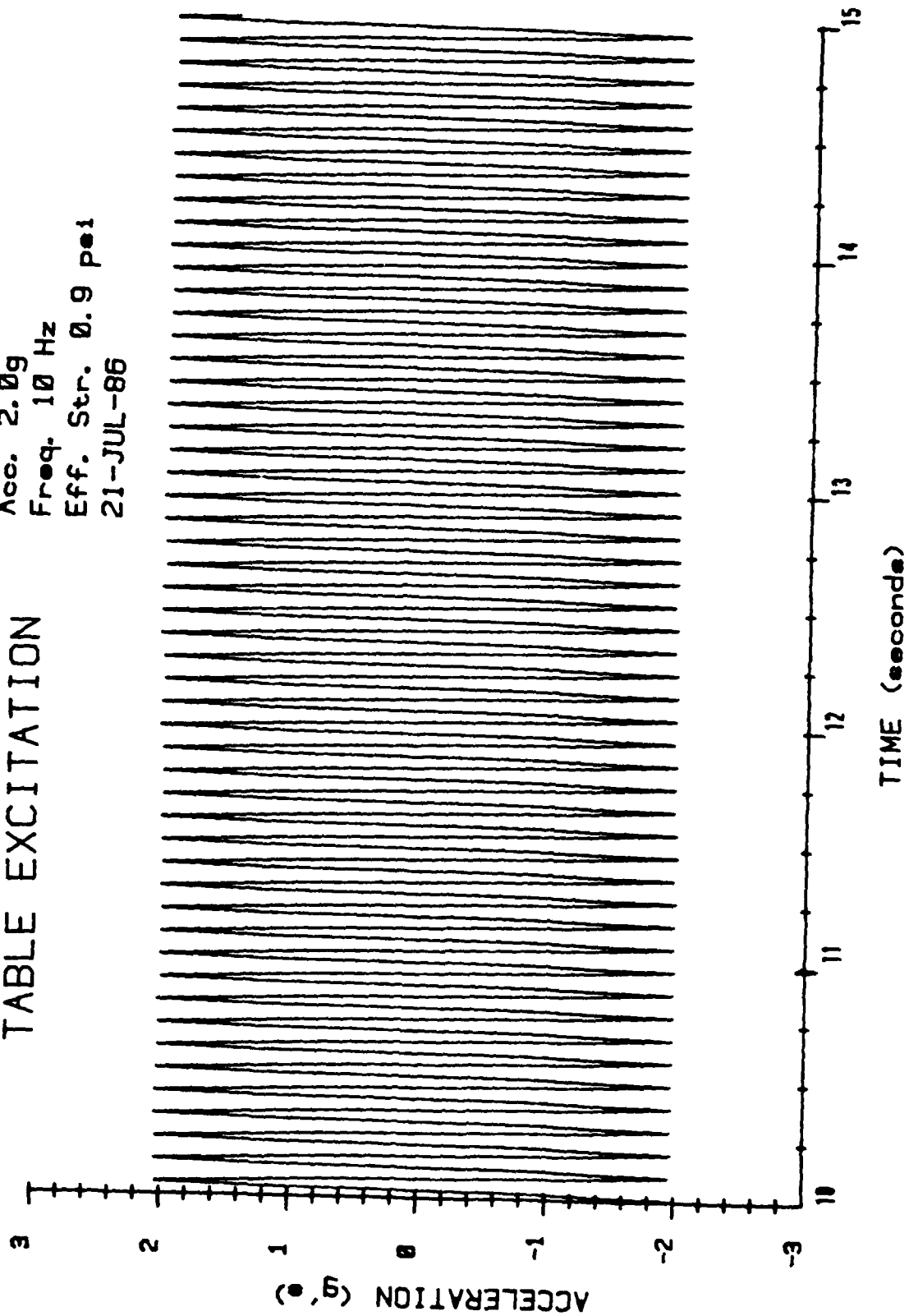


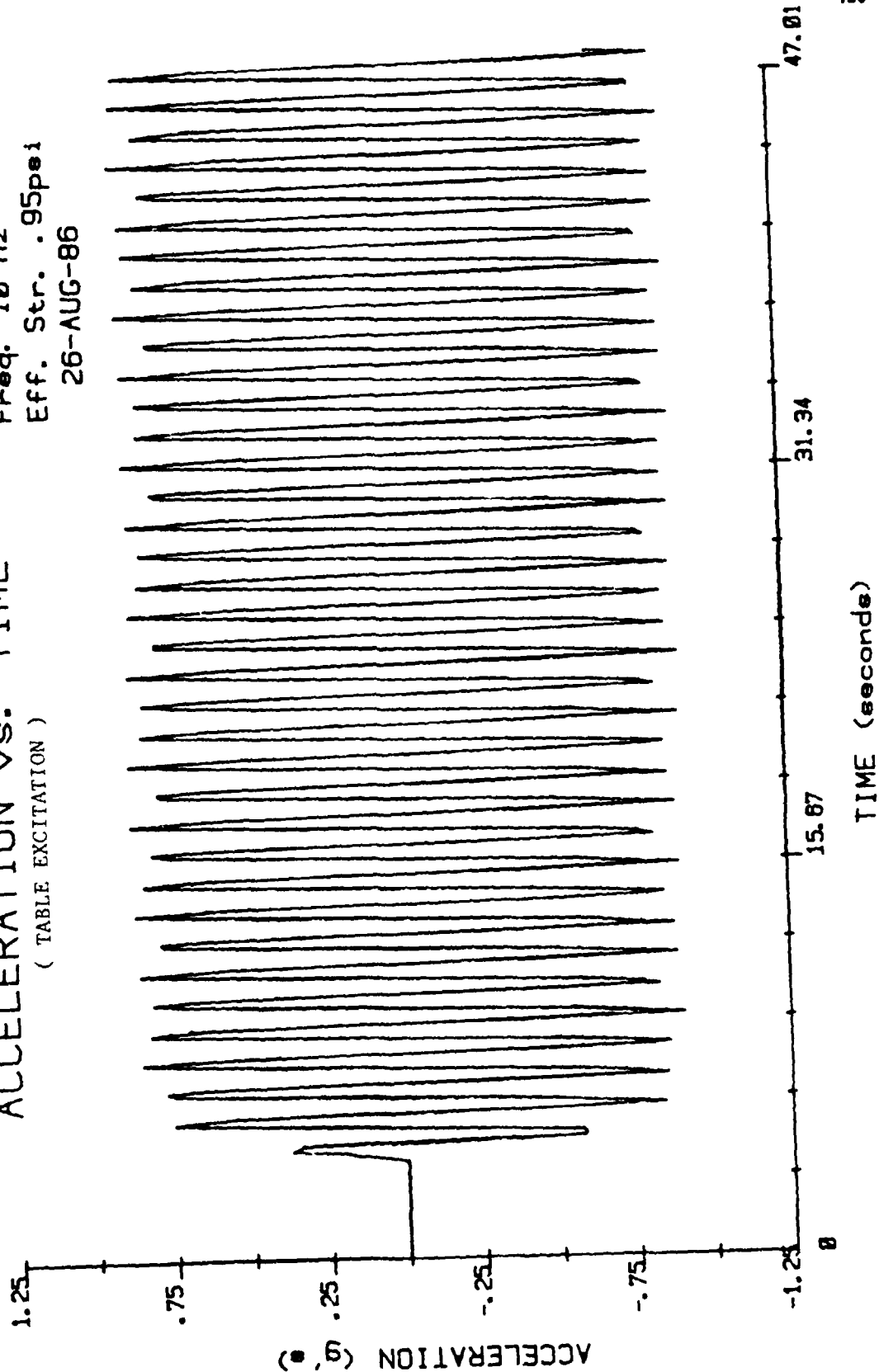
TABLE EXCITATION

Acc. 2.0g
Freq. 10 Hz
Eff. Str. 0.9 psi
21-JUL-86



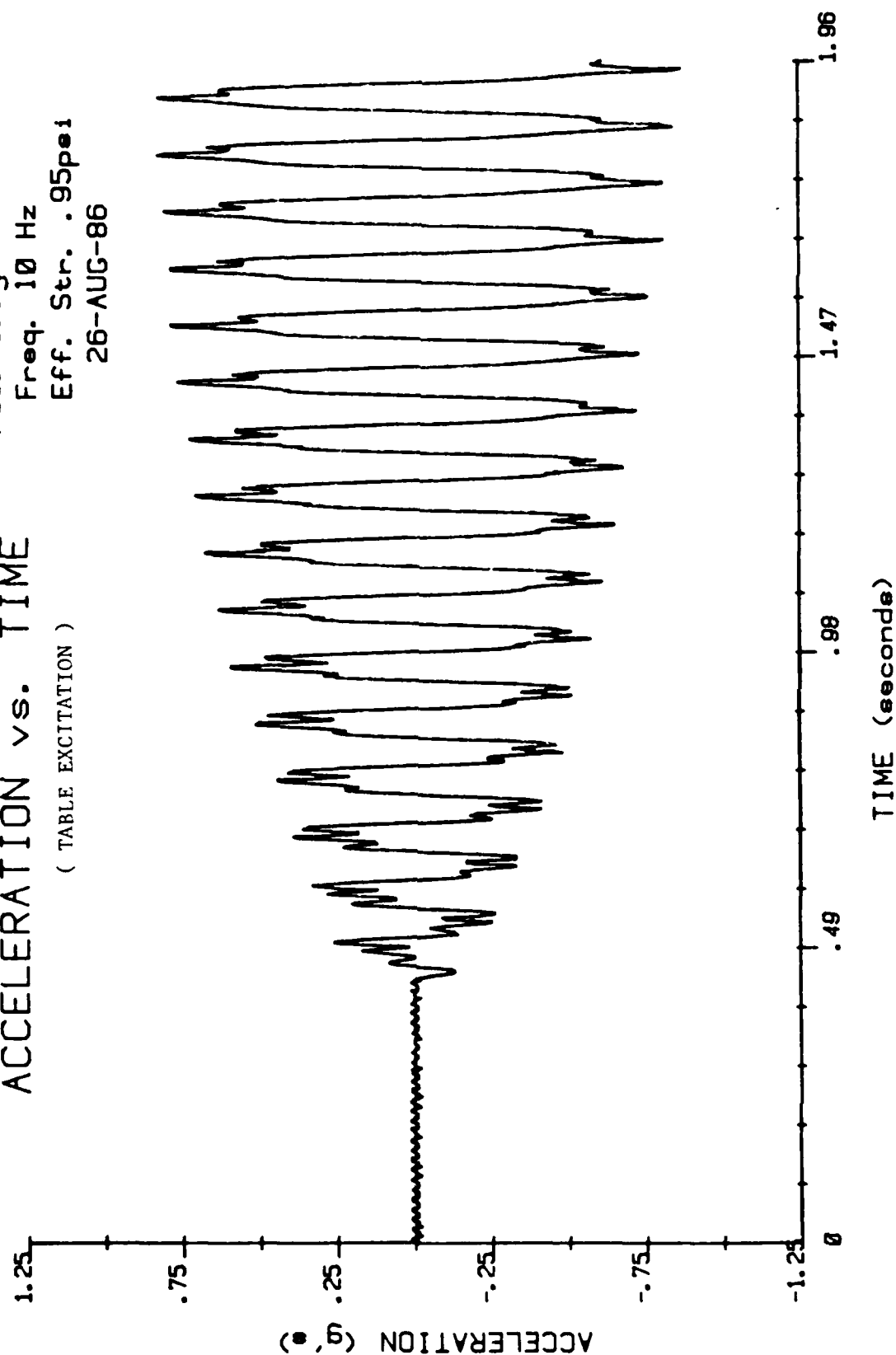
Acc. 1.0g
Freq. 10 Hz
Eff. Str. .95psi
26-AUG-86

ACCELERATION vs. TIME
(TABLE EXCITATION)



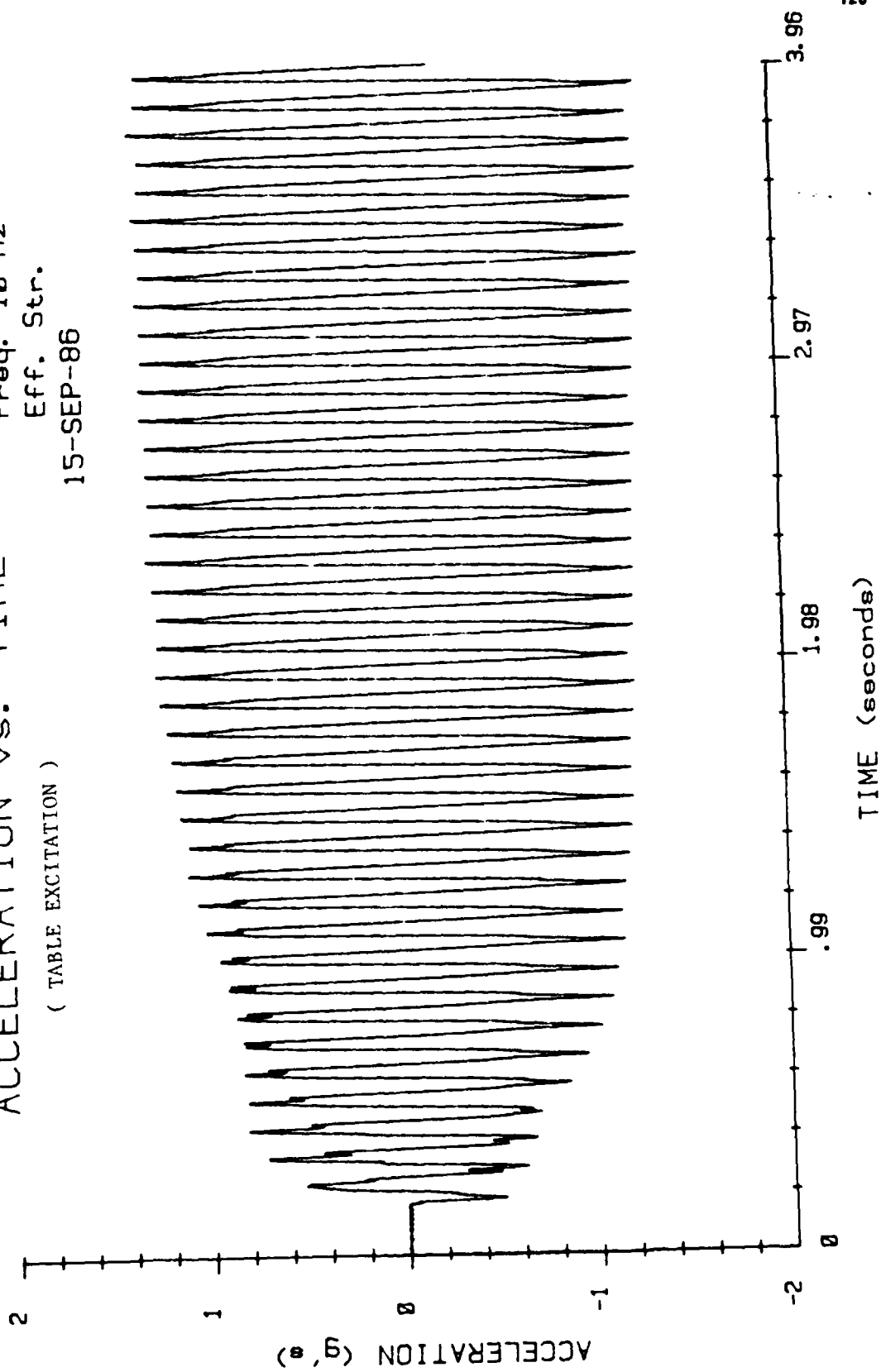
Acc. 1.0g
Freq. 10 Hz
Eff. Str. .95pei
26-AUG-86

ACCELERATION vs. TIME
(TABLE EXCITATION)



Acc. 1. g
Freq. 10 Hz
Eff. Str.
15-SEP-86

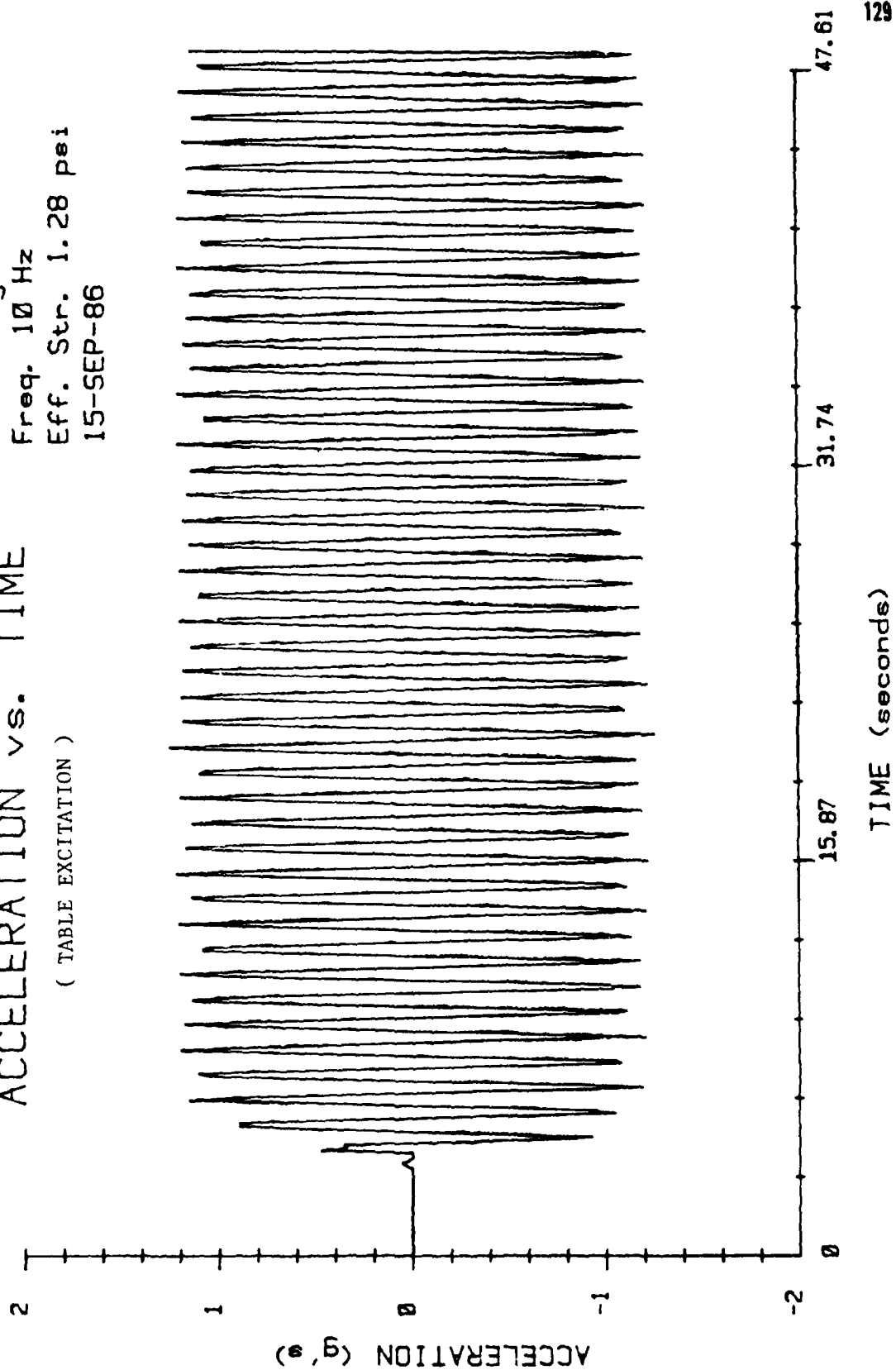
ACCELERATION vs. TIME
(TABLE EXCITATION)

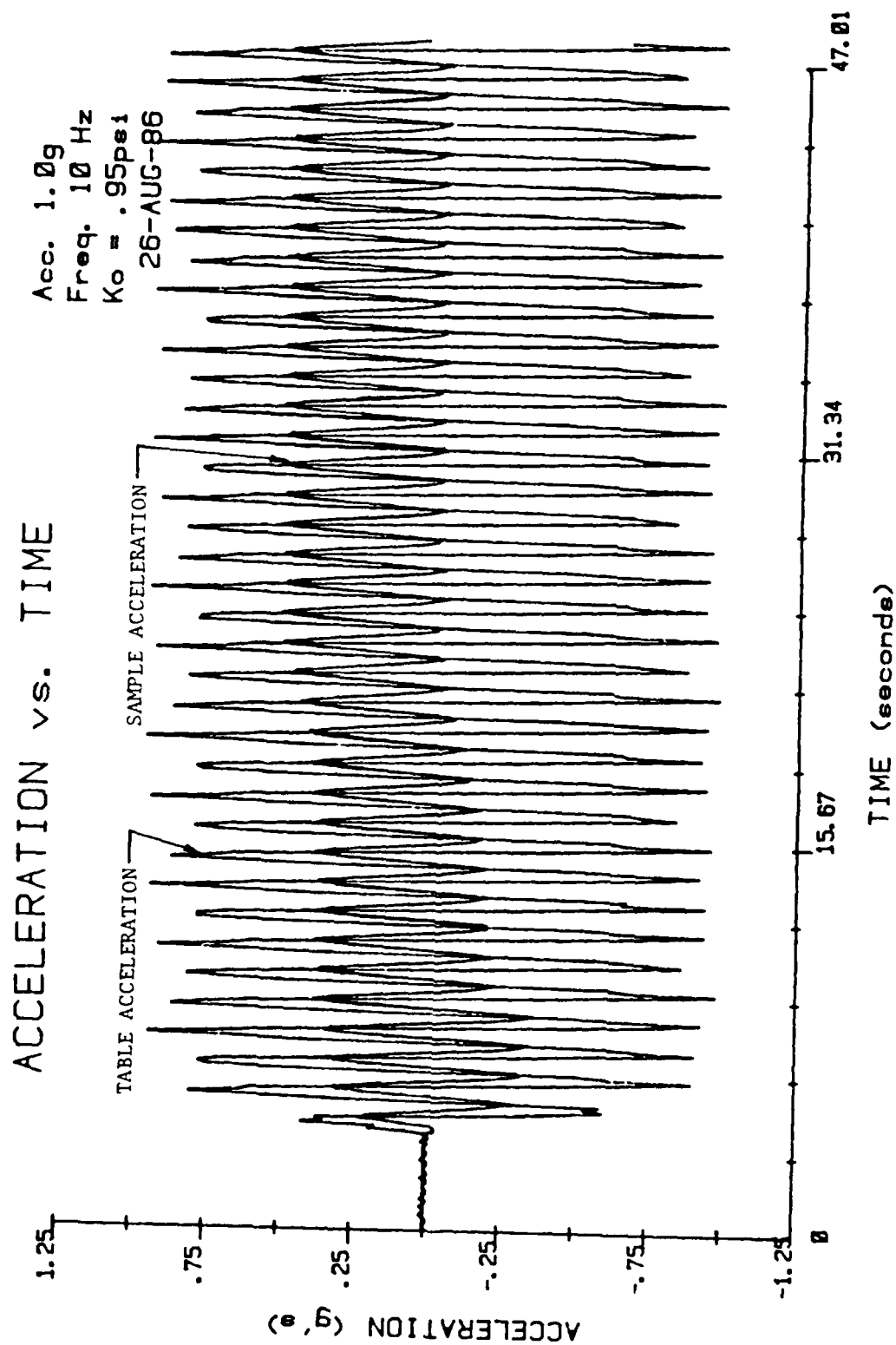


Acc. 1.3g
Freq. 10 Hz
Eff. Str. 1.28 psi
15-SEP-86

ACCELERATION vs. TIME

(TABLE EXCITATION)



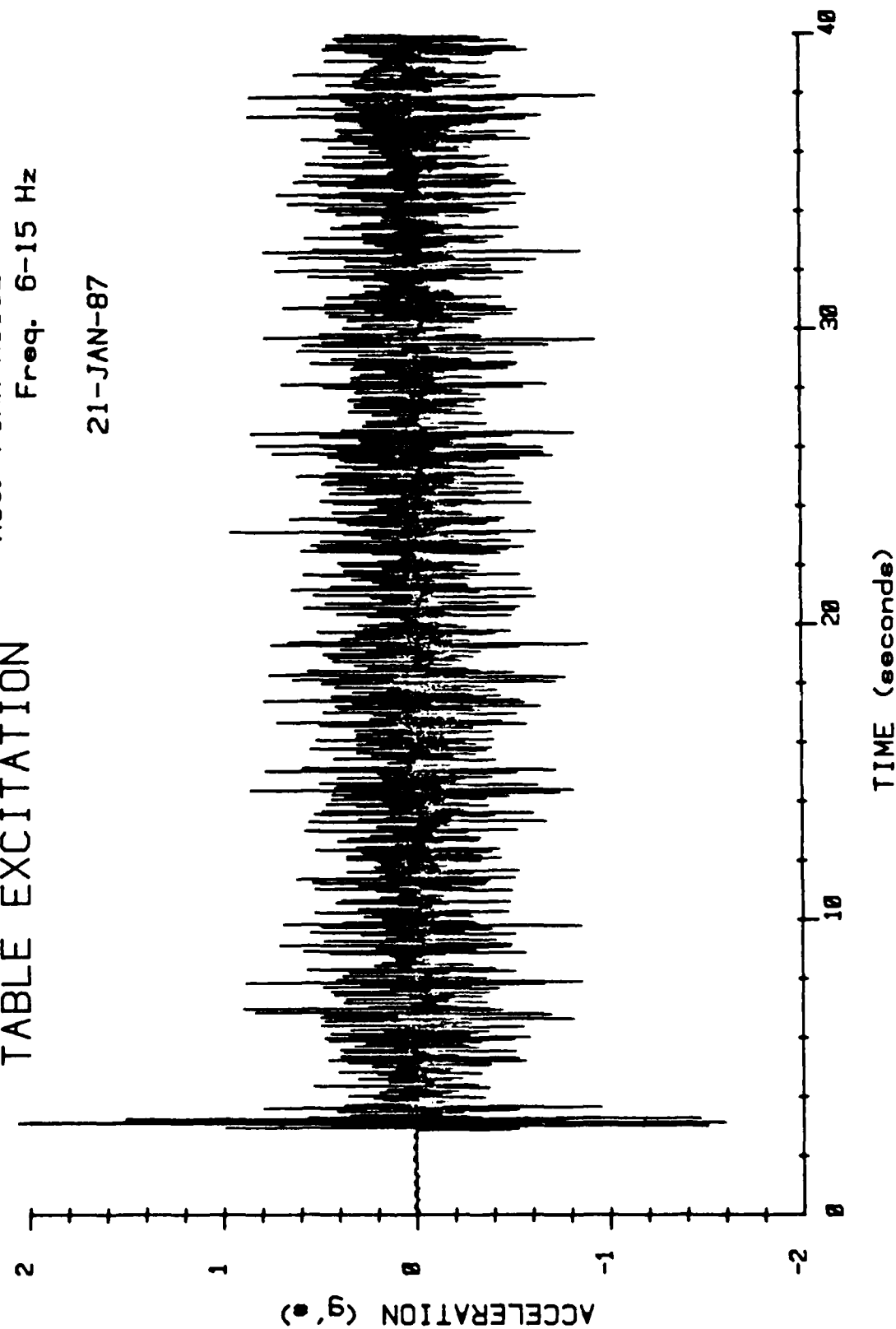


TO FACILITATE COMPARISON, THE MAGNITUDE OF THE SAMPLE ACCELERATION WAS GRAPHICALLY REDUCED BY ONE-FOURTH AND EVERY TWELFTH CYCLE IS REPRESENTED FOR BOTH ACCELERATION TIME HISTORIES

TABLE EXCITATION

Acc. PINK NOISE
Freq. 6-15 Hz

21-JAN-87



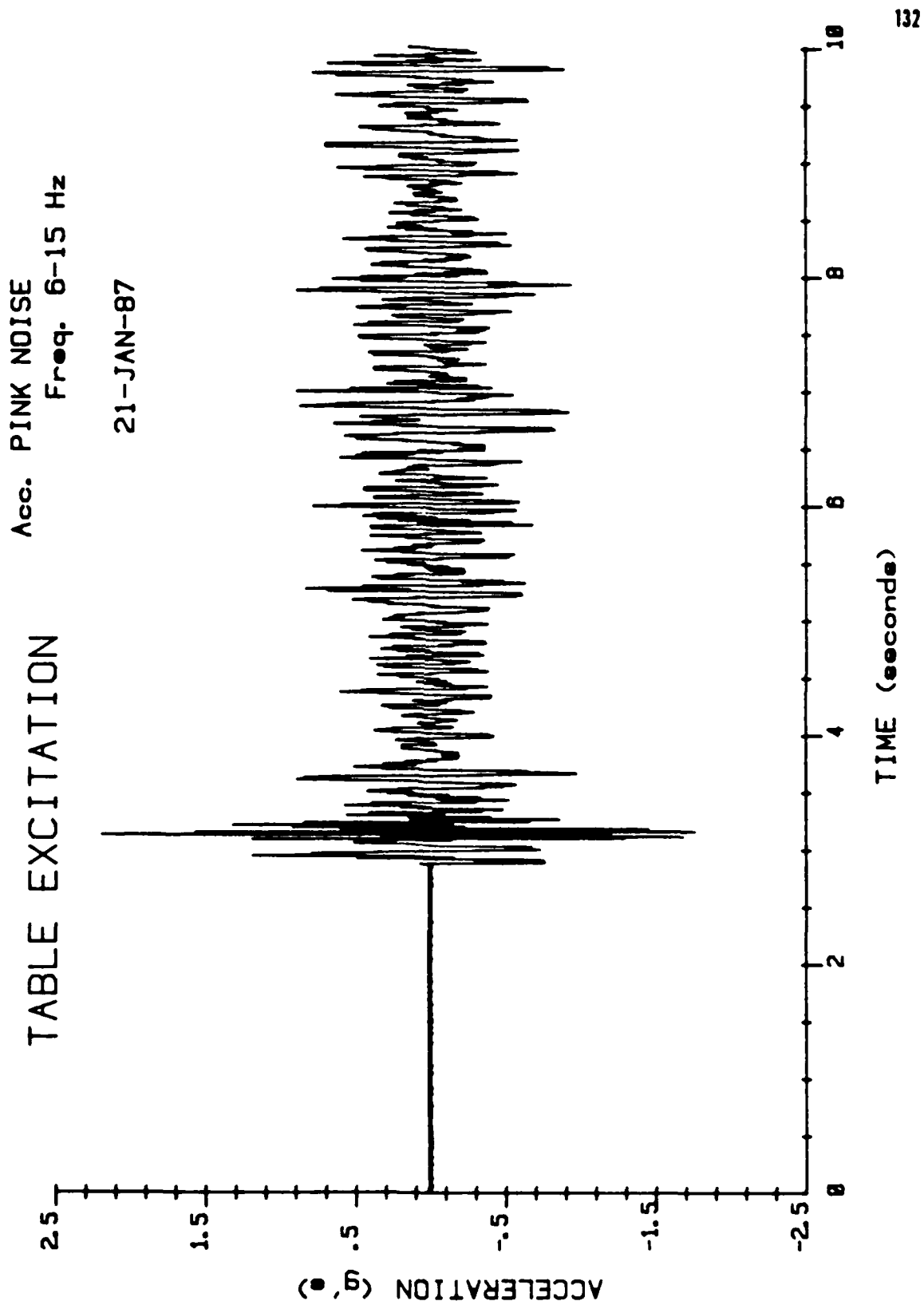
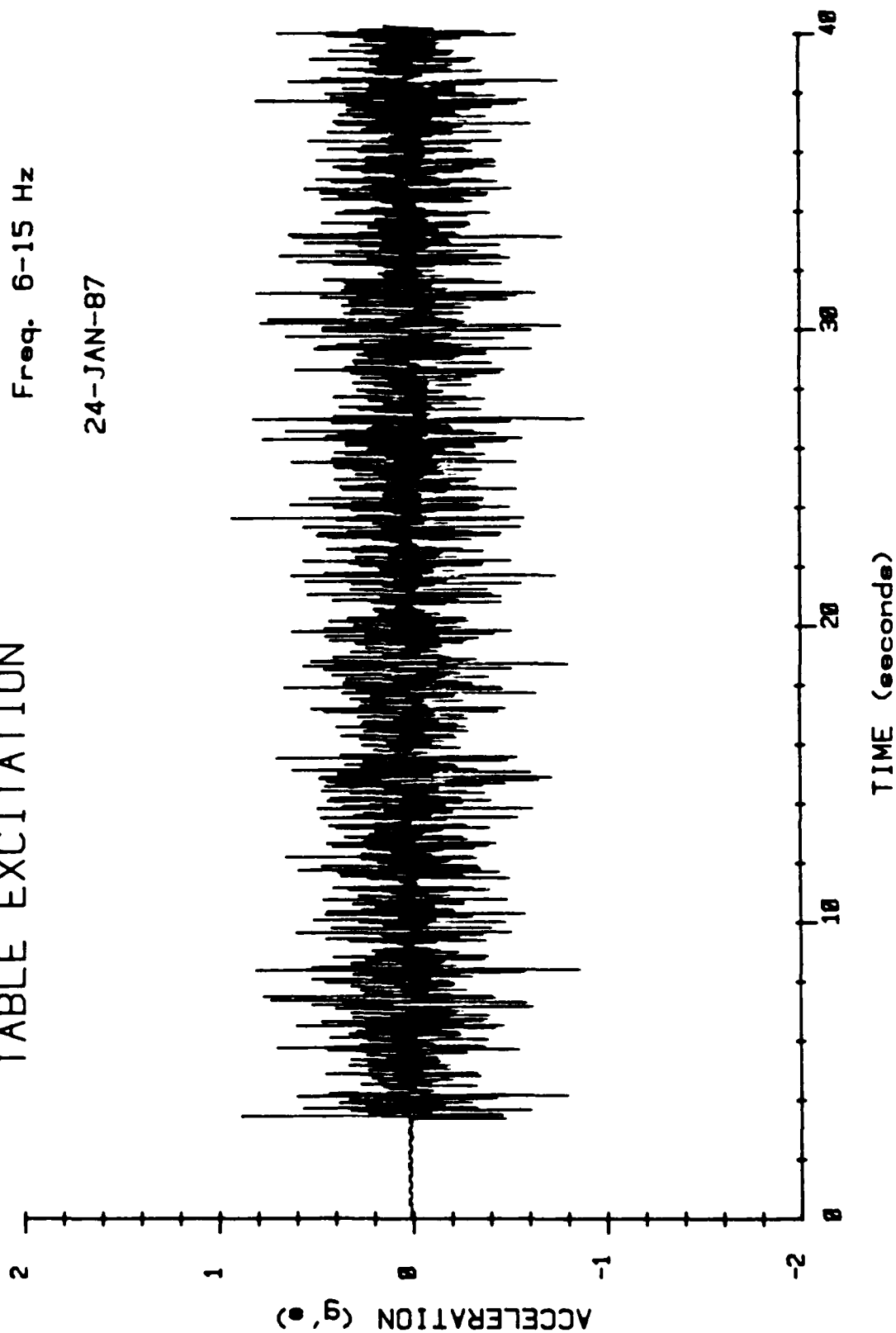


TABLE EXCITATION

Acc. PINK NOISE
Freq. 6-15 Hz

24-JAN-87



Acc. PINK NOISE
Freq. 6-15 Hz
24-JAN-87

SAMPLE EXCITATION

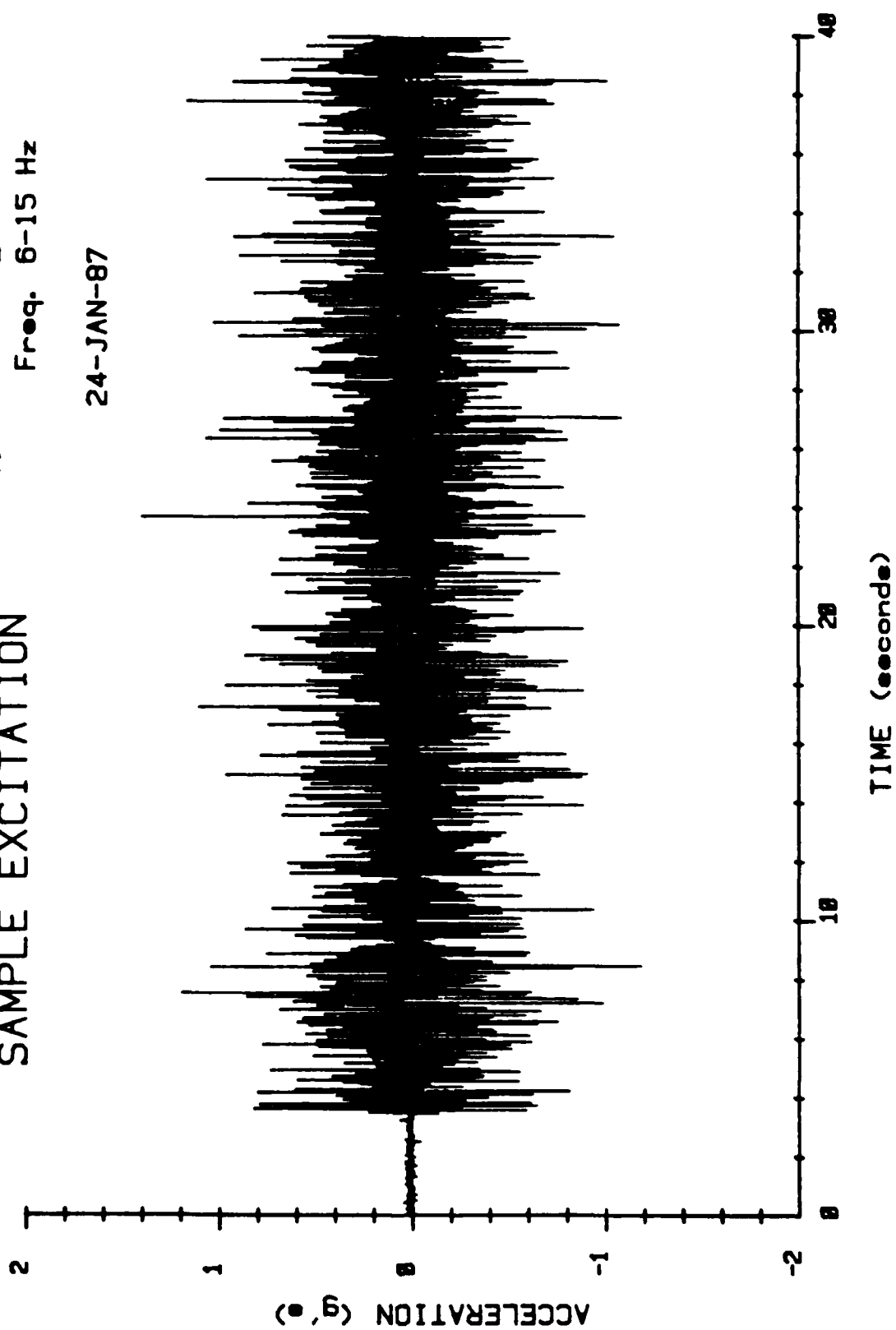
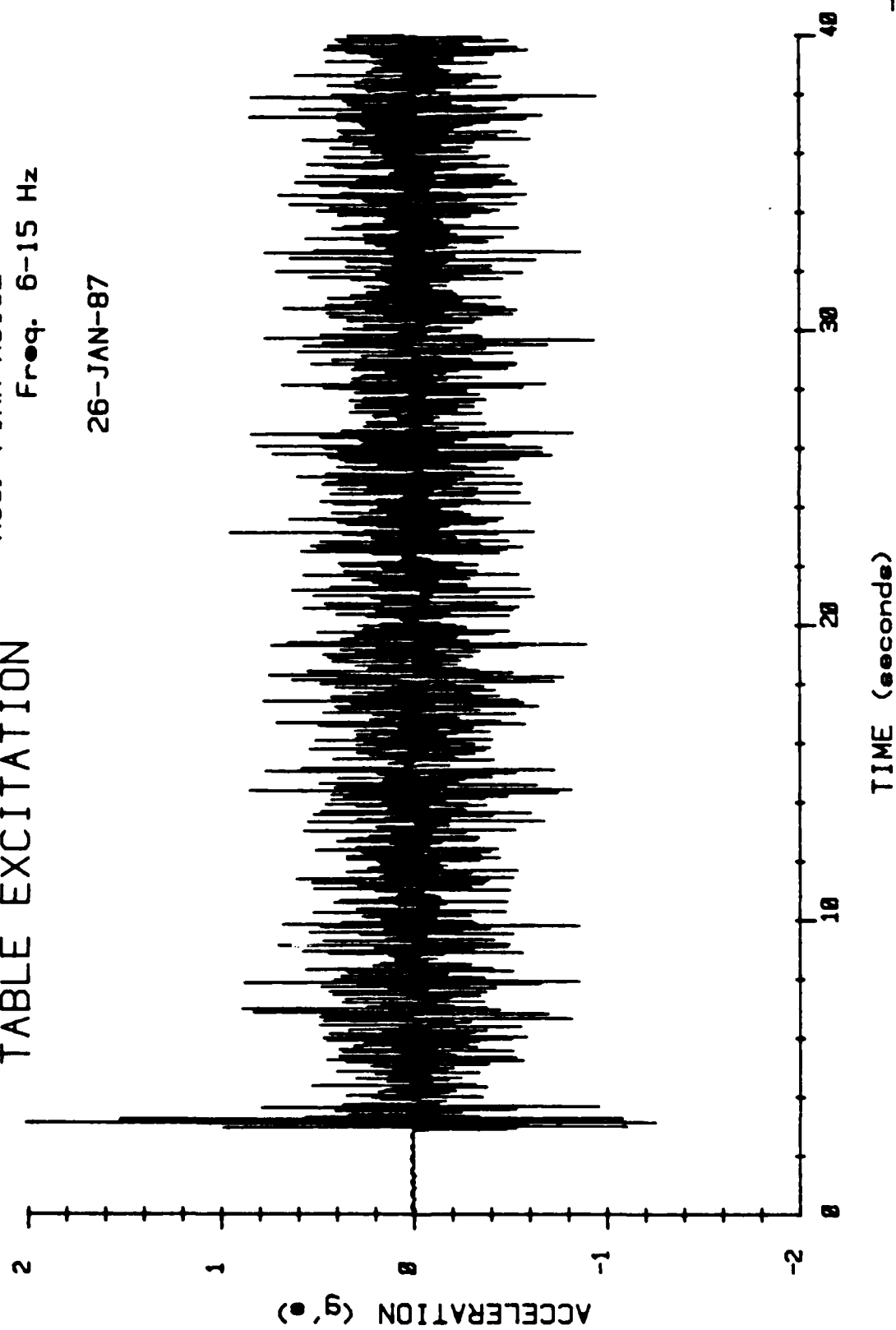


TABLE EXCITATION

Acc. PINK NOISE
Freq. 6-15 Hz

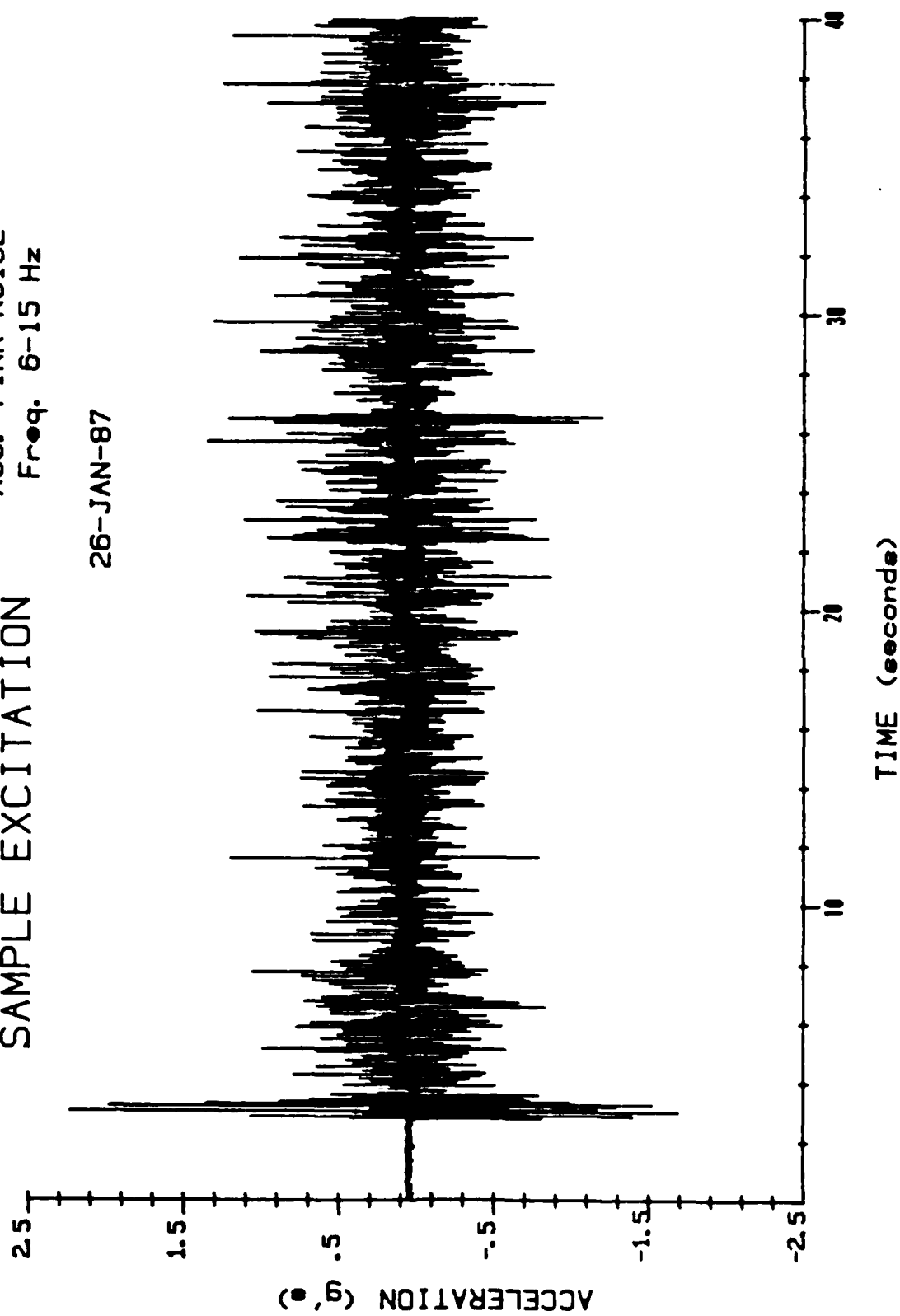
26-JAN-87



SAMPLE EXCITATION

Acc. PINK NOISE
Freq. 6-15 Hz

26-JAN-87



SAMPLE EXCITATION

Acc. PINK NOISE
Freq. 6-15 Hz

26-JAN-87

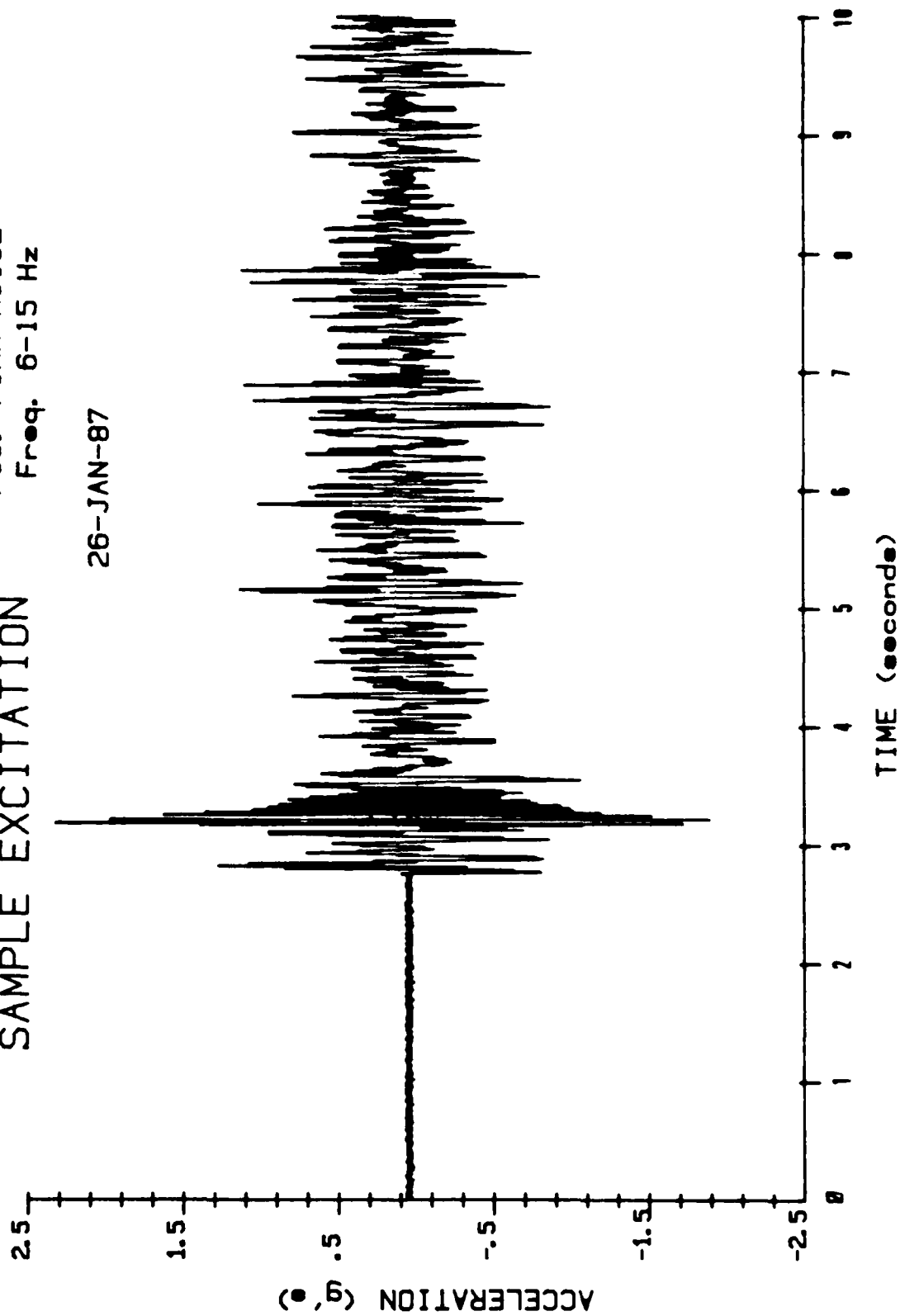
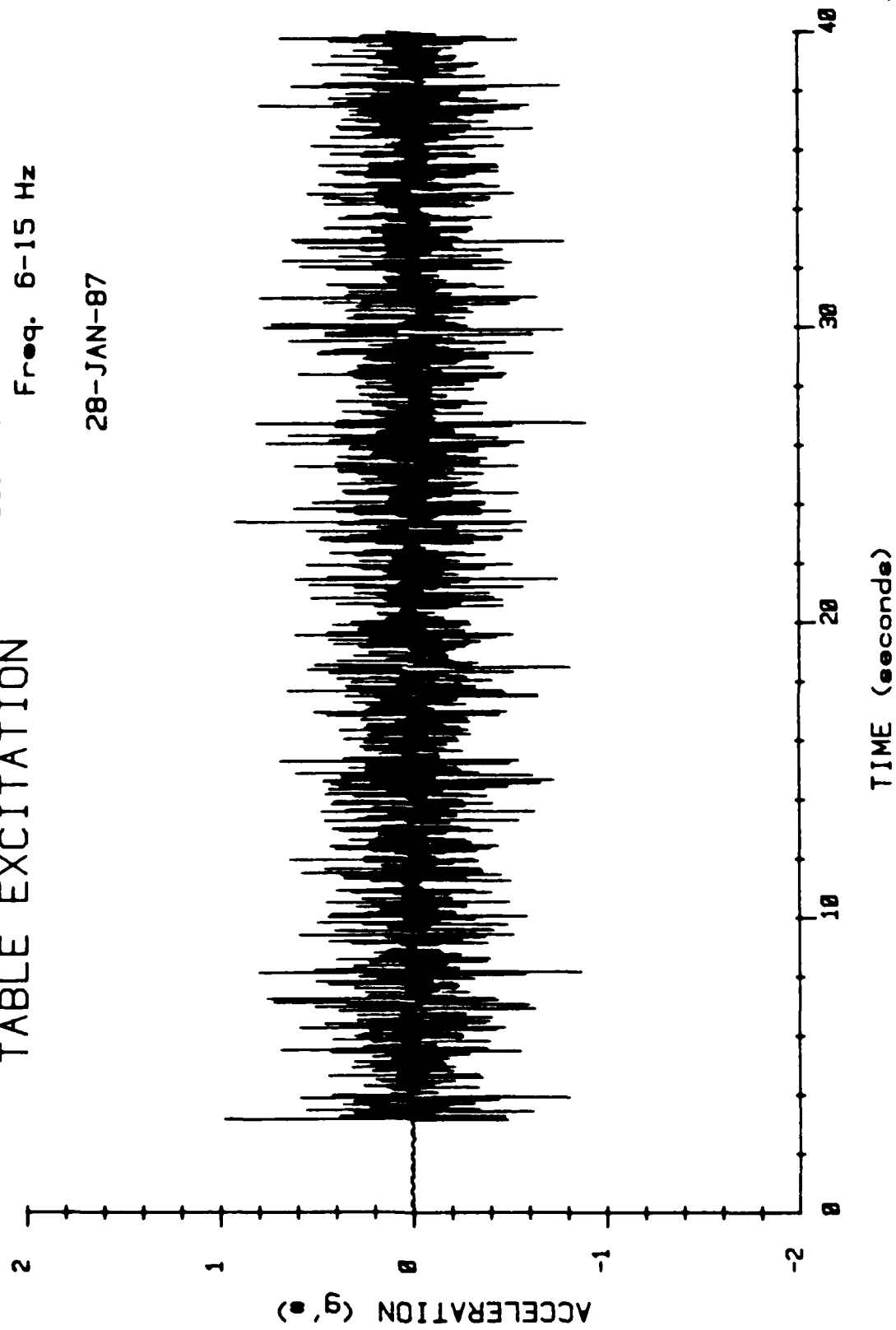


TABLE EXCITATION

Acc. PINK NOISE
Freq. 6-15 Hz

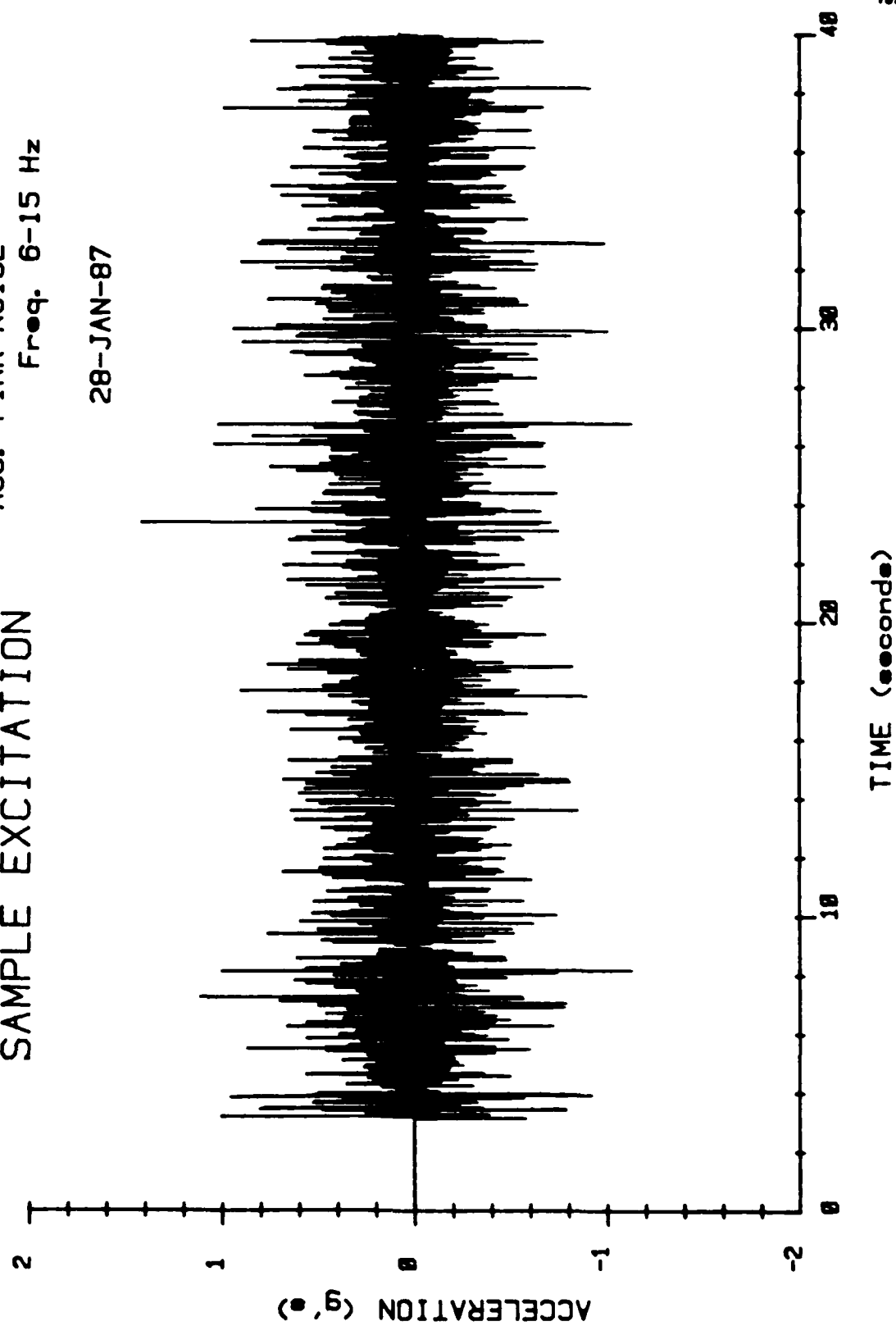
28-JAN-87



SAMPLE EXCITATION

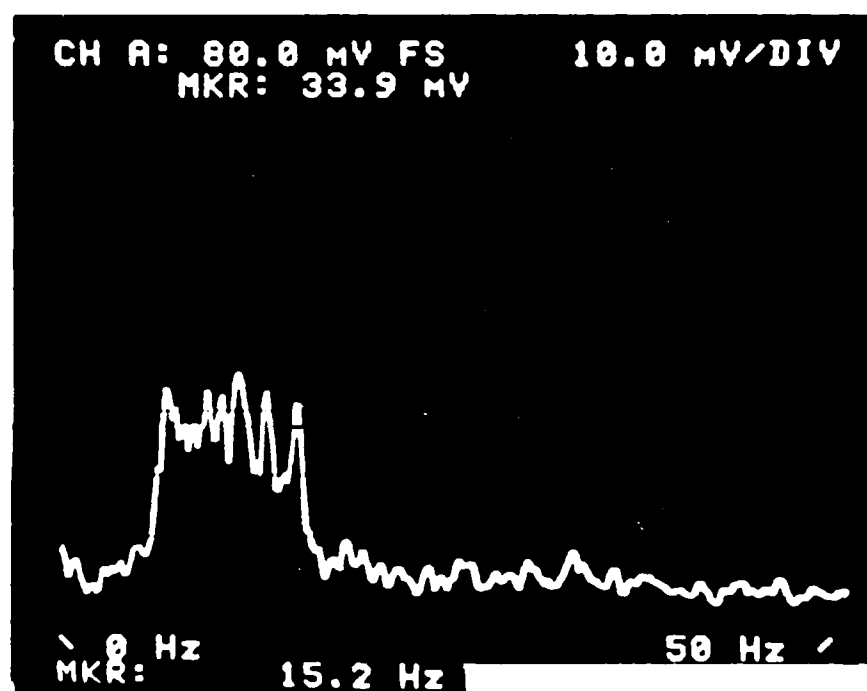
Acc. PINK NOISE
Freq. 6-15 Hz

28-JAN-87

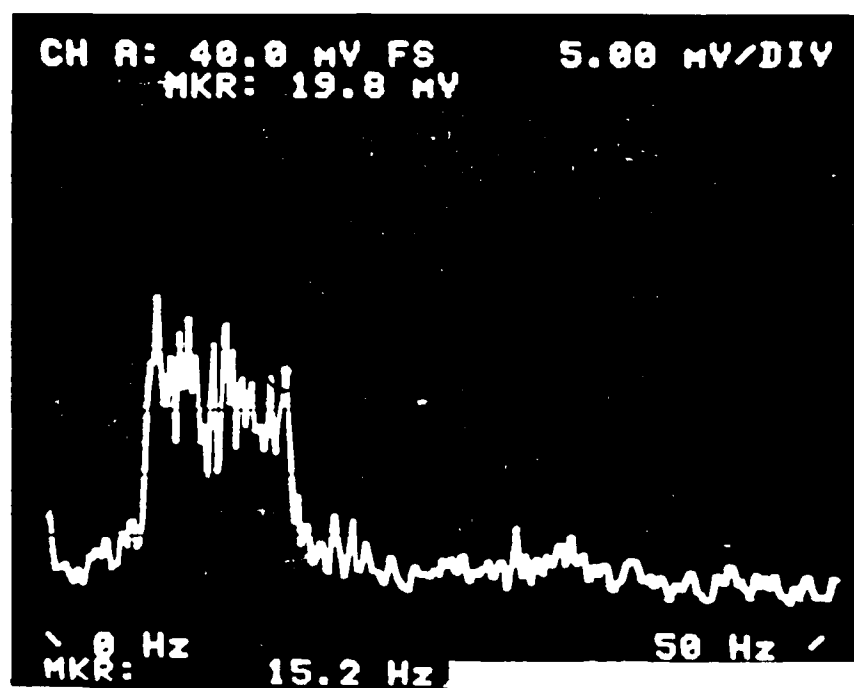


APPENDIX C
SPECTRUM ANALYSIS RECORDS

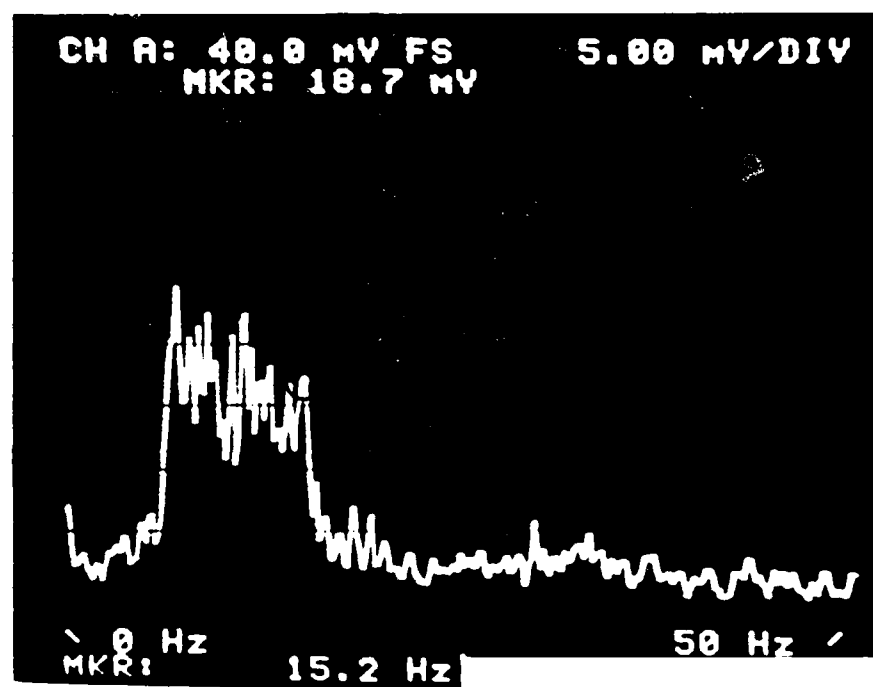
The following Fourier amplitude spectra were obtained by transmitting analog records of the excitations into a Hewlett-Packard 3582A Spectrum Analyzer. The plots are polaroid photos of the screen display having a horizontal scale of five hertz per division and the vertical scale displayed in the upper right-hand corner. The positioning of the screen marker within the frequency spectrum display is circled for clarity.



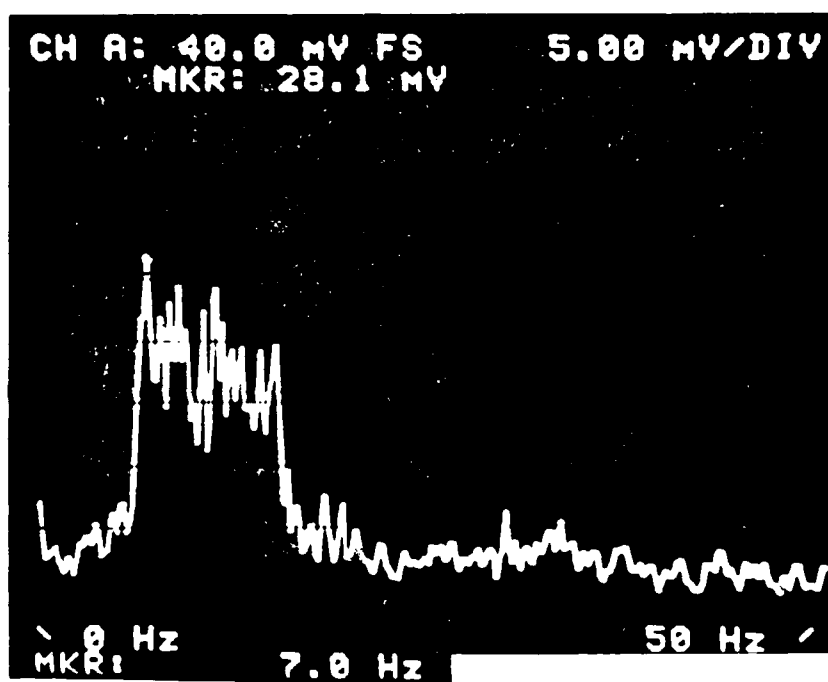
FOURIER SPECTRUM OF STAGE THREE INPUT MOTION



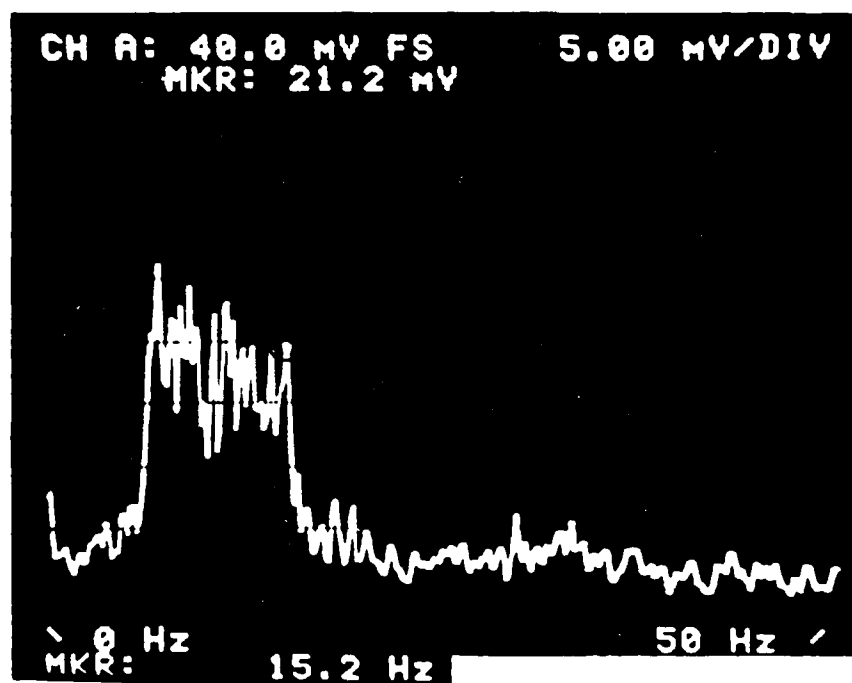
TYPICAL SAMPLE NON-SPIKED EXCITATION



TYPICAL TABLE NON-SPIKED EXCITATION



TYPICAL SAMPLE SPIKED EXCITATION



TYPICAL TABLE SPIKED EXCITATION

END

11-87

DTIC